Aus dem Institut für Experimentelle Biomedizin

der Universität Würzburg

Vorstand**:** Professor Dr. rer. nat. Bernhard Nieswandt

und Professorin Dr. rer. nat. Caroline Kisker

The role of septins and other regulatory proteins in abscission and midbody fate in *C. elegans* embryos

Inaugural - Dissertation

zur Erlangung der Doktorwürde der

Medizinischen Fakultät

der

Julius-Maximilians-Universität Würzburg

vorgelegt von

Linda Irmisch

aus Karlsruhe

Würzburg, Juni 2018

Inhalt

Abbildungsverzeichnis

Teile dieser Arbeit wurden veröffentlicht in:

Fazeli, G., et al., *C. elegans midbodies are released, phagocytosed and undergo LC3-dependent degradation independent of macroautophagy.* J Cell Sci, 2016. **129**(20): p. 3721-3731.

Beer, K., et al., *Degron-tagged reporters probe membrane topology and enable the specific labelling of membrane-wrapped structures*. Nature Communications, 2019, in press.

1. Introduction

1.1. Midbody formation during cytokinesis

Cytokinesis is a well-coordinated process that marks the last step of cell division, when the two daughter cells are physically separated. Even though the molecular mechanisms of cytokinesis are well studied (reviewed in [1]), some mysteries remain. For example, how exactly the two daughter cells physically separate at abscission is unclear.

Abscission is important to avoid multinuclear cells [2]. There are multiple examples of the profound clinical relevance of multinucleation. For instance, infection with *Chlamydia trachomatis* causes multinucleation of the host cell due to abscission failure, resulting in aneuploidy, which has been proposed to contribute to cellular transformation and cervical cancer [3]. Furthermore, Reed-Sternberg cells, part of the neoplastic population in classical Hodgkin lymphoma, arise from small mononucleated cells through abscission failure [4]. Thus, abscission timing needs to be tightly regulated to prevent aneuploidy, which is linked to tumor development (reviewed in [5]).

Cytokinesis begins after the mitotic spindle starts to segregate chromosomes. The anaphase spindle signals the cell cortex to conduct the assembly of an actomyosin ring at the spindle midzone, where antiparallel bundles of microtubules overlap. In this process, the small GTPase RhoA accumulates at the equatorial cell cortex [6]. RhoA promotes contractile ring assembly through activating actin nucleation [7] and myosin II [8]. The contractile ring also contains actin crosslinking proteins [9], like anillin [10, 11] and septin filaments [12, 13], discussed further in section 1.2. The amount of myosin, anillin and septins decreases with decreasing ring perimeter, indicating that ring contraction is coupled with filament disassembly [14].

As the actomyosin ring contracts, the cleavage furrow draws in until the daughter cells are only connected by an intercellular bridge. At the center of the bridge, composed of the contractile ring and the spindle midzone, the midbody forms. The midbody serves as a platform for proteins coordinating the final separation through abscission [15] by recruiting proteins that constrict and thin the cell membrane. Most actin filaments disassemble after

1

actomyosin ring ingression and microtubule bundles also disassemble as the intercellular bridge further narrows. Helices of 17 nm filaments encircle the intercellular bridge in a constriction zone [16, 17]. The composition of the 17 nm filaments is not known, however, they are thought to be composed of or regulated by the endosomal sorting complex required for transport (ESCRT). The ESCRT-III complex is essential for abscission [18]. TSG101, a component of the ESCRT-I complex, is recruited to the midbody to trigger ESCRT-III assembly [19]. It remains to be determined how exactly ESCRT-III contributes to abscission. One model proposes that the filaments form spirals that decrease in diameter and cause membrane constriction [16]. A second model proposes that part of the ESCRT-III filament is cut off to slide away from the midbody and constrict the cortex [20]. There are also models where ESCRT-III only has a stabilizing role at the intercellular bridge [17]. Once the membrane is thinned enough for the membranes to come together, membrane fusion occurs. Abscission thus separates the two sister cells, leaving behind a remnant of the midbody [16, 21], discussed further in 1.3.

Membrane trafficking has also been shown to play an important role in the abscission process. Abscission requires endosomes to be delivered to the intercellular bridge and then fuse with the plasma membrane [22]. While it was first thought that endosomes contribute to plasma membrane expansion, they are now known to serve as platforms on which molecular machines assemble (reviewed in [23]). These endosomes have been linked to actin disassembly at the intercellular bridge and also to ESCRT-III recruitment (reviewed in [24]).

Furthermore, the Class III phosphatidylinositol-3 kinase (PI3K), known to be involved in membrane trafficking through its role in endosome maturation [25], is also involved in localizing protein complexes at the intercellular bridge during cytokinesis (reviewed in [26]). The kinase VPS-34/Vps34 and modulatory subunits such as Bec-1/Beclin 1 are components of the Class III PI3K complex, which produces the phospholipid PI3P. PI3K and its product PI3P play many roles in membrane trafficking. PI3K helps initiate phagophore membranes during macroautophagy [27] and has trafficking roles during phagocytosis [28, 29], but has also been implicated in abscission. Upon depletion of PI3K,

Sagona et al. observed increased cytokinesis arrest and an increase in binucleate cells in cultured human cell lines and also *in vivo* in the follicular epithelium of the *Drosophila* egg chamber. Thus, they concluded that PI3K plays a role in abscission in addition to its numerous roles in membrane trafficking [30] (see also review [31]).

In summary, complex and precisely controlled mechanisms lead to abscission, the beginning of a new cellular generation.

1.2. The role of septins in abscission

Septins were first identified in yeast as cytokinesis mutants [32]. However, septins are regarded as the fourth component of the cytoskeleton and have more roles than just in cytokinesis [33].

Septins are a conserved, but diverse family of polymerizing GTP-binding proteins. The number of septin genes varies from two in *C. elegans* to 14 in humans [34-36]. Individual septin polypeptides assemble into oligomeric core complexes. In *C. elegans*, two copies of each septin protein UNC-59 and UNC-61 together form a tetrameric complex [37]. Septin oligomers then build higher-order structures such as filaments, rings and gauzes. These act as scaffold structures and boundaries that prevent diffusion of membrane-associated proteins and take part in key cellular processes like cell division, cytoskeletal organization and membrane-remodeling events (reviewed in [38]). Through distinguishing plasma membrane domains and cytoskeletal tracks from each other, septins are also thought to enable the formation of intracellular asymmetries and cell polarity [39]. Septins interact with other septins and also with numerous other proteins: proteins with roles in microtubule function, cell cycle control and dynamics, cell motility, protein modifications, endocytosis and intracellular trafficking, apoptosis and signaling cascades (reviewed in [38]).

During cytokinesis, septins are recruited to the contractile ring by anillin (reviewed in [11]). An anillin-septin complex narrows the intercellular bridge and is needed for ESCRT-III recruitment to the abscission site [40]. In septin-depleted vertebrate cells, contractile rings

open up again due to a defect in abscission, resulting in multinucleated cells [41]. However, in *C. elegans*, septin mutants have been found to have normal embryonic development. Defects were rather found in larval development, such as defects in vulva, gonad and male tails. Nguyen et al. reported that *unc-59* and *unc-61* double mutants show defects similar to each single mutant, indicating that these two proteins require each other for proper function [34].

In *C. elegans* embryos, septins are required for the timely isolation of the cytoplasm between daughter cells [42]. The lack of binucleation in septin-depleted *C. elegans* embryos prompted Green et al. to propose that various mechanisms ensure stable cell-cell boundaries [42]. Thus, the extent of the abscission defect in septin mutants remained unclear.

1.3. The midbody remnant and its fate

As the midbody remnant, from here on referred to as simply the midbody, is a product of abscission, studying the fate of the midbody could also lead to a better understanding of abscission. Several fates have been proposed for the post-mitotic midbody after abscission. In Fig. 1, possible pathways responsible for midbody degradation are depicted.

One suggested model is the macroautophagy model (Fig. 1A). It proposes that abscission takes place only on one side of the midbody, followed by retraction of the intercellular bridge. The cytoplasmic midbody is then engulfed by a double-membrane vesicle, the autophagosome, which later fuses with a lysosome [43, 44]. Proteins required for autophagy, such as Atg8/LC3, have been shown to associate with the midbody after abscission, supporting the autophagy model [45, 46].

Alternatively, the phagocytosis model (Fig. 1B) suggests that the midbody is released outside the cell by abscission taking place on both sides [47, 48]. Midbodies have been shown to be released into the cerebrospinal fluid *in vivo* in mouse embryos [49]. Midbodies of diverse mammalian cells are released into cell culture media *in vitro*, including

proliferating immortalized cells, cancer cell lines, and skeletal muscle stem cells [50]. Extracellular release of the midbody assures safe sequestration of midbody proteins to prevent further midbody signaling. It also allows the controlled internalization of midbodies via receptor-mediated phagocytosis, as seen in *C. elegans* embryonic blastomeres and neuroblasts *in vivo*, as well as in multiple mammalian cell types *in vitro* [50-52]. Not just daughter cells, but also neighboring cells take up midbodies *in vivo*. For example, somatic cells can internalize germ cell midbodies in *Drosophila* [53], which further supports the phagocytosis model.

A third possibility that has been suggested is that the midbody is degraded by a non-canonical autophagy pathway called LC3-associated phagocytosis (LAP) [50]. In LAP, autophagy proteins are required to degrade phagocytosed bacteria or phagocytosed cell corpses [54-56]. Most autophagy proteins are involved in LAP, including the Atg8/LC3-family proteins, the proteins involved in their lipidation, such as Atg7, and the PI3K subunits Vps34 and Beclin 1. Like the classical phagocytosis model, the LAP model suggests symmetric abscission on both sides of the midbody releases the midbody into the extracellular space before internalization of the midbody by phagocytosis (Fig. 1C). The autophagy-associated Atg8/LC3 is then recruited to the phagosome by a PI3K complex that, in contrast to the autophagy model, lacks the Atg14 subunit. Also in contrast to the autophagy model, proteins of the pre-initiation complex, such as ULK1, are not involved in LAP [56, 57]. Though suggested by Crowell et al., they did not favor midbody degradation via LAP, as they rarely observed LC3 staining on midbodies in cultured cells [50]. However, LC3 staining was previously reported on internalized mammalian midbodies [45, 46]. The LAP model could explain why some groups working with mammalian cells thought the midbody to be degraded by phagocytosis and others by autophagy. No one had looked at both phagocytosis and autophagy markers in an intact physiological system to test whether the midbody is degraded by LAP.
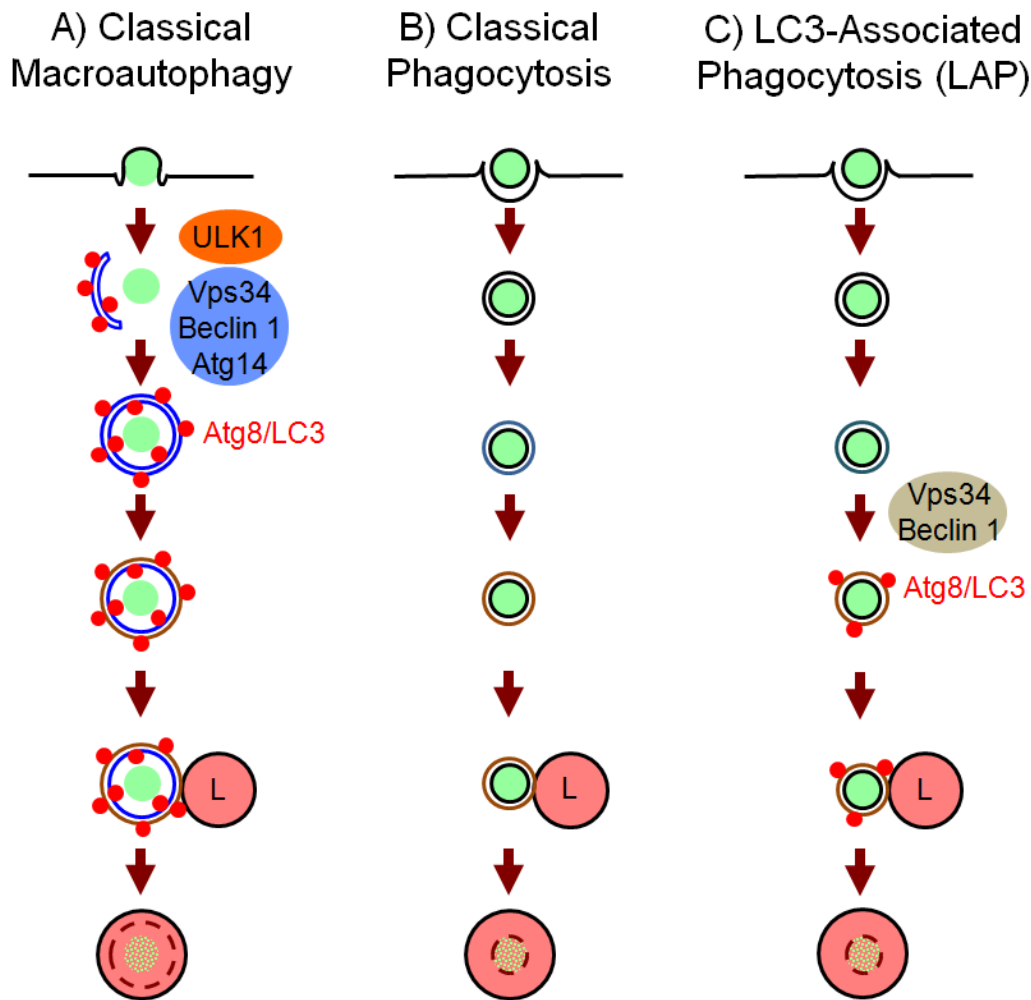
Fig. 1: Three different pathways by which the midbody could potentially be resolved. Lysosomes are marked with "L". The image is adapted from Fazeli and Wehman [58] and shown here with permission.

Thus, the fate of the midbody remains unclear. Though all three pathways converge on the lysosome, there are crucial differences. The autophagy model initially leaves signaling proteins free in the cytoplasm before they are wrapped in the autophagosome, a potential source of misregulation of the cytoskeleton or vesicular trafficking. The phagocytosis model fails to explain the observations of autophagy proteins in midbody degradation. In

view of the regulatory roles of midbody proteins during cytokinesis, the cell needs to carefully resolve the midbody.

In addition to roles during mitosis, inheritance of the midbody has been observed to correlate with the proliferative potential of cells [59]. Furthermore, several studies have implicated midbody positioning in influencing cell polarity and cell fate [46, 60, 61]. Thus, there is evidence that the midbody is able to influence cells after abscission, further suggesting that cells must regulate the fate of the midbody. Given the proposed roles of the midbody after abscission, elucidating the mechanisms of midbody release, uptake and elimination is of particular interest.

1.4. *C. elegans* as a model system for midbody fate

The nematode *Caenorhabditis elegans* is an attractive model organism for studying the role and fate of the midbody. It is an organism that has been studied for more than 50 years, which has become indispensable in today's research of molecular cell biology [62].

C. elegans is a small nematode, with adult worms measuring 1 mm long. Its rapid generation time (sixteen hours from fertilized egg to larva; 2.5 days to reach the adult stage), primary existence as a self-fertilizing hermaphrodite and high number of offspring have contributed to making *C. elegans* an important model of choice for genetic studies. Other advantages are its simple anatomy and eutely, i.e. its fixed, invariant cell lineage.

Also important to research is the ability to create transgenic animals [63]. Furthermore, *C. elegans* is amenable to RNA interference to knock down protein levels [64]. Its short cell cycle, as well as previous detailed studies of cell division in *C. elegans* (reviewed in [65]), and also the ease of time-lapse analyses of cells during the first cell divisions [66], are further appealing features of this organism for studies related to cell division and the fate of the midbody.

Finally, after cytokinesis, midbody remnants are inherited according to a stereotypical distribution pattern in the *C. elegans* embryo, both in respect to time and also the inheriting

cell [52, 61]. This allows easy detection of anomalies in midbody internalization patterns in genetically modified *C. elegans* embryos.

Green et al. found the first embryonic midbody in *C. elegans* to be released into a specific daughter cell after isolation of the cytoplasm between the daughter cells. They also observed membrane shedding, possibly a result of membrane remodeling events that lead to the release of the midbody [42]. They did not observe a membrane around the internalized midbody and favored the autophagy model for midbody fate.

Ou et al. tracked the first three embryonic midbodies in *C. elegans* and found that the first and third midbodies are internalized into daughter cells. However, the second midbody is internalized by a neighboring, non-daughter cell, indicating that at least the second midbody must have been released. Furthermore, through depleting the cell corpse engulfment genes *ced-1* and *ced-2,* Ou et al. showed that all three midbodies are phagocytosed like cell corpses [52].

Singh and Pohl proposed that stereotyped differences in cortical tension determine which cell internalizes the midbody. They also found that the P0 midbody remnant is positioned asymmetrically at the future ventral side of the embryo through rotational flow, concluding that there must be a functional attachment between the midbody and one of the sister cells, either through cell surface molecules or continuity of the plasma membrane [61].

Thus, although many interesting observations on the fate of the midbody have been made in *C. elegans* embryos, various questions remain open. Does abscission occur on both sides of the midbody in all the midbodies? What mechanisms lead to the release of the midbody into daughter or neighboring cells? Is the midbody securely enclosed by a membrane after internalization?

1.5. ZF1-mediated degradation technique

The release and further fate of the midbody can be studied by putting a degradation tag on midbody reporters. Specifically, the ZF1 degradation technique can be used. ZF1, the first

CCCH finger of PIE-1, marks proteins for proteasome-mediated degradation in somatic blastomeres [67]. ZIF-1, a SOCS-box adaptor protein, recruits ZF1-containing proteins to an E3 ubiquitin ligase complex to mark ZF1-containing proteins for proteasome-mediated degradation [68]. The ZF1-mediated degradation technique was developed to selectively remove persisting maternal proteins in *C. elegans* embryos [69, 70]. Moreover, the ZF1 technique can be used to test whether tagged proteins are accessible to the cytoplasm. For example, released extracellular vesicles are protected from ZF1 degradation [71].

In our workgroup, the ZF1-tag technique was further developed to test whether the midbody is released into the extracellular space. Non-muscle myosin NMY-2, which localizes superficially on the midbody [1], was tagged with the ZF1 domain. G. Fazeli showed that the ZF1 tag did not disrupt midbody internalization [29]. Thus, the NMY-2::GFP::ZF1 reporter could be used to test whether midbodies are separated from both daughter cells, thereby released in the extracellular space. Furthermore, this technique could potentially be applied to detect defects in abscission.

1.6. Aims of this work

Further experimental research is needed to give answers to the open questions on abscission, midbody uptake, and midbody fate. This work studies abscission by examining the extent of the abscission failure in *C. elegans* septin and ESCRT mutants with the help of the ZF1-degradation technique. The ZF1 technique is also applied to discern a possible role for PI3K during abscission. Lastly, we assess the role of autophagy proteins in midbody degradation and elucidate the fate of the midbody by testing the role of proteins required for LAP and/or macroautophagy. Thus, this work analyzes the role of different proteins in abscission, midbody internalization, and midbody degradation.

2. Materials and Methods

2.1. Worm strains

Basic methods of *C. elegans* culture and handling were according to standard protocols [72]. A list of the strains used in this work is given in Table 1.

Strain	Genotype	Source
BV113	*zuIs45 [nmy-2::NMY-2::GFP + unc-119(+)] IV;* *zbIs2 [pie-1::lifeACT::RFP + unc-119(+)]*	(Singh and Pohl, 2014)
CB261	*unc-59(e261) I*	(Sulston and Horvitz, 1981)
LP162	*nmy-2(cp13 [nmy-2::gfp + LoxP]) I*	(Dickinson et al., 2013)
WEH02	*ltIs38 [pie-1::GFP::PH(PLC1∂1) + unc-119(+)]* *xnIs8 [pJN343: nmy-2::NMY-2::mCherry + unc-119(+)]* *unc-119(ed3) III*	(Fazeli et al., 2016)
WEH03	*ltIs38 [pie-1::GFP::PH(PLC1∂1) + unc-119(+)]* *xnIs8 [pJN343: nmy-2::NMY-2::mCherry + unc-119(+)]* *unc-119(ed3) III; bec-1(ok691) IV / nT1 [qIs51] (IV; V)*	(Fazeli et al., 2016)
WEH51	*unc-119(ed3) III; xnIs65 [nmy-2::gfp::zf1 + unc-119(+)] IV;* *ltIs44 [pie-1p::mCherry::PH(PLC1∂1) + unc-119(+)] V*	(Fazeli et al., 2016)
WEH55	*vps-34(h510) dpy-5(e61) I;* *ltIs38 [pie-1::GFP:: PH(PLC1∂1) + unc-119(+)]* *xnIs8 [pJN343: nmy-2::NMY-2::mCherry + unc-119(+)]* *unc-119(ed3) III; enEx441 [vps-34(+) + ced-1C::mRFP]*	(Fazeli et al., 2016)
WEH69	*bec-1(ok691) xnIs65 [nmy-2::gfp::zf1 + unc-119(+)] / nT1 IV;* *ltIs44 [pie-1p::mCherry::PH(PLC1∂1) + unc-119(+)] /* *nT1 [qIs51] V*	(Fazeli et al., 2016)
WEH71	*ced-2(e1752) xnIs65 [nmy-2::gfp::zf1 + unc-119(+)] IV;* *ltIs44 [pie-1p::mCherry::PH(PLC1∂1) + unc-119(+)] V*	(Fazeli et al., 2016)
WEH73	*vps-34(h510) dpy-5(e61) I; unc-119(ed3) III;* *xnIs65 [nmy-2::gfp::zf1 + unc-119(+)] IV;* *ltIs44 [pie-1p::mCherry::PH(PLC1∂1) + unc-119(+)] V;* *enEx441 [vps-34(+) + ced-1C::mRFP]*	(Fazeli et al., 2016)
WEH78	*ltIs38 [pie-1::GFP::PH(PLC1∂1) + unc-119(+)]* *xnIs8 [pJN343: nmy-2::NMY-2::mCherry + unc-119(+)]* *unc-119(ed3) III; ced-2(e1752) IV*	(Fazeli et al., 2016)
WEH85	*ced-2(e1752) zuIs45 [nmy-2::NMY-2::GFP + unc-119(+)] IV;* *zbIs2 [pie-1::lifeACT::RFP + unc-119(+)]*	(Fazeli et al., 2016)

Strain	Genotype	Source
WEH98	*lgg-1(tm3489) II;* *ltIs38 [pie-1::GFP::PH(PLC1∂1) + unc-119(+)]* *xnIs8 [pJN343: nmy-2::NMY-2::mCherry + unc-119(+)]* *unc-119(ed3) III; lgg-2(tm5755) IV;* *wurIs36 [lgg-1::gfp fosmid WRM06 8A_G10]*	(Fazeli et al., 2016)
WEH106	*zbIs2 [pie-1::lifeACT::RFP + unc-119(+)] I; bec-1(ok691)* *zuIs45 [nmy-2::NMY-2::GFP + unc-119(+)] IV /* *nT1 [qIs51] (IV; V)*	(Fazeli et al., 2016)
WEH132	*unc-59(e261) I; unc-119(ed3) III;* *xnIs65 [nmy-2::gfp::zf1 + unc-119(+)] IV;* *ltIs44 [pie-1p::mCherry::PH(PLC1∂1) + unc-119(+)] V*	(Fazeli et al., 2016)
WEH176	*ltIs38 [pie-1::GFP::PH(PLC1∂1) + unc-119(+)]* *xnIs8 [pJN343: nmy-2::NMY-2::mCherry + unc-119(+)]* *unc-119(ed3) III; unc-51(e369) V*	(Fazeli et al., 2016)

Table 1: Strains used in this work.

Maternal-zygotic *vps-34* mutants were obtained as in [73]. Homozygous progeny of *vps-34* heterozygous mothers undergo larval developmental arrest. Therefore, a strain was used in which homozygous mutants received an extrachromosomal array carrying the *vps-34(+)* genomic DNA to prevent larval arrest and an mRFP marker to label embryos carrying the array. Isolation of maternal-zygotic embryos was performed by G. Fazeli.

Maternal-zygotic *lgg-1; lgg-2* double mutants were obtained similar to [74]. *lgg-1; lgg-2* mutants were rescued with a *lgg-1::gfp* transgene that is not visibly expressed in the early embryo. This transgene rescued the embryonic lethality in *lgg-1; lgg-2* mutants. For further depletion of maternal protein, L3 worms were also treated with *lgg-1* RNAi. Staining with an anti-GFP antibody ensured the absence of LGG-1::GFP transgene expression. These mutants were isolated and verified by G. Fazeli.

2.2. Crossing septin mutants

To analyze the role of septins in abscission, a new worm strain was established, WEH132. The WEH132 strain contains a mutant allele of *unc-59(e261),* a missense mutation in one of the two *C. elegans* septins [34], and two fluorescent transgenes: the green fluorescent protein GFP labels the ZF1 degron-tagged non-muscle myosin (NMY-2), thus labeling the midbody ring and remnant to allow tracking of the midbody and the ZF1 degradation assay [69], and the red fluorescent protein mCherry labels the plasma membrane marker PH(PLCd1) for better judgment of midbody internalization [61].

To create this new strain, *unc-59* hermaphrodites of the strain CB261 were mated with males of the strain WEH51. WEH51 is a genetically modified strain with the described fluorescent markers (*nmy-2::gfp::zf1* and *pie-1p::mCherry::PH*). On the next day, the hermaphrodites were isolated onto separate plates to be able to analyze the amount of males in the F1 generation, an indicator for successful mating with a male. After two days, hermaphrodites of the F1 generation were singled onto separate plates, predicted to be heterozygote for the mutation and two transgenes.

Four days later, uncoordinated worms (Uncs) of the F2 generation were singled out onto 24-well plates. These Uncs were identified by their disturbed backwards movement and a protruding vulva, the characteristic phenotypes of *unc-59* mutants [34].

To identify an F2 that was homozygous for the fluorescent transgenes from the wells that only contained Unc worms (i.e. homozygous for the *unc-59* mutation), 12 adults of the next generation, F3, were mounted on a slide and expression of the fluorescent markers was examined. A single F2 strain homozygous for the mutation and expressing the fluorescent transgenes was identified and named WEH132.

Noteably, *unc-59(e261)* mutants still express UNC-59 protein, with the function of septin partly remaining [34]. Therefore, the WEH132 strain was additionally treated with *unc-59* RNAi to further deplete UNC-59 protein levels.

2.3. RNAi experiments

RNAi experiments were performed by standard feeding protocols [75]. Briefly, bacteria carrying double-stranded RNA (dsRNA) expression plasmids were seeded onto NGM Lite plates supplemented with Ampicillin and 20% ß-lactose. Gravid adult worms were bleached onto seeded plates and their progeny was fed dsRNA from the L1 larval stage through adulthood at 25°C, roughly 60-70 hours. RNAi constructs were obtained from available libraries (Source BioScience). The following clones were used for feeding: *atg-7* (sjj_M7.5), *lgg-1* (mv_C32D5.9), *par-1* (*sjj_H39E23.1)* and *unc-59* (mv_W09C5.2).

For RNAi experiments with *tsg-101* and *zif-1*, dsRNA was injected into the gonad of young adult worms (0.5-2 µg/µl *tsg-101*, 0.5 µg/µl *zif-1*) and their progeny was analyzed 20-26 hours later. The dsRNA was transcribed using T7 RNA Polymerase (ThermoFisher) from T7 PCRs of cDNA cloned into the RNAi plasmid L4440 [76]. The *tsg-101* dsRNA was designed according to the Cenix clone 49-f7 [77]. The *zif-1* dsRNA was cloned with the following primers: forward, 5′-CGTCAAGAACATCAGAGCATAGCA-3′; and reverse, 5′-CGGCAGTTTCTTTTTCAAGTTCTTC-3′. To determine the efficiency of *tsg-101* RNAi, embryos were screened for a mild delay in internalization of the AB midbody. Embryos were excluded from ZF1 degradation analysis if internalization of the AB midbody was not delayed, i.e. internalized at the six-cell stage. All RNAi experiments were performed by G. Fazeli.

2.4. Time-lapse imaging

Embryos were released from gravid adult worms with a scalpel blade in M9 buffer and then placed on a slide with an agarose pad. The coverslip was sealed with petroleum jelly to prevent embryos from drying out. For imaging, a Leica DM5500 wide-field fluorescence microscope with a HC PL APO 40X 1.3 NA oil objective lens was used together with a Leica DFC365 FX CCD camera controlled by LAS AF software. 16 „z-steps" (z-planes) with distance of 1.2 µm were recorded sequentially for GFP and mCherry every 20

seconds. All imaging was conducted at controlled room temperature. Time-lapse imaging of all strains other than WEH132 was conducted by G. Fazeli.

2.5. Analysis of time-lapse series

Time-lapse movies were analyzed using Imaris (Bitplane). First, the times of cell stages up to the 15-cell stage were recorded (the cell lineage of early *C. elegans* embryos is depicted in Fig. 2). Each cell stage was defined as the beginning of furrow ingression of the cell undergoing cytokinesis, a time point that can be easily determined. Thus, as shown in Fig. 3, the two-cell stage corresponds to the beginning of P0 furrow ingression, the three-cell stage corresponds to the beginning of AB furrow ingression, and so on.
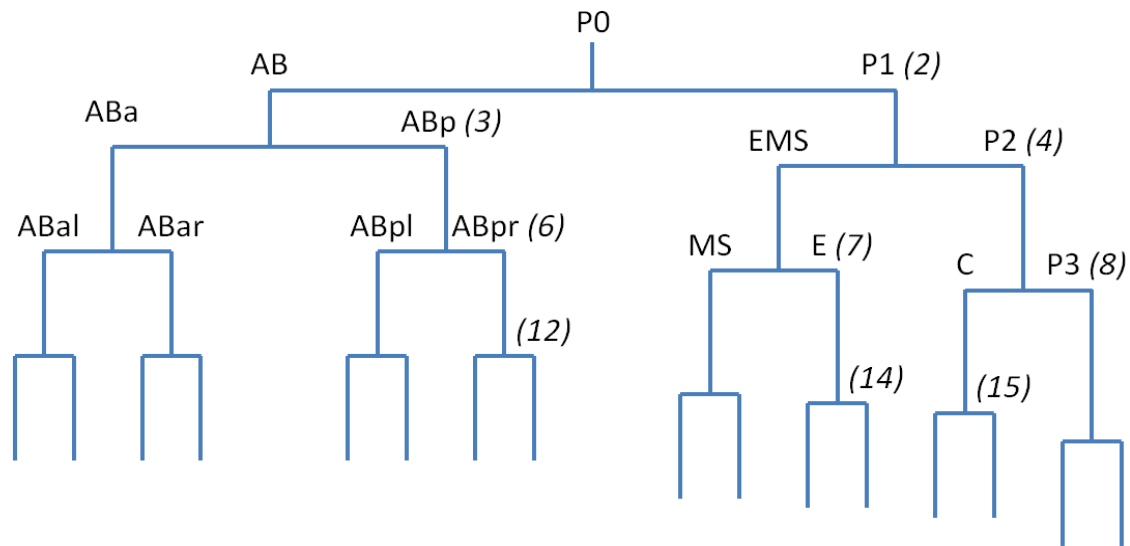
Fig. 2: Cell lineage of early *C. elegans* embryos. The numbers in parentheses indicate the cell stage. Adapted from [78].
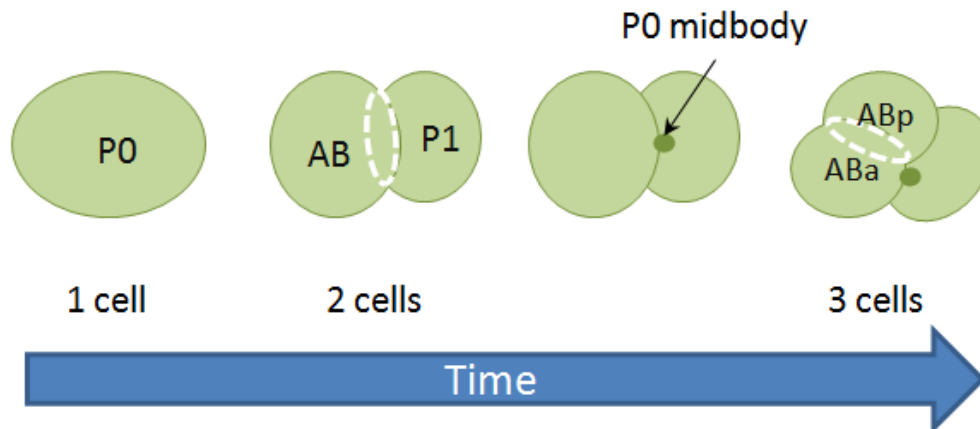
Fig. 3: Development of a *C. elegans* embryo up to the early three-cell stage (time not to scale).

When analyzing midbody remnant internalization, the time of internalization was defined as the first time frame at which the midbody moves away from the plasma membrane into the internalizing cell.

2.6. Cell cycle timing

First, the times required to reach specified developmental stages up to the 15-cell stage were determined in mutant and control embryos according to section 2.5. Next, to quantify the change in cell cycle time in mutants to the cell cycle time in controls, ratios between the required time in mutant and control embryos were computed. To avoid biasing the calculations on the AB lineage alone, a ratio for each of the following times was created: two cell divisions of the anterior AB lineage (from three- to six- and 12-cell stages), two cell divisions of the ventral EMS lineage (from four- to seven- and 14-cell stages) and two cell divisions of the posterior P2 lineage (from four- to eight- and 15-cell stages). The average of these six ratios then presented a total ratio.

2.7. Calculating the velocity of contractile ring closure

The diameter of the contractile ring was measured using ImageJ. For each time frame during ring closure, the diameter of the remaining aperture was determined by drawing a line in the z-plane with the largest ring diameter (Fig. 4). The results are reported in μm.
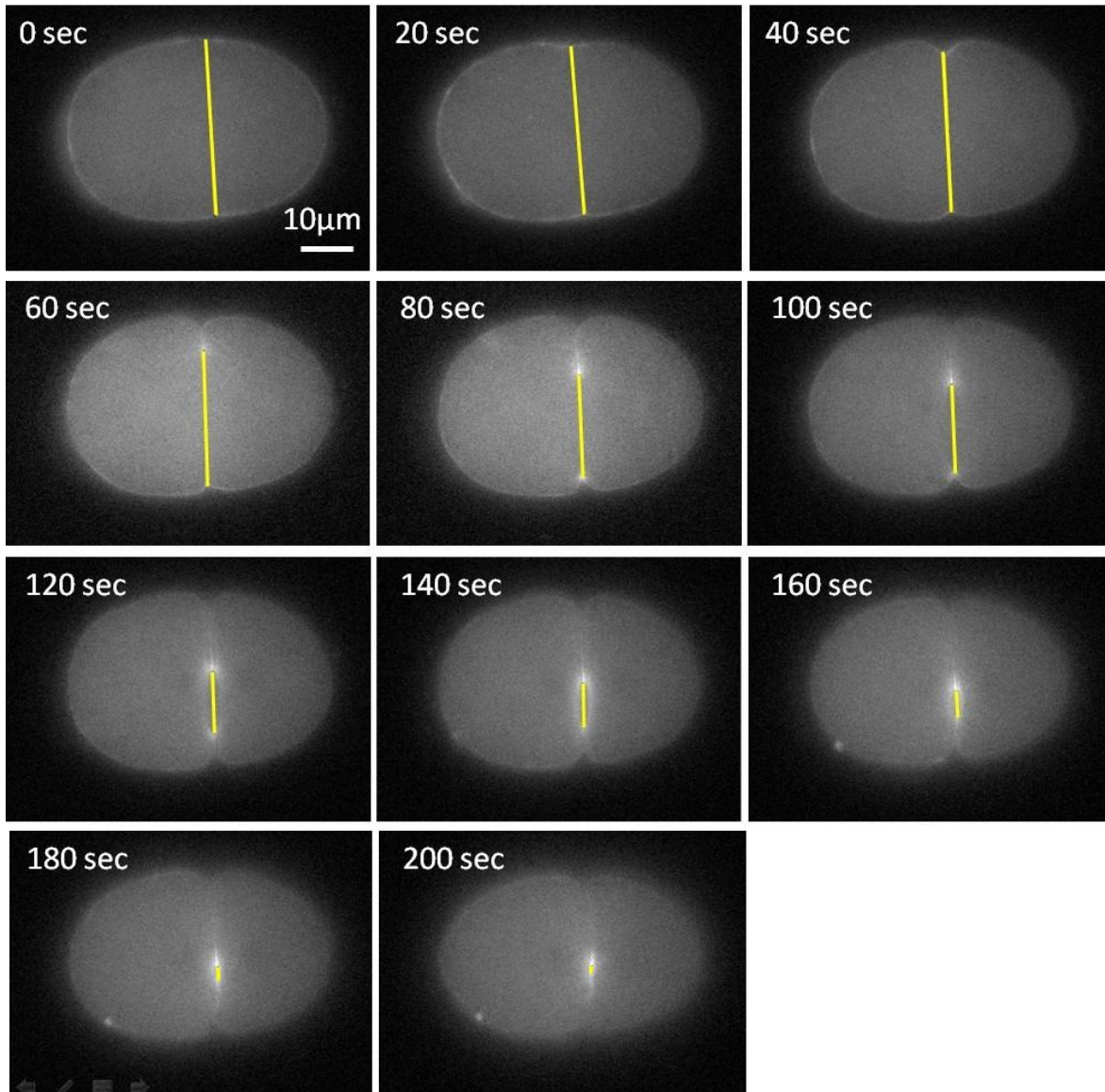
Fig. 4: Measurement of the ring aperture during the first embryonic cell division in a *C. elegans* embryo of the strain WEH51, expressing NMY-2::GFP::ZF1. For each time frame, the ring diameter was measured in one z-plane.

The analysis of 20 to 80% of ring closure was adapted from [79]. First, initial ring size (d_0) was measured in the last frame before furrow ingression. Next, a linear regression, modeling all time points within 20% and 80% of ring closure, was created for the AB cell division (Fig. 5). Using the linear regression, time points of 20% and 80% ring closure were calculated (t_{20} and t_{80}). The slope of the linear regression lines represents the speed between 20% and 80% of ring closure.

$$y = -10.632x + 40.092$$
$$R^2 = 0.999$$
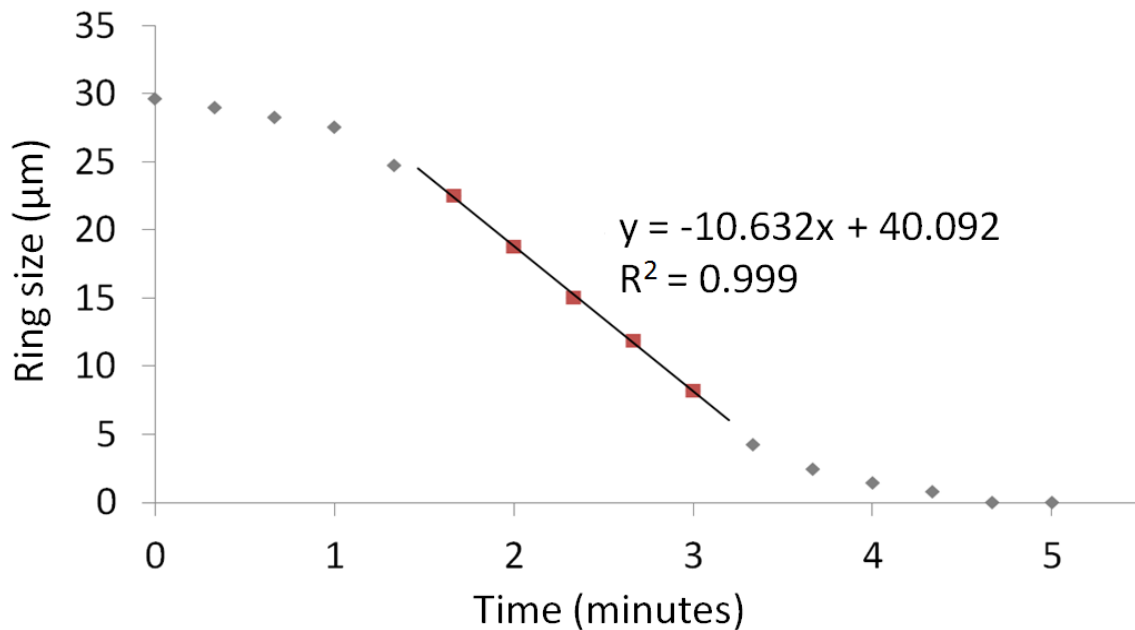
Fig. 5: Ring closure during AB cell division in a control embryo (WEH51). The values marked in red are within 20-80% of the initial ring size and were used to create a linear regression.

2.8. ZF1-mediated degradation of NMY-2::GFP::ZF1

The NMY-2::GFP::ZF1 reporter was used to reveal the release of midbodies or connections to the cytoplasm, as described in section 1.5. To determine when ZF1 degradation of this reporter begins, ZF1-disappearance in the cytoplasm of the AB daughter cells ABa and

ABp was examined by eye. The first time point when the fluorescence appeared to drop in the cytoplasm was noted. This time point served as a reference, indicating at what time a drop of fluorescence on midbodies was to be expected if they had a remaining connection to the ABa or ABp cytoplasm.

2.9. Quantification of fluorescence intensity of midbody reporters

Measurement of the fluorescence intensity of NMY-2::GFP::ZF1 and NMY-2::mCherry reporters was conducted on midbodies using ImageJ. Mean fluorescence intensity was measured in a circle with an area of 0.5 μm^2 in the z-plane where the midbody was brightest. Measurements were started a few minutes after visible closure of the contractile ring (Fig. 6), due to midbody compaction still taking place, and continued for every time frame until the end of the movie or until the midbody could no longer be distinguished from the cytoplasm. Embryos were excluded from the analysis when the P0 and AB midbodies were too close to each other to distinguish.

In addition to midbodies, mean fluorescence intensity of the first polar body was measured in a circle of the same size for every time frame of the time-lapse movie (Fig. 7). Since the first polar body is extruded very early during embryonic development and is trapped in the eggshell [80], these measurements serve as an internal control to account for bleaching due to fluorescent light [81]. Using OriginPro (OriginLab), the measured values from the polar body were fit to an exponential decay curve (Fig. 8). When the polar body measurements did not fit an exponential decay function, the embryo was excluded from midbody analysis.
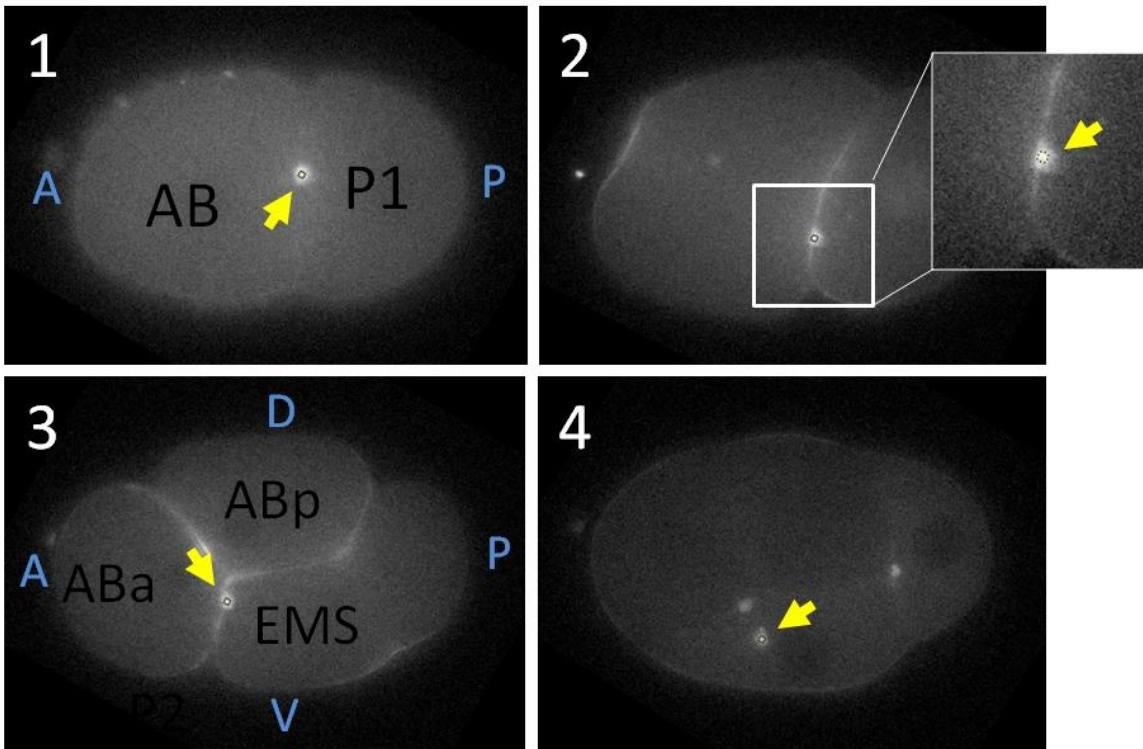
Fig. 6: Fluorescence measurement of the P0 midbody (yellow arrow) in a representative WEH51 embryo expressing the NMY-2::GFP::ZF1 reporter. Only one z-plane is displayed. Fluorescence was measured in the z-plane where the midbody appeared brightest. The early (1) and late (2) two-cell stage and the early (3) and late (4) four-cell stage are depicted. At the late four-cell stage, the P0 midbody has internalized into the EMS cell. Axes are as labeled in blue letters (A = anterior, P = posterior, D = dorsal, V = ventral).
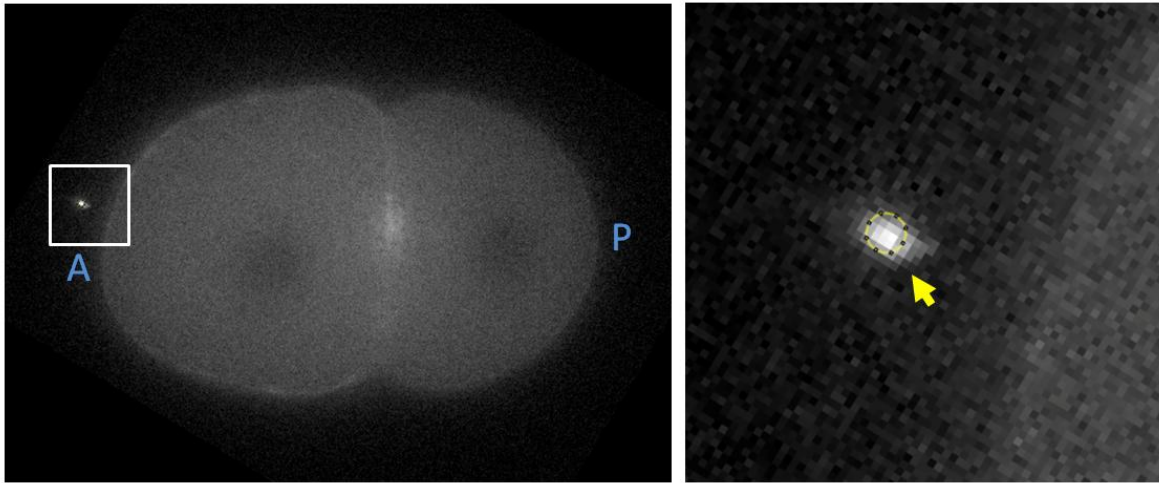
Fig. 7: Fluorescence measurement of the first polar body (yellow arrow) in a representative two-cell *C. elegans* embryo of the strain WEH51, expressing the NMY-2::GFP::ZF1 reporter. The anterior-posterior axis is labeled in blue letters (A = anterior, P = posterior).
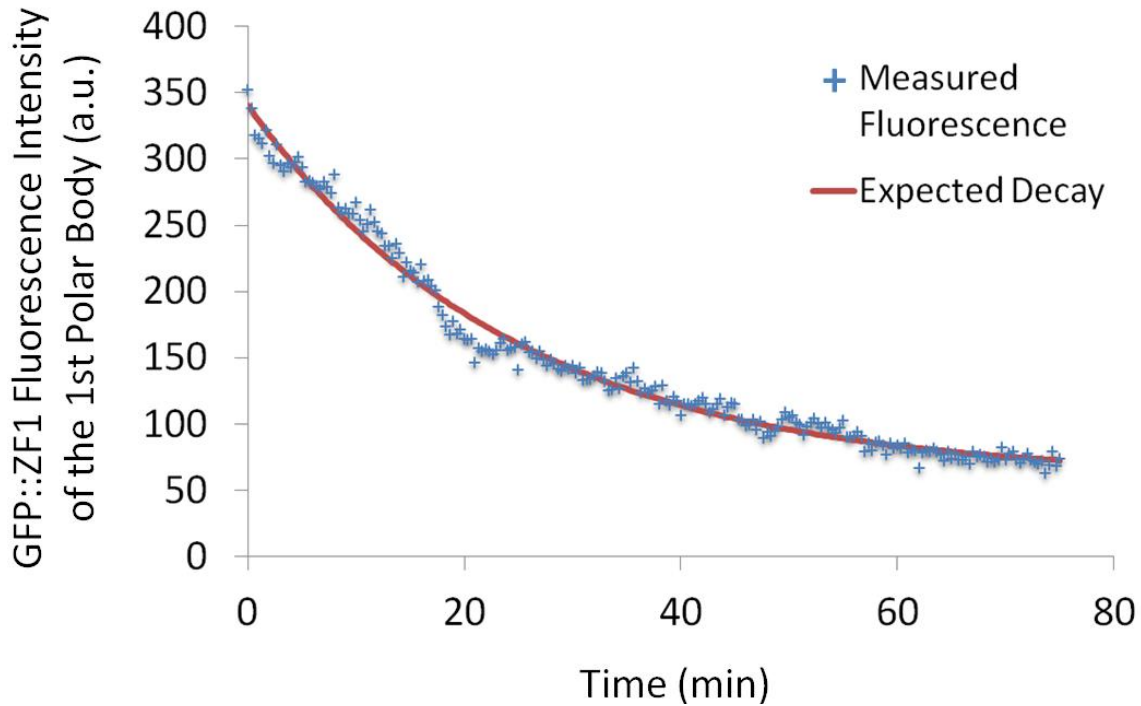
Fig. 8: Measured GFP fluorescence of the first polar body in a representative WEH51 embryo expressing NMY-2::GFP::ZF1. The function of the exponential decay curve was used to normalize midbody fluorescence.

Midbody fluorescence was normalized with the help of the exponential decay function fit to the polar body measurements. Normalized midbody fluorescence N(t) was defined as the ratio of measured fluorescence of the midbody to the calculated fluorescence of the polar body according to the exponential decay function at time t:

$$Normalized\ fluorescence\ N(t) = \frac{Brightness\ of\ Midbody\ (t)}{Predicted\ brightness\ of\ Polar\ body\ (t)}$$

Next, to allow comparisons between samples, fluorescence intensity was fit to values between 0 and 1:

$$Fitted\ fluorescence\ F(t) = \frac{N(t) - Minimum}{Maximum - Minimum}$$

For P0 midbody measurements, the maximum was defined as the highest value of normalized midbody fluorescence starting at the four-cell stage. For the AB midbody, the maximum was defined to be the fluorescence intensity halfway in-between the four- and six-cell stages, hence $N(\frac{t6+t4}{2})$. This time point was 5 minutes after the four-cell stage in control embryos (WEH51; n=12), which is in accordance with the beginning of ZF1-degradation in ABa and ABp (see section 2.8).

The minimum was defined as the last measurement of the disappearing midbody. However, when the midbody was not degraded within the time boundaries given below, a cytoplasmic background measurement at the indicated time was used as the minimum. For background measurements, ten measurements of the brightness of the cytoplasm in daughter cells of AB were conducted at a defined time point after the four-cell stage, and their normalized mean was then set to be the minimum.

Time boundary values were based on the time that the P0 and AB midbodies usually disappeared in control embryos. Time boundary values for NMY-2 reporters were defined as following:

mCherry: When the P0 midbody had not disappeared by 45 minutes after the four-cell stage or the AB midbody had not disappeared by 70 minutes after the six-cell stage, then cytoplasm measurements at 45 minutes after the four-cell stage were used to calculate the minimum.

GFP: When the P0 midbody had not disappeared by 30 minutes after the four-cell stage or the AB midbody had not disappeared by 40 minutes after the six-cell stage, then cytoplasm measurements at 30 minutes after the four-cell stage were used to calculate the minimum.

2.10.   Extrapolation of midbody disappearance

When calculating the average time of midbody disappearance or the statistical difference between mutants and controls, we included midbodies that did not disappear before the end of time-lapse imaging by extrapolating their time of disappearance. Disappearance was set to 0.33 minutes after the last time frame recorded. Since the time lapse series were collected every 20 sec, this was the first possible time point when the midbody could have theoretically disappeared.

2.11.   Quantification of dorsoventral movement of the P0 midbody

The time points at which the position of the P0 midbody was to be measured, as previously performed in [61], were determined using Imaris. The first time point, t_0, was set to the time of NMBD (nuclear membrane breakdown). The breakdown of the nuclear membrane in prometaphase allows cytosolic GFP to enter the previously dark nucleus, resulting in a nuclear flash. The second time point, t_2, was defined as the beginning of ring contraction in the AB-cell division.

Next, ImageJ was used to stack all z-planes ("z-stack") at the first time frame (t_0). The embryo was then rotated until a vertical line could be drawn on the plane between the AB cell and the P1 cell. This line measured the width of the embryo from its dorsal to its ventral side. If necessary, the line was moved laterally to ensure that it would cut directly through the brightest point of the P0 midbody (Fig. 9). The position of the maximum of fluorescence on this line equaled the position of the midbody in respect to the dorsal side of the embryo. The same measurement was done for t_2 and also for 40 seconds after t_2 (t_3).
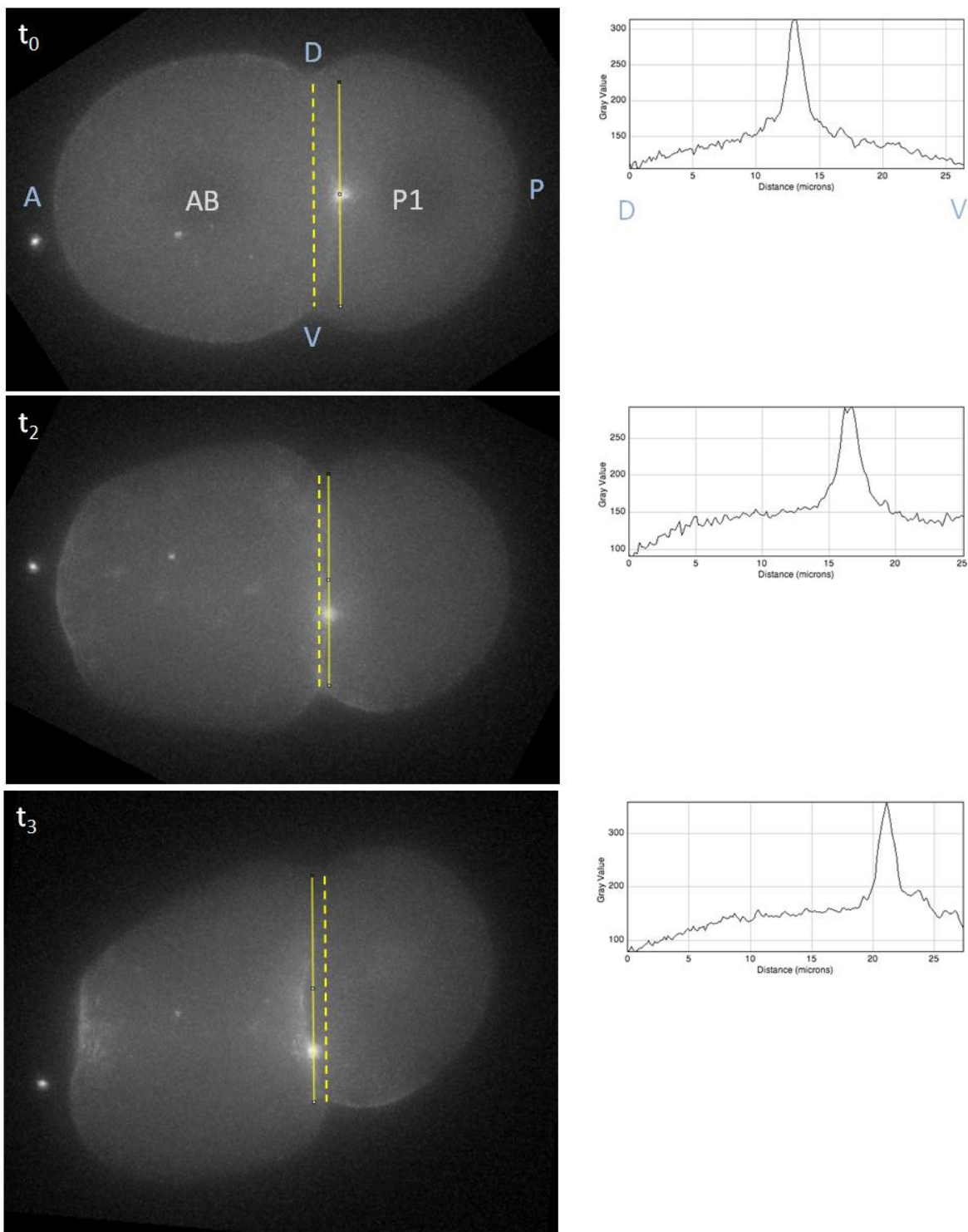
Fig. 9: Measurement of the P0 midbody position on the dorsoventral axis at t_0, t_2 and t_3 in a representative *C. elegans* WEH51 embryo, expressing a NMY-2::GFP::ZF1 reporter. First,

the dashed line was drawn and then moved horizontally to cut through the brightest point of the midbody (yellow line). By analyzing the plot profile of the yellow line (right panels), movement of the midbody was quantified. Axes are as labeled in blue letters (A = anterior, P = posterior, D = dorsal, V = ventral).

2.12. Image manipulation

The images of the embryos displayed in materials and methods were exported from ImageJ and later rotated with Microsoft Office Picture Manager for better demonstration. The embryo displayed in the results was rotated in Imaris. For clarity, it was colorized in cyan and yellow and the intensity was adjusted with the help of Adobe Photoshop. Only one z-plane is displayed in all images.

2.13. Statistical evaluation

For all comparisons presented in this study, statistical significance was tested using a one-tailed Student's t-test for samples of unequal variance. For multiple comparisons, the Bonferroni correction was applied.

In the text, mean ± standard deviations are reported. In graphs, error bars represent standard deviations (SD) or standard errors of the mean (SEM).

3. Results

3.1. The role of UNC-59/Septin in abscission and midbody fate in *C. elegans*

Our first aim was to determine the role of septins during abscission with the help of the ZF1-degradation technique in *C. elegans*. In septin mutants, the cytoplasm of sister cells takes 2-3 minutes longer to separate during the first embryonic division than control embryos [42]. Therefore, we expected to observe a delay in abscission in septin mutants, which could also affect internalization of embryonic midbodies.

We created a new strain, WEH132, by crossing the *unc-59*/septin mutant strain CB261 with a reporter strain WEH51 (see section 2.2). The new strain, WEH132, is homozygous for two fluorescent proteins (mCh::PH and NMY-2::GFP::ZF1) as well as the septin mutation. The ZF1 degron and degradation assay enabled us to detect connections to the cytoplasm and they are explained in sections 1.5 and 2.8.

For both control (WEH51) and mutant embryos (WEH132), time lapse imaging of the first cell divisions was conducted (roughly 60 minutes). These data sets were then annotated in regard to internalization timing and pattern of the first three midbodies (section 3.1.1), including the so-called bridge phenotype (section 3.1.2). We also analyzed the fluorescence intensity of the first and second midbody after their formation in order to test their accessibility to the cytoplasm (section 3.1.3) and compared the results to another abscission mutant (section 3.1.4).

3.1.1. Characterizing internalization of the first three midbodies in septin mutants

3.1.1.1. Control

First, data was collected for the fluorescent reporter strain WEH51, which served as our control. For this strain, time lapse imaging had already been carried out by G. Fazeli in the lab. We expected to see midbodies internalized with a stereotypical timing and an asymmetric pattern of inheritance, as reported with other fluorescent midbody strains [52,

61]. We therefore analyzed the time of internalization and the identity of the cell that internalizes the midbody for the first three embryonic midbodies in WEH51.

Time of internalization: The P0 midbody was internalized 5 ± 6 minutes after the four-cell stage. All of the P0 midbodies were internalized by the end of the eight-cell stage (n=18). The AB midbody was internalized 5 ± 6 minutes after the six-cell stage (n=17/18). The midbodies were normally taken up between the six- and 12-cell stage (n=17), while one midbody did not internalize by the 12-cell stage. On average, the P1 midbody was internalized 2 ± 3 minutes after the six-cell stage. All P1 midbodies were internalized within the four- to eight-cell stage (n=18). In conclusion, a stereotypical timing of internalization was observed in WEH51 (Table 2), similar to other midbody reporter strains [52, 61]. While the P0 midbody was internalized shortly after the four-cell stage, the AB and P1 midbodies were internalized shortly after the six-cell stage.

Internalizing cell: The P0 midbody was mainly internalized by EMS (n=15/18, including four midbodies that were internalized on the EMS-side of P1). We also observed internalization of the P0 midbody by AB and its daughter cells (n=3/18). Internalization of the AB midbody also mainly took place into EMS and its daughter cell MS (n=16/18), with the exception of one midbody that was internalized by a daughter cell of AB and one midbody that did not internalize and lost GFP fluorescence by the 12-cell stage. The P1 midbody was exclusively taken up by P2 and its daughter cell P3 (n=18). In conclusion, a stereotypical pattern of internalization is observed in WEH51 (Table 3), similar to other midbody reporter strains [52, 61]. The P0 and AB midbodies were primarily taken up by EMS and its daughter cell MS, whereas the P1 midbody was taken up by P2 and its daughter cell P3.

3.1.1.2.   unc-59/Septin

Next, I analyzed the UNC-59-deficient strain WEH132 in respect to midbody internalization.

Time of internalization: On average, the P0 midbody was internalized 12 ± 9 minutes after the four-cell stage (n=6), versus 5 ± 6 minutes in the control (n=18), thus with a significant delay (p<0.05). The P0 midbodies were internalized between the four-and 12-cell stages, whereas all P0 midbodies had been internalized by the end of the eight-cell stage in control embryos. The AB midbody was internalized 13 ± 4 minutes after the six-cell stage (n=7), also significantly delayed in comparison to the control (p<0.01). Midbodies were taken up between the eight- and 12-cell stage. Lastly, the P1 Midbody was internalized 6 ± 3 minutes after the six-cell stage, which was also significantly later than in the control (p<0.01). The P1 midbodies were internalized between the six- and eight-cell stage (n=8) (Table 2). Thus, septin mutants displayed a mild, but significant delay in internalization times of the first three midbodies.

Internalizing cell: The P0 midbody was taken up by EMS and its daughter cell MS in all *unc-59* mutant embryos (n=8), similar to control group. The AB midbody was internalized by daughter cells of EMS (n=6) and AB (n=1), similar to the control except for one AB midbody being internalized by E rather than MS. Similarly, the P1 midbody was mainly internalized by P2 and its daughter cells (n=6/8, Table 3). Altogether, these results showed no evidence of difference in internalization pattern in *unc-59* mutants versus the control.

3.1.1.3. *unc-59* with *unc-59* RNAi

Since it had been previously reported that septins are required for internalization of the P0 midbody into a daughter cell [42], we had expected to see a stronger defect in internalization timing of all three midbodies. Considering that *unc-59(e261)* is a missense mutation, it is possible that some septin function remained. Therefore, we additionally treated the WEH132 strain with *unc-59* or *unc-61* RNAi with the goal of creating a stronger loss-of-function.

The RNAi treatment caused sterility in both *unc-59* and *unc-61* RNAi-treated worms, implying a more severe effect compared to mutants. For example, only two of 26 WEH132 worms treated with *unc-61* RNAi became gravid adults. This made isolating embryos more

difficult and we were only able to perform time-lapse imaging on very few embryos. Thus, we chose to focus our analysis on WEH132 worms treated with *unc-59* RNAi.

Time of internalization: The P0 midbody in *unc-59* mutants treated with *unc-59* RNAi was internalized 21 ± 14 minutes after the four-cell stage (n=7), significantly later than in control embryos (6 ± 5 minutes after the four-cell stage, n=18) (p<0.05). The P0 midbodies were internalized between the four- and 24-cell stages, taking place at later cell stages than in the control. For AB midbodies, the time of internalization averaged 18 ± 13 minutes after the six-cell stage (n=5/7), compared to 5 ± 6 minutes after the six-cell stage in the control (n=17), this also being a statistically significant delay (p<0.05). Two of the seven AB midbodies did not internalize before ZF1 fluorescence disappeared completely, hindering further tracking of the midbody. Thus, it is unknown whether they fail to internalize or do internalize with a delay, after having lost fluorescence due to ZF1 degradation. Lastly, internalization of the P1 midbody took place 12 ± 12 minutes after the six-cell stage. This is a significant delay compared to the control (p<0.05). The P1 midbodies were internalized between the eight- and 24-cell stage, hence also at later cell stages than in control (n=8) (Fig. 10, Table 2 and 4). In summary, all three midbodies were observed to internalize with a significant delay in *unc-59* mutants treated with RNAi, and in two of the AB midbodies ZF1 fluorescence disappeared completely before the midbodies internalized.

Comparing the internalization times of *unc-59* mutants treated with RNAi to mutants without RNAi, no statistically significant difference was given (p>0.05). However, seeing the RNAi to cause a stronger effect and taking in account the low amount of embryos and the increase in variance of values for the mutants with RNAi, we concluded that the strain additionally treated with RNAi has a stronger delay in internalization times of the first three midbodies in *C. elegans* embryos, which may imply a stronger defect in abscission (Table 2, Fig. 10).

Internalizing cell: The P0 midbody was mostly taken up by EMS and its daughter cells (n=6/7), but also by a daughter cell of AB (n=1/7). The AB midbodies that were internalized were exclusively taken up by EMS and its daughter cell MS (n=5). The P1

29

midbody was not only internalized by P2 (n=3/7), but also by the further anterior cells AB (n=1/7) and MS (n=3/7) (Table 3). Thus, the pattern of internalization only differed for the P1 midbody, as it was taken up by further anterior cells than in the control.
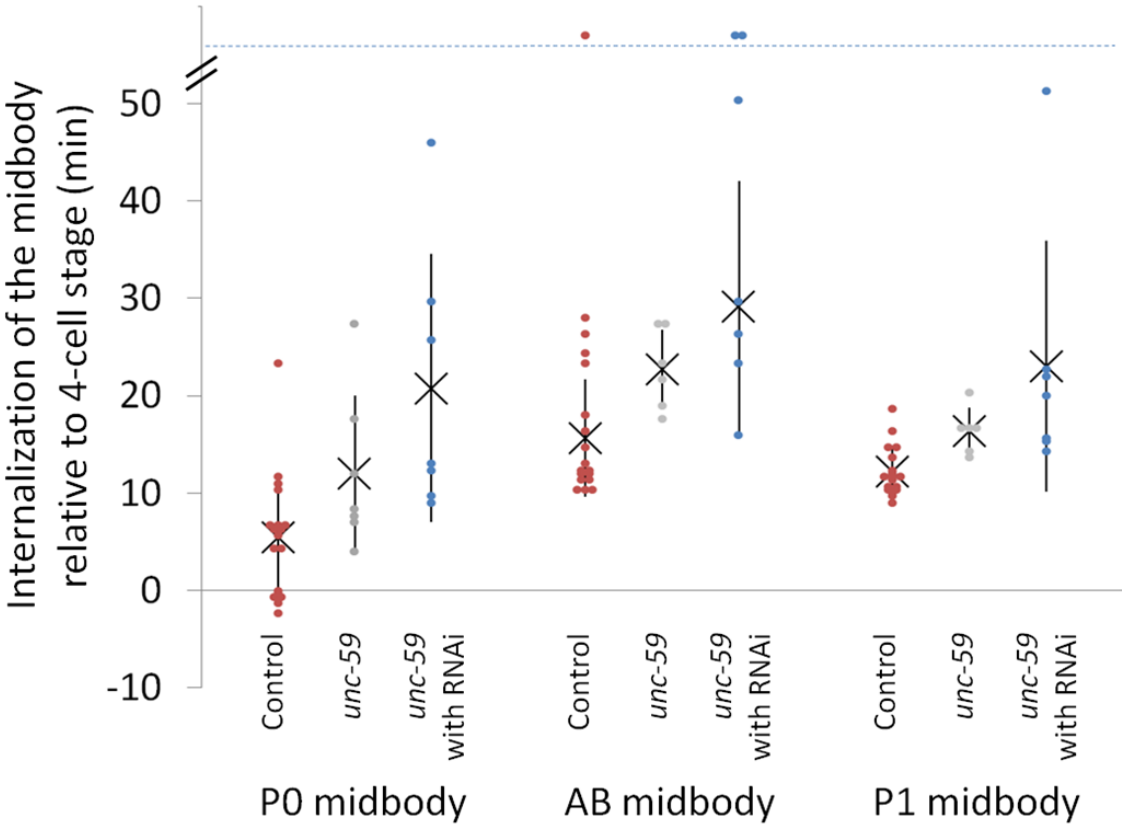
Fig. 10: Time of internalization of the first three midbodies in control, *unc-59* and *unc-59* with *unc-59* RNAi. Time is given relative to the four-cell stage for all three midbodies. Points above the dashed line represent the midbodies that did not internalize by the end of recorded time-lapse series (45-75 minutes after the four-cell stage). Error bars indicate the standard deviation.

	Control	*unc-59*	*unc-59* with RNAi
P0 midbody	5 ± 6 (n=18)	12 ± 8* (n=7)	21 ± 14* (n=7)
AB midbody	5 ± 6 (n=17)	13 ± 4** (n=7)	18 ± 13* (n=5)
P1 midbody	2 ± 3 (n=18)	6 ± 3** (n=7)	12 ± 12* (n=7)

Table 2: Time of internalization of the first three midbodies (mean $\pm$ SD). The time is expressed in minutes relative to the four-cell stage for the P0 midbody or relative to the six-cell stage for the AB and P1 midbodies. Significant differences to the control are marked (*p<0.05 and **p<0.01).

P0 midbody

Strain	n	2-cell		4-cell			8-cell or later					No int.
		AB	P1	ABx	EMS	P2	ABxx	MS	E	C	P3	-
WEH51	18	-	22%	11%	61%	-	6%	-	-	-	-	-
WEH132	8	-	-	-	63%	-	-	38%	-	-	-	-
WEH132 + RNAi	7	-	-	14%	43%	-	-	43%	-	-	-	-

AB midbody

Strain	n	2-cell		4-cell			8-cell or later					No int.
		AB	P1	ABx	EMS	P2	ABxx	MS	E	C	P3	-
WEH51	18	-	-	-	50%	-	6%	39%	-	-	-	6%
WEH132	7	-	-	14%	-	-	-	71%	14%	-	-	-
WEH132 + RNAi	7	-	-	-	14%	-	-	57%	-	-	-	29%

P1 midbody

Strain	n	2-cell		4-cell			8-cell or later					No int.
		AB	P1	ABx	EMS	P2	ABxx	MS	E	C	P3	-
WEH51	18	-	-	-	-	94%	-	-	-	-	6%	-
WEH132	8	-	-	13%	-	63%	13%	-	-	13%	-	-
WEH132 + RNAi	7	-	-	-	-	43%	14%	-	43%	-	-	-

Table 3: Cell stage at time of internalization and cells that internalize each of the first three embryonic midbodies in control, *unc-59* and *unc-59* with RNAi. "No int." means internalization did not occur before the end of the recorded time-lapse series (45-75 minutes after the four-cell stage). In case of the septin mutants with RNAi "no int." means that the midbody was not seen to internalize before its fluorescence disappeared due to ZF1 degradation. The displayed numbers are rounded and therefore may not add up to 100%.

3.1.2. „Bridge" phenotype of the P0 midbody in *unc-59* with *unc-59* RNAi

We observed an interesting novel phenotype for the P0 midbodies in *unc-59* with *unc-59* RNAi that could explain the observed delay in internalization. In control embryos, the P0 midbody changes its position within one time-frame (20 seconds) from being seen on the membrane to floating freely in the cytoplasm of the internalizing cell. In our septin mutants, however, the membrane wrapping the P0 midbody extended into the cytoplasm of the EMS cell that would later internalize it while still being attached to the plasma membrane (Fig. 11). This phenotype was named the "bridge" phenotype, as a bridge from the previous position of the midbody on the membrane to the new position in the cytoplasm remains (Fig. 12).
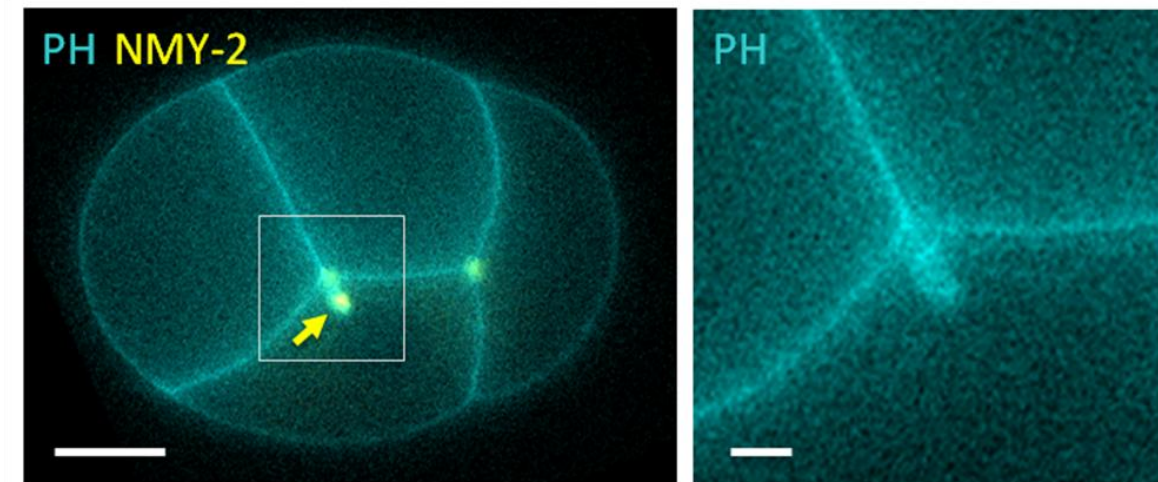
Fig. 11: A representative WEH132 embryo expressing mCh::PH(PLC1d1) on membranes (cyan) and NMY-2::GFP::ZF1, which labels midbodies (yellow), treated with *unc-59* RNAi. The membrane wrapping the P0 midbody (arrow) extends into EMS but remains connected to the AB cells with the cell membrane. The embryo is shown at the late four-cell stage. The left panel shows a merged image (scale bar measures 10 µm) and the right panel shows mCh::PH alone at higher magnification (scale bar measures 2 µm).
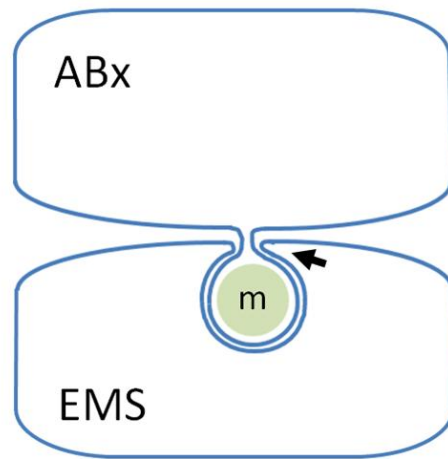
Fig. 12: Hypothetical model of the bridge phenotype in septin mutants. We predict that abscission defects leave a connection to at least one daughter cell, corresponding to the observed bridge (marked with arrow). This hinders the completion of internalization of the midbody (m) and thus restricting its movement in the cytoplasm of the EMS cell.

The bridge phenotype of the first midbody was found in four out of seven *unc-59* mutant embryos treated with *unc-59* RNAi. The bridge appeared 3 ± 3 minutes after the four-cell stage (n=4). Internalization was defined to be effective only upon the midbody being disconnected from the membrane and released freely into the cytoplasm. In all four embryos with the bridge phenotype, the P0 midbodies were released for definite internalization at 28 ± 15 minutes after the four-cell stage, showing a significant delay in comparison to the control ($p<0.05$). In contrast to the P0 midbody, the AB and P1 midbodies did not show a bridge phenotype.

This bridge phenotype of the P0 midbody, observed for the first time in *unc-59* mutant embryos treated with *unc-59* RNAi, offered new insights into the mechanism of abscission and midbody internalization in early *C. elegans* embryos, which will be discussed later.

3.1.3. Early loss of ZF1 fluorescence on the AB midbody in *unc-59*

To gain further understanding of abscission and the release of the midbody into the extracellular space, we used the ZF1-mediated degradation technique, as introduced in section 1.5, to test whether midbodies were accessible to the cytoplasm.

The start of ZF1-mediated degradation of the NMY-2::GFP::ZF1 reporter in the daughter cells of AB was determined by observing by eye at what time GFP fluorescence starts to diminish in the cytoplasm of ABa and ABp. In both control (n=8) and septin mutants (n=7), it begins 5 ± 1 minutes after the four-cell stage (6 ± 1 minutes before the six-cell stage), as shown in Fig. 13.
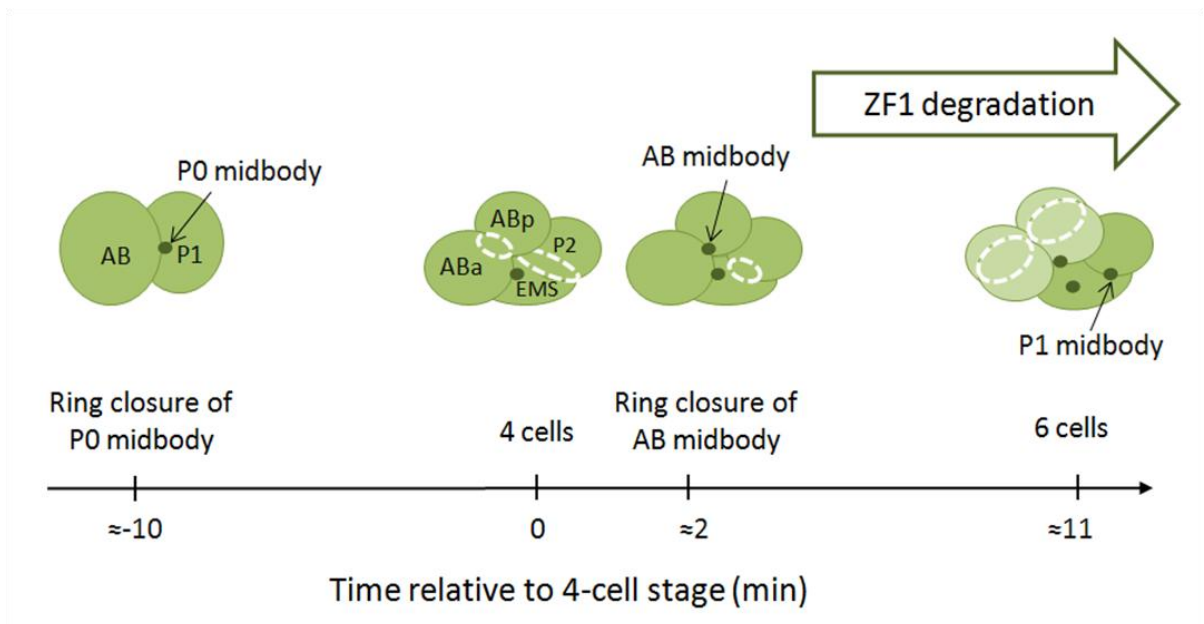
Fig. 13: Formation of the first embryonic midbodies during development of the *C. elegans* embryo. The white dashed ovals depict cytokinetic rings and green dots are midbody remnants. NMY-2::GFP::ZF1 degradation starts in the anterior and dorsal AB cells (ABa and ABp), a few minutes after apparent ring closure of the AB midbody.

At the time of P0 midbody remnant formation and abscission, about 10 minutes before the four-cell stage, NMY-2::GFP::ZF1 degradation has not yet started. It starts about 15 minutes later. Therefore, we expected to find stable GFP fluorescence intensity for the P0 midbody at least until the onset of ZF1 degradation (5 minutes after the four-cell stage), in control embryos (measured by M. Trinkwalder) and in *unc-59(e261)* mutants treated with *unc-59* RNAi. This was confirmed by the results of NMY-2::GFP::ZF1 fluorescence measurements and analysis of the P0 midbody in these mutants. As shown in Fig. 14, no significant difference in fluorescence intensity of the P0 midbody was measured before ~5 minutes after the four-cell stage ($p>0.05$), due to NMY-2::GFP::ZF1 degradation having not yet begun. There was also no significant loss in GFP fluorescence after ZF1 degradation began in the cytoplasm (starting at 5 minutes after the four-cell stage). These results show that by the time ZF1 degradation in ABa and ABp begins, the midbody is isolated from the ABx cytoplasm by abscission. Furthermore, the ZF1-mediated degradation technique reveals that abscission has occurred in septin mutants by ~15 minutes after apparent P0 ring closure.
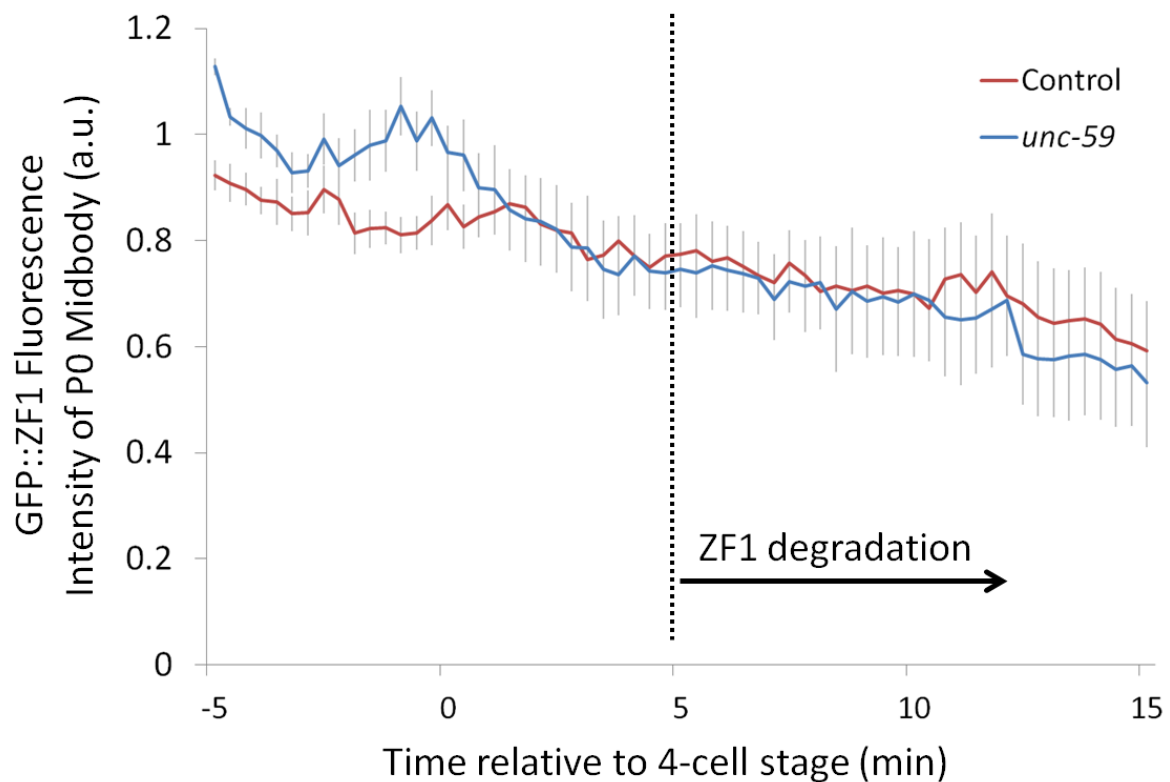
Fig. 14: NMY-2::GFP::ZF1 fluorescence remained constant on P0 midbodies in *unc-59* mutants treated with *unc-59* RNAi (n=5), similar to controls (n=9). NMY-2::GFP::ZF1 degradation begins in ABa and ABp five minutes after the four-cell stage, depicted by the dotted line. Error bars indicate SEM.

However, closure of the second midbody ring, which forms the AB midbody remnant, takes place a few minutes before the onset of NMY-2::GFP::ZF1 degradation in ABa and ABp (Fig. 13). Therefore, the ZF1 method can be used to find out how long the AB midbody remains in contact with the cytoplasm of at least one of the AB daughter cells in septin mutants.

In control embryos (analyzed by M. Trinkwalder), NMY-2::GFP::ZF1 fluorescence on the AB midbody remained steady while the midbody was at the cell surface (Fig. 15 and 17). This implies that NMY-2::GFP::ZF1 on the midbody was protected from degradation due

to bilateral abscission and extracellular release. GFP fluorescence was also steady for ~5 minutes after internalization (internalization occurring 5 ± 6 minutes after the six-cell stage, see Table 2), demonstrating that the phagosome also protects the midbody from ZF1 degradation after internalization.
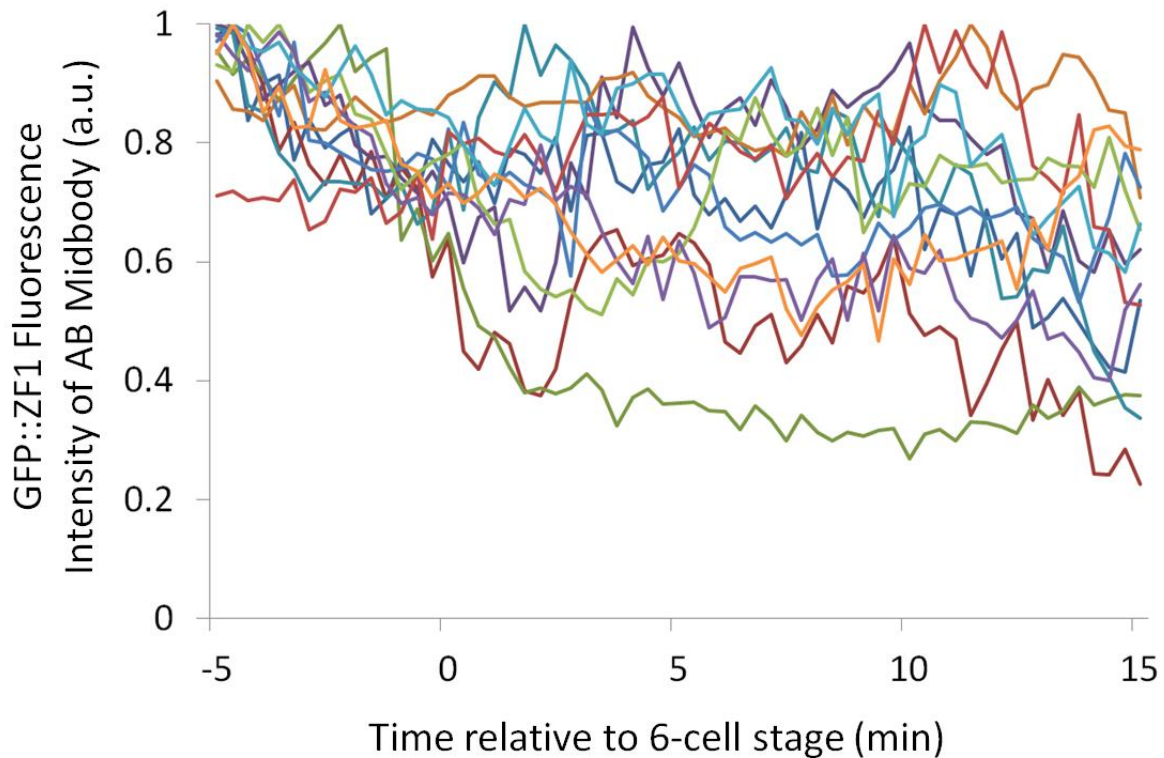
Fig. 15: NMY-2::GFP::ZF1 fluorescence is steady on AB midbodies in control embryos. Fluorescent intensity on the midbody was measured by M. Trinkwalder and each embryo was plotted in a different color (n=12). ZF1 degradation begins ~6 minutes before the six-cell stage.

In contrast to control embryos, the AB midbody showed an early loss of NMY-2::GFP::ZF1 fluorescence in septin mutants. NMY-2::GFP::ZF1 fluorescence on the AB midbody diminished rapidly after the onset of ZF1 degradation in septin mutants, while the

midbody was at the cell surface (Fig. 16). NMY-2::GFP::ZF1 fluorescence intensity of the AB midbody was significantly lower in *unc-59* than in control embryos starting at one minute before the six-cell stage (Fig. 17, p<0.01). This continuous drop of fluorescence was observed in all AB midbodies. The rapid decrease of fluorescence on the AB midbody in septin mutants suggests that a cytoplasmic bridge remains open between the AB midbody and one or both of the AB daughter cells for at least five minutes after ZF1 degradation initiates.
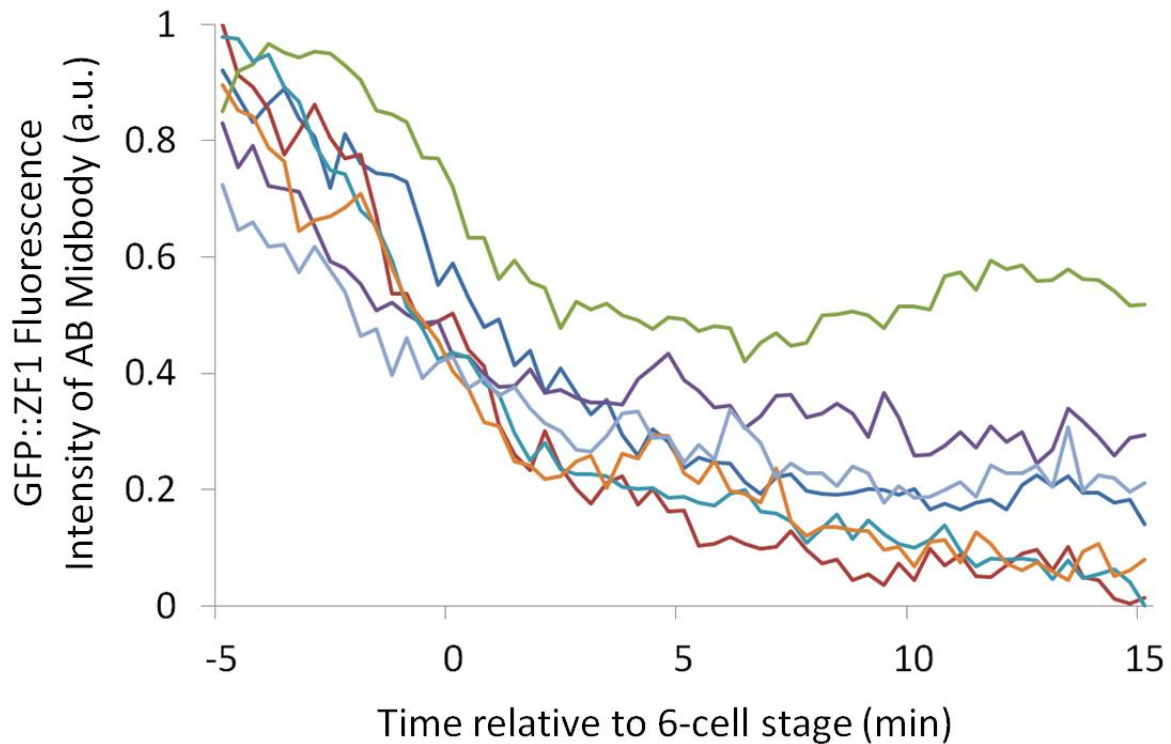
Fig. 16: NMY-2::GFP::ZF1 fluorescence drops rapidly on AB midbodies in septin mutants. Intensity of NMY-2::GFP::ZF1 fluorescence on the AB midbodies in *unc-59* with *unc-59* RNAi (n=6). Each embryo was plotted in a different color. ZF1 degradation begins ~6 minutes before the six-cell stage.
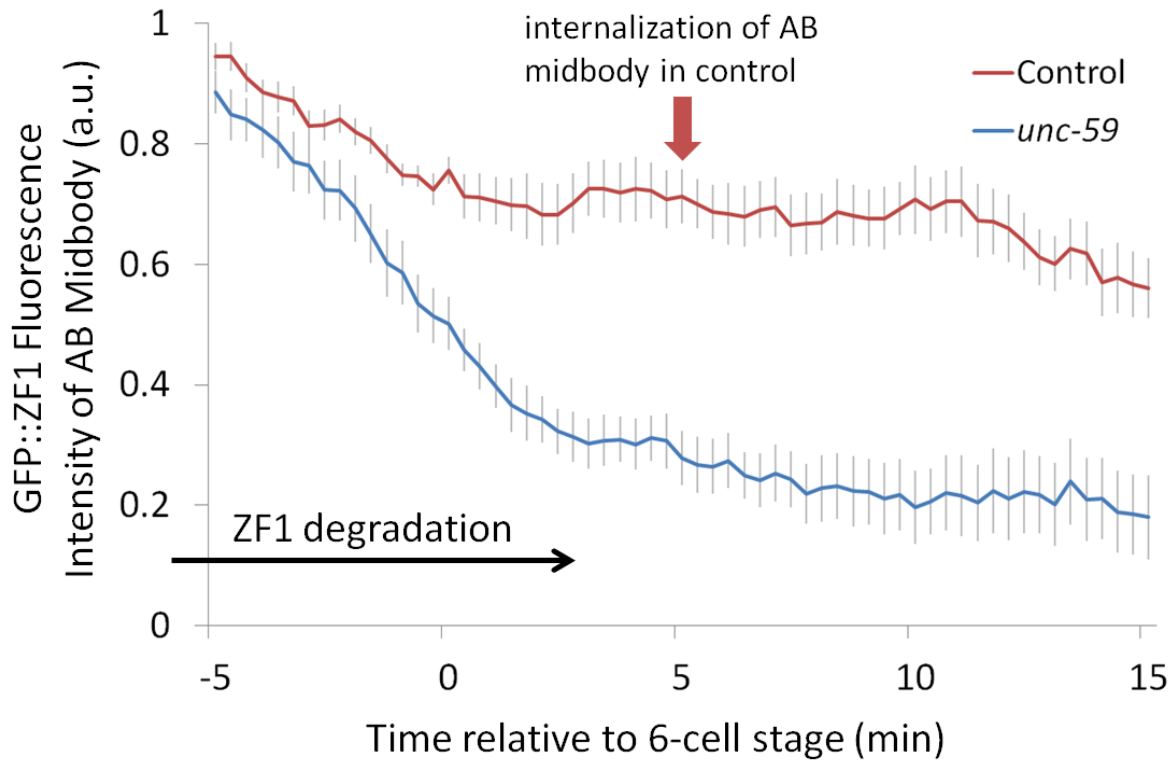
Fig. 17: Comparison of control embryos with septin mutants. Average intensity of ZF1 fluorescence on the AB midbody is plotted for septin mutants (n=6, blue) versus control embryos (n=12, red). ZF1 degradation begins ~6 minutes before the six-cell stage. Control midbodies internalized ~5 min after the six-cell stage, while septin midbodies were internalized ~18 min after six-cell stage (see Table 2). Error bars indicate SEM.

In conclusion, these findings show that the NMY-2::GFP::ZF1 of the midbody remnant is degradable and that the ZF1-mediated technique is a sensitive test for abscission defects. They also emphasize that in control embryos, abscission takes place on both sides of the midbody and the midbody is released into the extracellular space, protecting the midbody from the process of NMY-2::GFP::ZF1 degradation. In contrast, in septin mutants, ZF1 marked NMY-2 can be degraded through the remaining connection to the cytoplasm. In these septin mutants, abscission is delayed by at least three minutes, which results in significant delays in midbody internalization.

3.1.4. *tsg-101* RNAi and *tsg-101 zif-1* double RNAi

To confirm the findings in septin-depleted embryos, we next tested whether other abscission mutants act similarly in the ZF1 degradation assay. The ESCRT-I component TSG-101 is involved in late stages of abscission and has also been shown to be required for timely internalization of the midbody [42]. Therefore, the WEH51 strain expressing NMY-2::GFP::ZF1 was treated with RNAi for TSG-101. Time-lapse imaging was conducted by G. Fazeli and I measured NMY-2::GFP::ZF1 fluorescence intensity. The focus was set on measuring the AB midbody, as it is the remnant that forms right before ZF1-degradation begins in ABa and ABp.
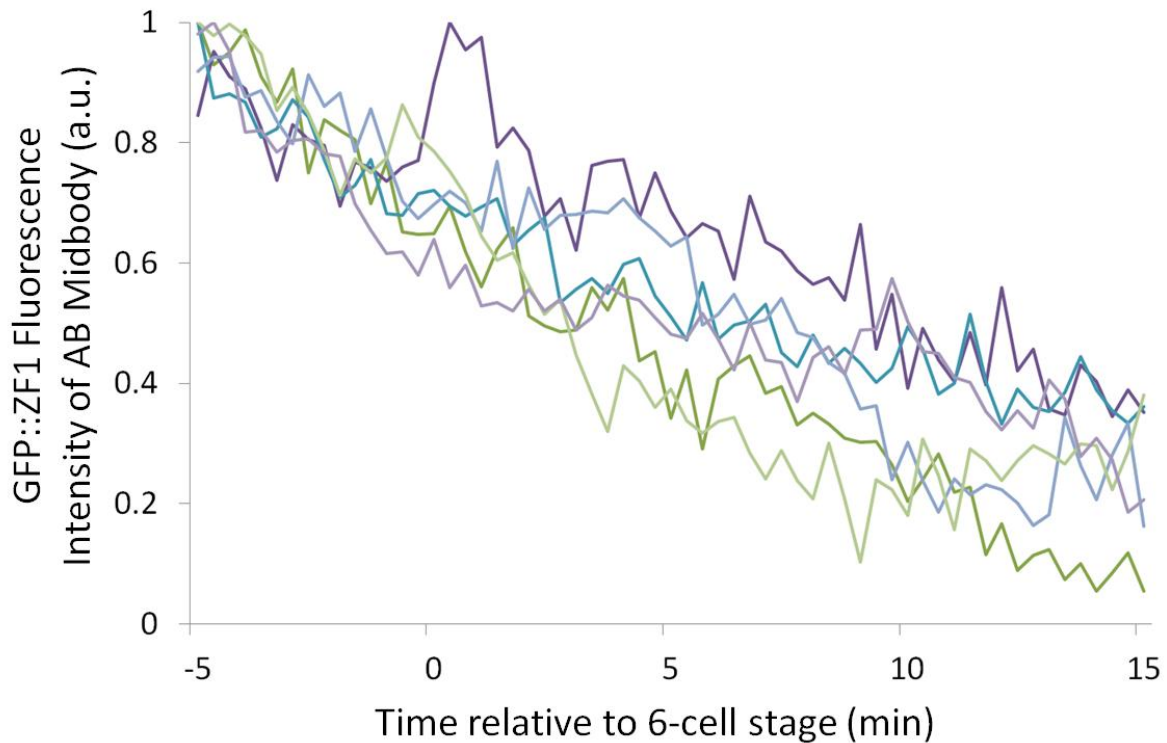
Fig. 18: NMY-2::GFP::ZF1 fluorescence drops on AB midbodies in *tsg-101* mutants. Intensity of NMY-2::GFP::ZF1 fluorescence on the AB midbodies in *tsg-101* RNAi (n=6). Each embryo was plotted in a different color. ZF1 degradation begins ~6 minutes before the six-cell stage.

Similar to septin mutants, NMY-2::GFP::ZF1 underwent degradation on the AB midbody in embryos treated with *tsg-101* RNAi (n=6) (Fig. 18). Consistent with the report that *unc-59* RNAi disrupted cytoplasmic flow more than *tsg-101* RNAi [42], *tsg-101* RNAi embryos lose fluorescence significantly later than *unc-59* mutants (p<0.01). The difference to controls is first statistically significant starting at 4.3 minutes after the six-cell stage for *tsg-101* RNAi embryos (p<0.01) (Fig. 19). Therefore, even mild abscission defects can be detected with the ZF1 assay. These findings confirm that the ZF1-mediated degradation technique can sensitively detect abscission defects.
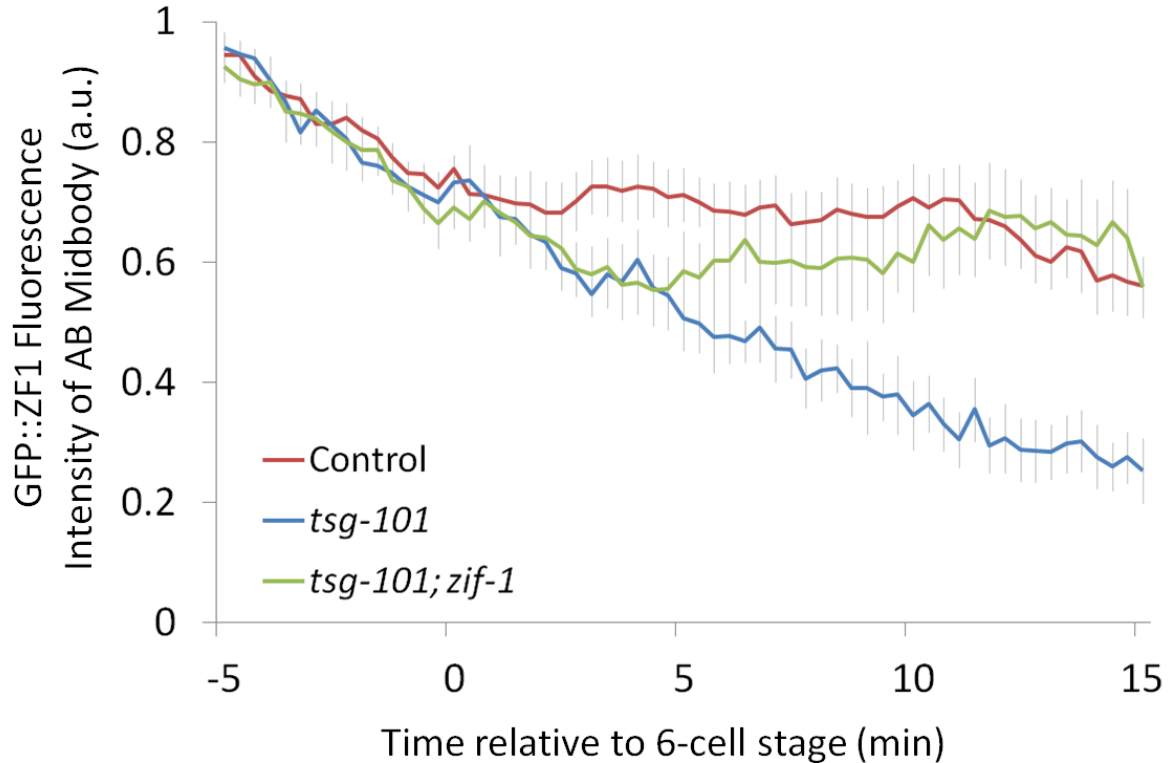
Fig. 19: Average intensity of ZF1 fluorescence on the AB midbody in *tsg-101* mutants (n=6, blue) and *tsg-101; zif-1* double mutants (n=5, green) versus control embryos (n=12, red). ZF1 degradation begins ~6 minutes before the six-cell stage. Error bars indicate SEM.

In order to confirm that the loss of NMY-2::GFP::ZF1 fluorescence intensity on the AB midbody is due to ZIF-1-mediated proteasomal degradation, we next performed the same analysis of fluorescence intensity on the AB midbody in *tsg-101 zif-1* double RNAi-treated WEH51 embryos.

Indeed in embryos treated with *tsg-101 zif-1* double RNAi (n=5) NMY-2::GFP::ZF1 fluorescence on the AB midbody remained stable, as shown in Fig. 19. T-tests showed no significant difference in *tsg-101 zif-1* double RNAi-treated WEH51 embryos compared to the control (p>0.05), but *tsg-101 zif-1* doubles differed significantly from *tsg-101* mutants starting at 11 minutes after six-cell stage (p<0.01).

Thus, the ZF1 reporter undergoes degradation by the ZIF-1 dependent pathway and NMY-2::GFP::ZF1 assay is a reliable tool to examine whether midbodies are connected to the cytoplasm.

Taken together, the delay in internalization in septin mutants, the bridge phenotype and the rapid drop of ZF1 marked NMY-2 give new insights into the process of midbody abscission and internalization in early *C. elegans* embryos, which will be discussed later.

3.2. Slower cell cycle in PI3K mutants

While analyzing the role of the Class III PI3Kinase in midbody internalization and degradation, G. Fazeli noticed that midbodies were not internalized in *bec-1* and *vps-34* mutants. In light of the many roles of PI3K (as described in 1.1), we next wanted to use the ZF1 degradation assay to find out whether the Class III PI3K complex is also required for timely abscission in *C. elegans*. However, G. Fazeli also noticed that *bec-1* and *vps-34* mutant embryos appeared to develop slower. Thus, we first wanted to find out what phase of the cell cycle took longer in these mutants – interphase or cytokinesis. If cytokinesis was delayed, it could be more specifically analyzed by looking at the two main steps of cytokinesis, contractile ring constriction and abscission [1].

3.2.1. Longer cell cycle time in *bec-1* and *vps-34*

To determine the extent of the developmental delay, we measured the timing of cell divisions up to the 15-cell stage. We quantified the cell cycle time for the PI3K-mutants *bec-1* (WEH69, WEH03, WEH106) and *vps-34* (WEH73, WEH55), as well as for control transgenic embryos (WEH51, WEH02, BV113). Table 4 gives an overview of the average time required to reach distinctive cell stages in control *C. elegans* embryos. As additional controls, we also analyzed *ced-2* phagocytosis mutants (WEH71, WEH78, WEH85) and *unc-59/Septin* abscission mutants (WEH132 with *unc-59* RNAi). The time points for each cell stage were assessed and compared to determine a developmental rate.

Cell stage	Time (min)	n=
2-cell	-14 ± 2	7
3-cell	-3 ± 1	28
4-cell	0	-
6-cell	11 ± 1	40
7-cell	15 ± 1	37
8-cell	18 ±2	36
12-cell	26 ± 2	36
14-cell	34 ± 3	36
15-cell	39 ± 4	32

Table 4: Time to reach the indicated cell stage relative to the four-cell stage in WEH51 (n=17), WEH02 (n=9) and BV113 (n=14) control embryos.
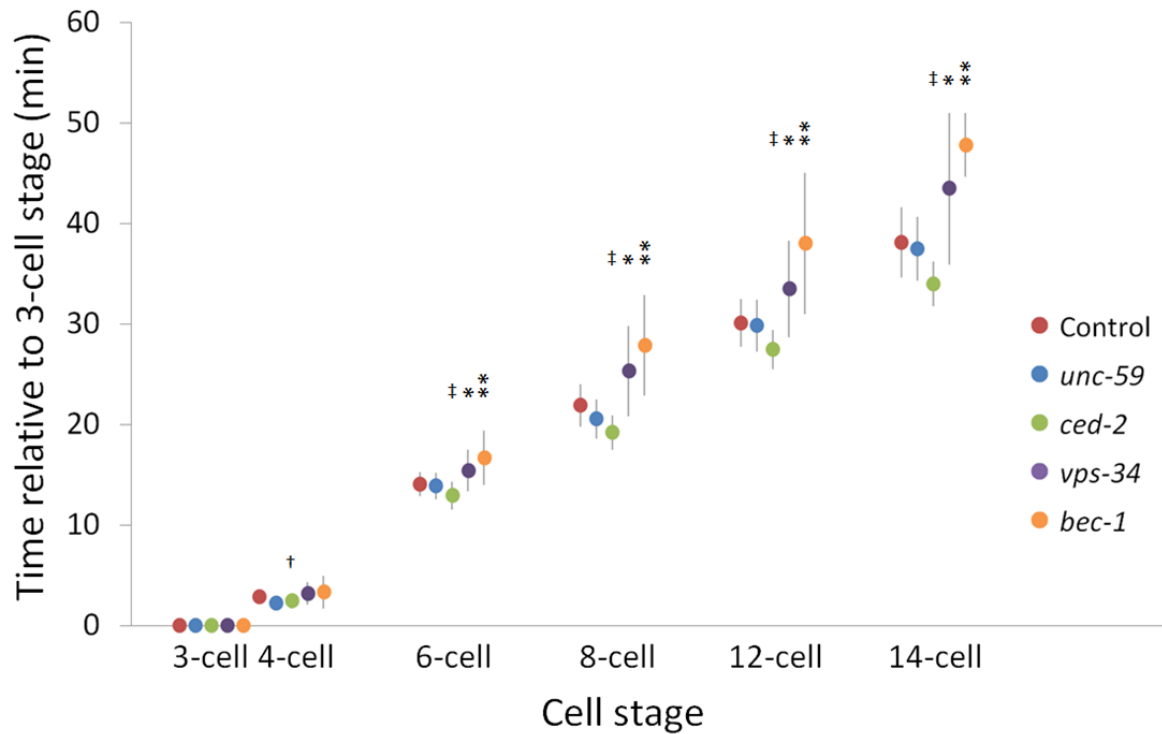
Fig. 20: Time required to reach the specified developmental stages. Graph of average time relative to the three-cell stage in control (n=24), *unc-59* (n=5), *ced-2* (n=22), *vps-34* (n=12) and *bec-1* (n=12). The PI3K mutant embryos required a significantly longer time for their cell cycle compared to the control (*p<0.05, **p<0.01). The phagocytosis mutant embryos *ced-2* developed significantly faster (†p<0.05, ‡p<0.01). Error bars indicate SD.

The AB lineage is the least variable lineage in *C. elegans* embryos [78], therefore we calculated the time from the three- to the 12-cell stage, which corresponds to two cell divisions of the AB lineage. Control embryos from the three transgenic strains took 29 ± 3 minutes (WEH51, n=7), 30 ± 3 minutes (WEH02, n=7) and 30 ± 2 minutes (BV113, n=10) to get from the three- to 12-cell stage. There was no statistically significant difference between these control strains (p>0.05). Therefore, data from the three strains were pooled for all analyses.

To confirm the data from the AB lineage, we next analyzed the times required to reach specified developmental stages up to the 15-cell stage in mutants and control embryos, thus also including the lineages of EMS and P2. As displayed in Fig. 20, significant delays in the cell cycles of *vps-34* and *bec-1* were detected as early as the six-cell stage. To get from three- to the 15-cell stage, control embryos required 43 ± 4 minutes (n=22). PI3K mutants required significantly longer times of 52 ± 4 minutes (n=9, p<0.01) in *bec-1* and 48 ± 8 minutes (n=12, p<0.05) in *vps-34*. One *bec-1* embryo that had to be excluded in this calculation didn't even reach the 15-cell stage within 69 minutes after the 3-cell stage and another slowly developing embryo died before reaching the 15-cell stage, thus also could not be taken into account. As expected, *ced-2* and *unc-59* mutants did not develop significantly slower (37 ± 2 minutes (n=22) and 42 ± 5 minutes (n=4) respectively).

To quantify the change in cell cycle time in mutants to cell cycle time in the control, we computed ratios between mutant and control embryos, taking in account the anterior AB, ventral EMS, and posterior P2 lineages (as described in 2.6). The ratio of cell cycle time in mutants to the control (n=37) averaged 1.28 ± 0.04 in *bec-1* (n=16), 1.16 ± 0.04 in *vps-34* (n=13), 0.92 ± 0.01 in *ced-2* (n=28) and 0.99 ± 0.02 in *unc-59* (n=7). Thus, the delay in the cell cycle amounts to a statistically significant $28 \pm 4\%$ in *bec-1* (p<0.01) and $16 \pm 4\%$ in *vps-34* (p<0.05), confirming our impression of a developmental delay. Surprisingly, the cell cycle was faster by $8 \pm 1\%$ in *ced-2* mutants. However, this indicates that blocking phagocytosis does not slow down cell cycle progression. This observation was of interest as PI3K is also required for midbody phagocytosis [29]. In *unc-59* mutants, the cell cycle was comparable to the control ($1 \pm 2\%$), indicating that the abscission and phagocytic delays described in Section 1.3 do not lead to overall cell cycle delays.

In conclusion, the PI3K mutants *bec-1* and *vps-34* show a significant delay in their early cell divisions, requiring 5-10 minutes more to reach the 14-cell stage. Knowing the extent of the delay, we were prepared to identify which stage of the cell cycle was delayed (see section 3.3). Interestingly, although abscission is delayed in *unc-59* mutants and phagocytosis is defective in *ced-2* mutants, this does not delay their cell cycle time. This

suggests that the cell cycle delay in PI3K mutants is due to something other than abscission or phagocytic defects.

3.2.2. The effect of light exposure on early embryonic cell divisions

Having the cell cycle data in hand, we next wanted to examine whether there was evidence for cell cycle delays due to phototoxicity of fluorescent light exposure during time-lapse imaging on *C. elegans* embryos. It has been known that high-intensity excitation light during fluorescence microscopy is toxic for live cells [81], but it was unknown how problematic this was for the imaging setup used in the Wehman lab. As fluorescence microscopy was started at slightly different developmental stages, some variability in light exposure was given to embryos. Similarly, slower developing embryos (such as PI3K mutants) needed to be imaged for longer times to visualize the same developmental stages, resulting in increased light exposure.

In order to find out the extent of the damaging effect of light, the time from the three- to 12-cell stage, corresponding to two cell divisions of the AB lineage, was plotted in relation to the time of light exposure before the three-cell stage for all control embryos (WEH51 n=7, WEH02 n=7 and BV113 n=10). As shown in Fig. 21, the effect of the light exposure on embryonic development was not significant.

We fit a line to the data, which had a coefficient of correlation (Pearson R) of 0.13, indicating that the light exposure did not significantly explain the observed variability in cell cycle time (p=0.54). The slope of the line of regression was 0.06 (Fig. 21), indicating that if light exposure was harming development, ~17 minutes of additional imaging would be necessary to slow development by 1 minute. Therefore, we conclude that the harming effect of light exposure in early *C. elegans* embryos for ~20 minutes before the three-cell stage has no significant impact on the development through the 12-cell stage.
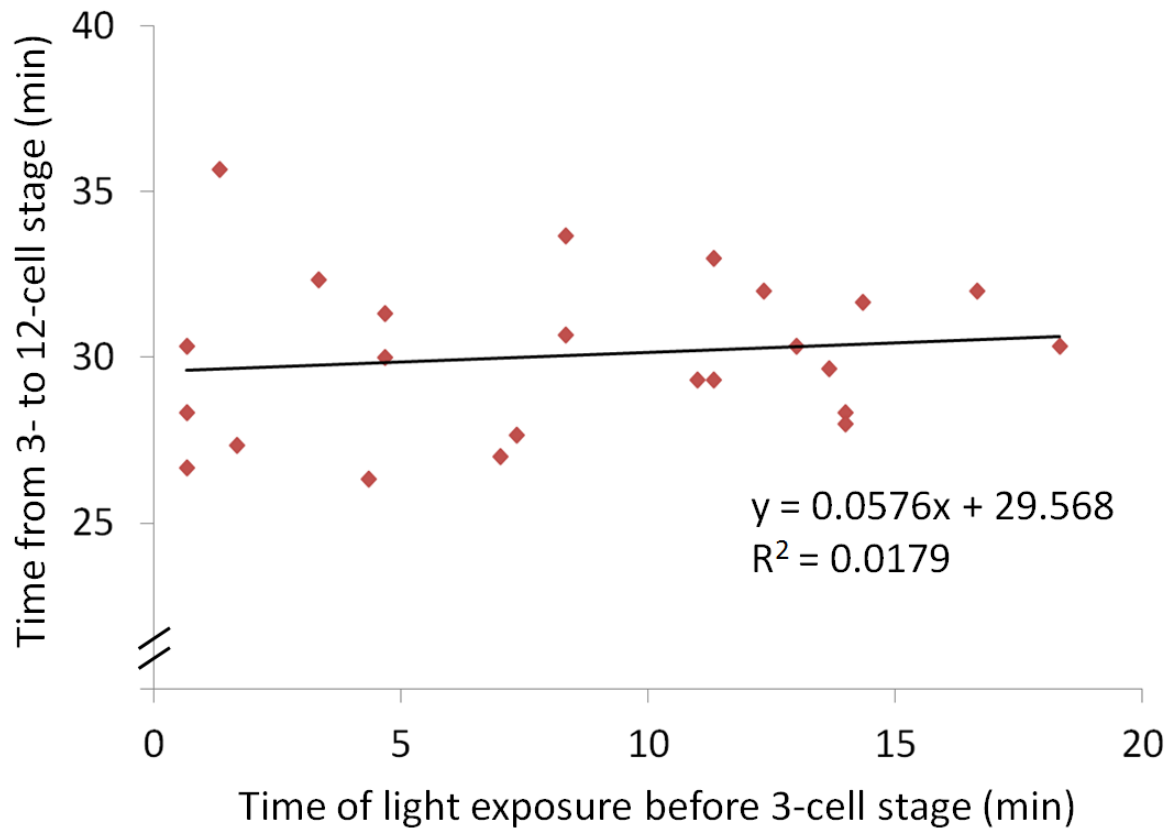
Fig. 21: Effect of light exposure on cell cycle time. The length of time from the three- to 12-cell stage is graphed as a function of light exposure before the three-cell stage in minutes (n=24).

The range of light exposure before the three-cell stage was quantified in the different groups of embryos and ranged $0.7 - 18.3$ minutes in control embryos, $0.3 - 20$ minutes in *bec-1*, $0.3 - 17.7$ in *vps-34*, $0.3 - 22.0$ in *ced-2* and $1.0 - 14.7$ in *unc-59*. The average light exposure before the three-cell stage varied little between the different groups of embryos that were compared: 9 ± 6 minutes in controls, 10 ± 7 minutes in *bec-1*, 6 ± 5 minutes in *vps-34*, 7 ± 7 minutes in *ced-2* and 7 ± 5 minutes in *unc-59*. Thus, the imaging conditions do not explain the observed cell cycle delays in PI3K mutants, because light exposure did not bias our cell cycle results. Therefore, the observed delay in cell cycle timing in *bec-1* and *vps-34* mutants was not caused by increased light exposure.

3.2.3. Quantification of ring closure in PI3K mutants

3.2.3.1. Time of ring closure

We next tested whether the developmental delay in *bec-1* and *vps-34* mutants was due to slower closure of the contractile ring. Time lapse series were annotated for time point t_0 and t_1. t_0 was the time point before furrow ingression started, and t_1 was the time point when the ring appeared closed. We annotated these time points for both the P0- and AB-cell division in control embryos (WEH51, BV113, LP162) in addition to *bec-1* (WEH106, WEH69) and *vps-34* (WEH55, WEH73) mutants.

Apparent ring closure of the P0 cell division ($\Delta t = t_1 - t_0$) lasted 4 min 20 sec ± 20 sec (n=8) in control, 5 min (n=2) in *bec-1* and 5 min 20 sec ± 50 sec (n=4) in *vps-34* (Fig. 22). Due to difficulties obtaining *bec-1* embryos at the appropriate stage, only two embryos were available for these measurements, preventing statistical analysis. No significant difference between *vps-34* and the control was observed ($p > 0.05$).

To confirm the P0 division results, we next analyzed the AB cell division (Fig. 23). Here, ring closure lasted 4 min 30 sec ± 30 sec (n=10) in control, 4 min 30 sec ± 30 sec (n=3) in *bec-1* and 4 min 50 sec ± 20 sec (n=4) in *vps-34*. There was no significant difference between mutants and control embryos ($p > 0.05$).

In conclusion, no significant difference in time needed for ring closure during P0 or AB cell divisions was observed in PI3K-mutants *bec-1* and *vps-34* versus control embryos. However, this method offered limited information on the process of ring closure because the end time point of completed ring closure was difficult to determine due to the limited resolution of wide-field fluorescence images. Therefore, we wanted to confirm these results using another measurement method independent of the end time point.

3.2.3.2. Velocity of ring closure

Another method to determine furrowing rate is to calculate the average speed between 20% and 80% of ring closure, as previously applied by Bourdages et al. in vulva precursor cells

in *C. elegans* [79]. Since the exact time point of ring closure could not be determined due to the limited resolution of light microscopy, this approach is a good method to determine the velocity of ring contraction independent of the end time point of ring closure.

In order to quantify this specific step of cytokinesis, the diameter of the contractile ring was measured every 20 seconds from time points t_0 to t_1. Again, t_0 was the time point before furrow ingression started, and t_1 was the time point when the ring appeared closed. Measurements were done for both the P0- and AB-cell division in control embryos (WEH51, BV113, LP162) in addition to *bec-1* (WEH106, WEH69) and *vps-34* (WEH55, WEH73) mutants (Fig. 22-23).
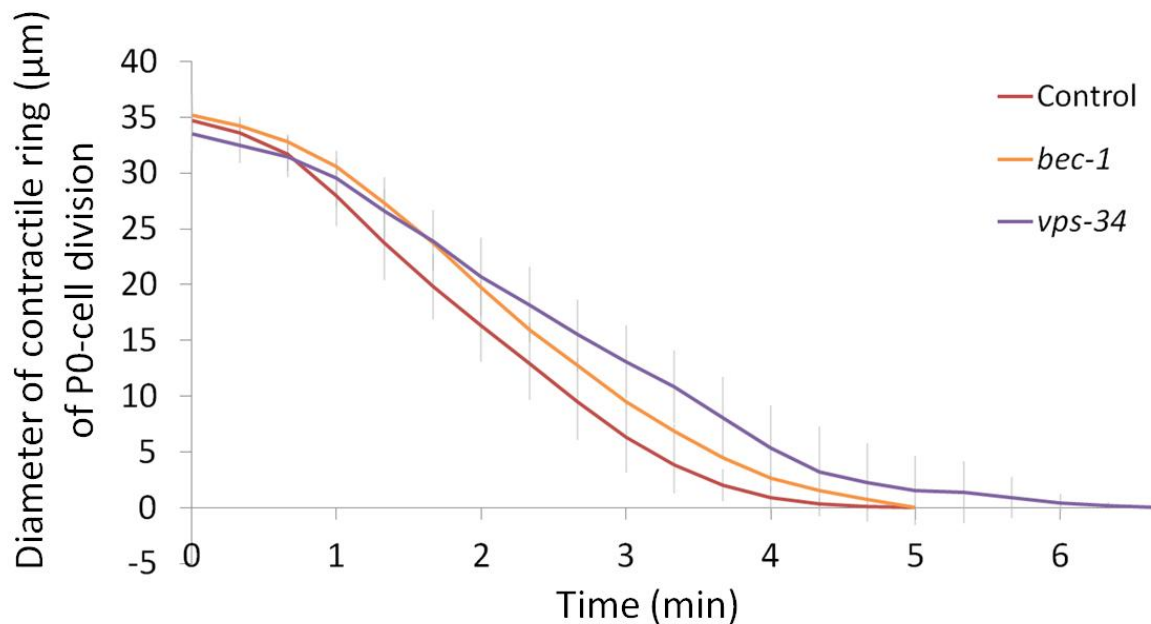
Fig. 22: Diameter of the contractile ring during P0 cell division in μm over time in minutes. Time 0 is the beginning of furrow ingression. Strains used: WEH51, BV113, and LP162 as control (n=8), WEH106 as *bec-1* (n=2) and WEH55 as *vps-34* (n=4). Error bars indicate SD.
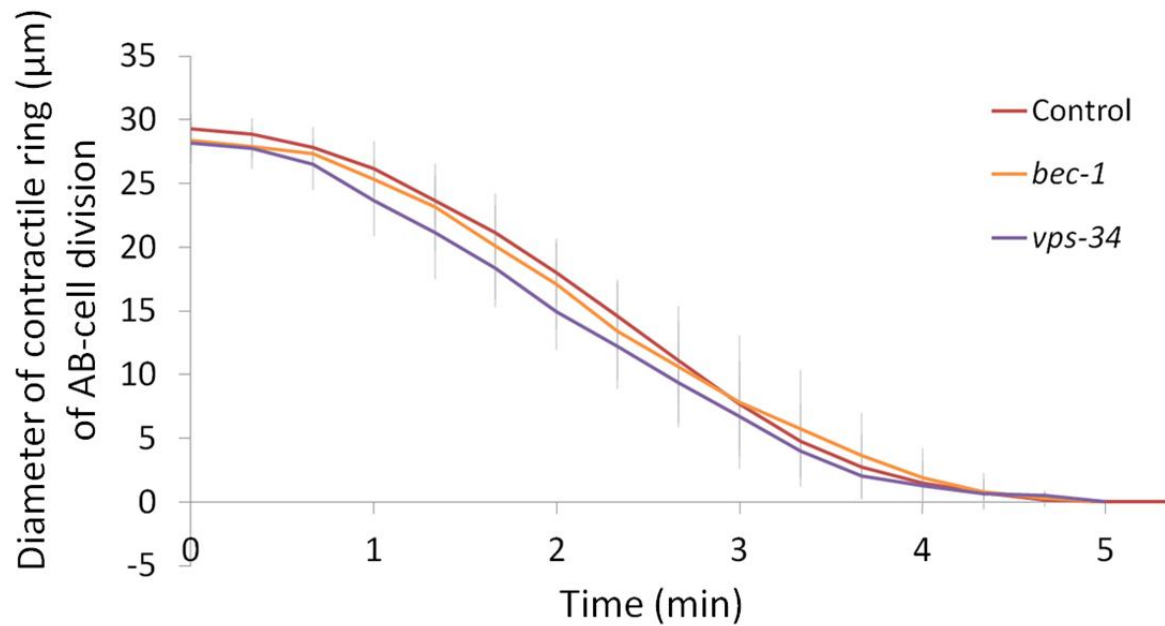
Fig. 23: Diameter of the contractile ring (μm) during AB cell division over time (minutes). Time 0 is the beginning of furrow ingression. Strains used: WEH51 as control (n=10), WEH106 and WEH69 as *bec-1* (n=3) and WEH73 as *vps-34* (n=4). Error bars indicate SD.

The initial ring size in the last frame before AB furrow ingression was also measured in *bec-1* and *vps-34* and compared to control embryos. The diameter averaged 28.4 ± 1.0 μm in *bec-1* (n=3) and 28.2 ± 1.4 μm in *vps-34* (n=4) and in both did not differ significantly from the control, where it averaged 29.3 ± 1.2 μm (n=10, $p > 0.05$). Therefore, the contractile ring had a comparable distance to cover in *bec-1, vps-34* and control.

Time points of 20% (t_{20}) and 80% (t_{80}) ring closure, according to a linear regression modeling all time points within 20% and 80% of ring closure (see section 2.7), are shown in Table 5. The time between 20% and 80% ring closure, ∂t, averaged 1.8 ± 0.2 minutes in control embryos (n=10), 1.9 ± 0.2 minutes in *bec-1* (n=3) and 1.9 ± 0.1 minutes in *vps-34* (n=4). Statistical analysis again showed no significant difference in either mutant compared to the control ($p > 0.05$).

	Control (n=10)	*bec-1* (n=3)	*vps-34* (n=4)
t_{20}	1.4 ± 0.2	1.4 ± 0.4	1.1 ± 0.3
t_{80}	3.2 ± 0.4	3.3 ± 0.6	3.1 ± 0.3
∂t	1.8 ± 0.2	1.9 ± 0.2	1.9 ± 0.1

Table 5: Times at which 20% and 80% ring closure of AB furrow are reached in control and PI3K mutant embryos relative to t_0 (in minutes). ∂t represents the time from 20 to 80% ring closure (in minutes).

The speed between 20% and 80% of ring closure, represented by the slope of the linear regression, averaged 9.9 ± 1.3 µm/minute in the control (n=10) versus 9.1 ± 1.2 µm/minute in *bec-1* (n=3) and 8.7 ± 0.3 µm/minute in *vps-34* (n=4). The average speed in *bec-1* was not significantly different from the control (p>0.05), but was significantly slower in *vps-34* (p<0.01). In other assays, we typically observe stronger defects in *bec-1* mutants than *vps-34*, but this may be due to the low number of embryos measured. Thus, we conclude that calculation of average speed between 20% and 80% of ring closure offers a sensitive method of quantifying speed of furrow ingression in early *C. elegans* cell divisions.

In summary, although distance and time span covered between 20% and 80% of ring closure were similar in *bec-1, vps-34* and control embryos, there is a significant difference between control embryos and the PI3K mutant *vps-34* in furrow ingression speed. This preliminary finding needs to be confirmed by analyzing more embryos to determine the true extent of the delay. However, a difference in furrow ingression in PI3K mutants versus control of about 10 seconds per division (see Table 5) would not explain the observed delay of 5-10 minutes in development in PI3K mutants between the three- and 15-cell stages (two rounds of division). Therefore, we predict that the cell cycle is delayed during another phase.

3.2.4. No delay in abscission in PI3K mutants

As longer cell cycle time in *bec*-1 and *vps-34* could not be attributed exclusively to slower ring contraction, we next wanted to know whether part of the delay could be caused by a delay in abscission. Therefore, we used the ZF1 degradation assay to test whether PI3K mutants had a delay in abscission similar to *unc-59/Septin* mutants (see section 3.1.3, Fig. 17).

M. Trinkwalder measured NMY-2::GFP::ZF1 fluorescence of the AB midbody in the PI3K mutant *bec-1* (WEH69) and control embryos (WEH51) and I compared it to the fluorescence in abscission mutants (WEH132 with *unc-59* RNAi), as shown in Fig. 24. In *unc-59* mutants, ZF1 fluorescence on the AB midbody dropped early because of a defect in abscission, as discussed in section 3.1.3. However, data measured by M. Trinkwalder showed that ZF1 fluorescence on the AB midbody in *bec-1* depleted embryos did not drop significantly below the fluorescence in control embryos (p>0.05).
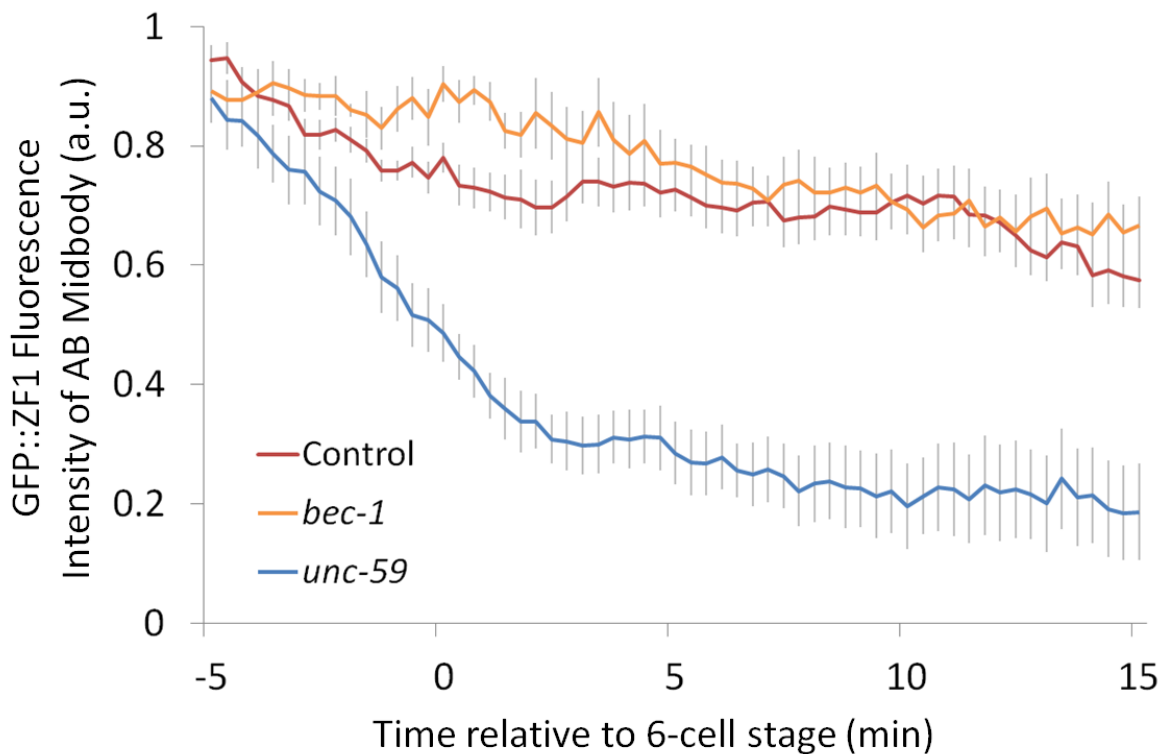
Fig. 24: NMY-2::GFP::ZF1 fluorescence intensity of the AB midbody in control (n=12), *bec-1* (n=6) and *unc-59* (n=6). Error bars indicate SEM.

Thus, the longer cell cycle time in *bec-1* mutant embryos is not caused by a defect in abscission, because at least in *C. elegans* the Class III PI3K complex is not required for abscission. Furthermore, given that ring contraction is not sufficiently delayed to explain the additional 5 - 10 minutes required to reach the 15-cell stage in the development of PI3K mutants, it appears that PI3K regulates another aspect of the cell cycle. The cause of this delay remains to be determined.

3.3. Dorsoventral movement of the P0 midbody at late two-cell stage

In a paper published in 2014, Singh and Pohl showed that the P0 midbody remnant has a role in dorsoventral axis formation in *C. elegans* [61]. They proposed that the P0 midbody becomes positioned asymmetrically at the future ventral side of the embryo due to rotational cortical flow orthogonal to the anteroposterior axis that occurs during the late two-cell stage. Since our data showed that midbodies are released, we wanted to see how dorsoventral axis formation would change in septin mutants. We started by first characterizing control embryos and *ced-2* and *par-1* mutants using the Singh and Pohl method.

3.3.1. Control embryos

I first measured the position of the P0 midbody in three control strains expressing fluorescent NMY-2 transgenes: WEH02, WEH51 and BV113. Using ImageJ, I measured the position of the P0 midbody on the AB cell - P1 cell interface (Fig. 25) at three defined time points during late two-cell stage:

t_0 Nuclear membrane breakdown in AB

t_2 Beginning of ring contraction in AB cell division

t_3 Two frames (40 seconds) after t_2
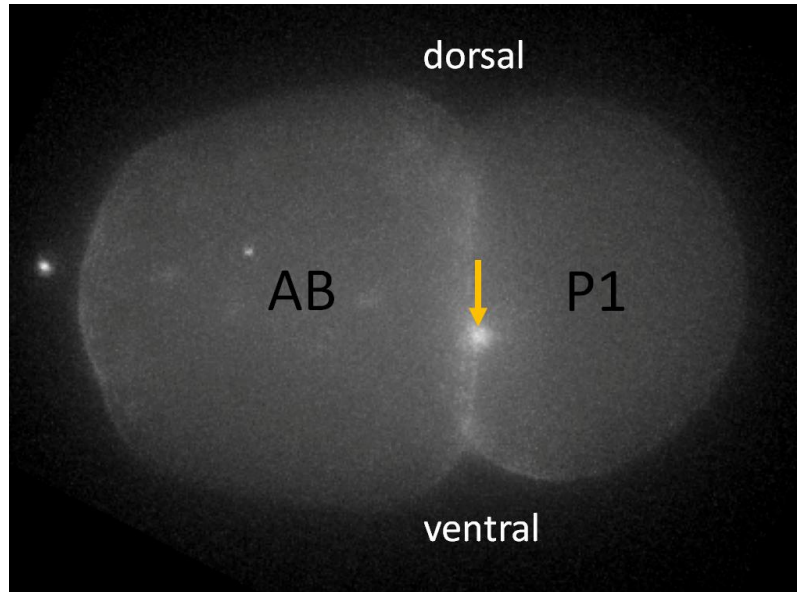
Fig. 25: A representative *C. elegans* embryo of the strain WEH51, expressing NMY-2::GFP::ZF1, at time t_2. The arrow indicates the ventral movement of the P0 midbody between t_0 and t_2.

t_0 and t_2 were the previously used time points of Singh and Pohl. However, during our analysis, we realized that much of the ventral movement takes place in the two time frames after t_2. Therefore, t_3 was introduced as an additional time point to measure ventral movement of the P0 midbody. At t_3, the interface between the AB cell and P1 cell is not yet curved by the cell division of the AB cell, although it is slightly curved due to different cortical pressures (see Fig. 9 in 2.11). Therefore, P0 midbody position on the DV axis could still be precisely determined at t_3.

	Position on DV-Axis (%) at time t		
	t_0	t_2	t_3
WEH51 (n=8)	48 ± 15	53 ± 17	63 ± 15
WEH02 (n=4)	42 ± 10	45 ± 12	64 ± 5
BV113 (n=10)	54 ± 11	56 ± 10	67 ± 15
Total (n=22)	50 ± 13	53 ± 13	65 ± 13

Table 6: Position of the P0 midbody on the dorsoventral axis expressed as percentage of the width of the embryo at the time t in three different control *C. elegans* strains (<50% corresponds to a dorsal position, >50% corresponds to a ventral position).

The three control genotypes were combined and viewed as one control group in the following results, because statistical analyses showed no significant difference between the three strains (p>0.05, Table 6).

From t_0 until t_2, the midbody moved only $3 \pm 12\%$, whereas from t_0 until t_3 it moved $16 \pm 20\%$ in the ventral direction (n=22). Moreover, between t_0 and t_2, 41% of the midbodies moved towards the dorsal side, i.e. in the opposite direction than previously reported [61]. Even between t_0 and t_3, 32% of the midbodies moved dorsal. However, five of the nine midbodies that moved dorsal between t_0 and t_2 later moved ventral between time points t_2 and t_3. In our analysis, 50% of the midbodies are located at the ventral half of the embryo at time t_0, 55% at t_2 and 91% at t_3.

Looking at the average movement of the P0 midbody in our control embryos, we were able to confirm that dorsoventral movement of the P0 midbody does take place. However, this movement was not as strongly conserved as reported by Singh and Pohl [61], where 100% of the midbodies (n=20) moved ventrally and were positioned on the ventral side at t_2. In conclusion, movement in the ventral direction in control embryos was observed, however the extent of the movement was not as previously reported.

3.3.2. *ced-2* and *par-1* mutants

Using the ventral movement assay, we next wanted to find out how P0 midbody position changes in mutants that disrupt midbody internalization. We expected to see no difference in ventral movement in the phagocytosis mutant *ced-2* (WEH71 and WEH85), where DV axis formation is not known to be disturbed. In contrast, the polarity protein PAR-1 is known to be required for normal cleavage patterns and *par-1* mutants show defects in anteroposterior polarity [82]. In addition, midbody-induced DV patterning is disrupted in Par polarity mutants [61]. Therefore, we expected little or no P0 midbody movement at the late two-cell stage in *par-1* RNAi treated embryos (WEH51 and BV113 with *par-1* RNAi).

Dorsoventral movement was determined at time points t_0 and t_3 in *ced-2* and *par-1* mutants (Table 7), because these were the time points at which midbody ventral movement was best detected in the control. While the P0 midbody moved 16 ± 20 % in the ventral direction in the control, it moved significantly less ventrally by 3 ± 11 % in *ced-2* mutants ($p<0.05$). Midbodies in *par-1* mutants moved in the ventral direction by 13 ± 14 %, showing no significant difference in comparison to the control ($p>0.05$).

	Position on DV axis (%) at time t		
	t_0	t_3	$t_3 - t_0$
Control (n=22)	50 ± 13	65 ± 13	16 ± 20
ced-2 (n=12)	51 ± 7	53 ± 13 *	3 ± 11 *
par-1 (n=11)	47 ± 14	60 ± 8	13 ± 14

Table 7: Position of the P0 midbody on the dorsoventral axis expressed as a percentage of the width of the embryo at time t in control and mutant embryos (<50% corresponding with a dorsal position, >50% corresponding with a ventral position). The last column shows the effective change in position to the ventral side. Asterisk (*) indicates statistically significant difference to the control ($p<0.05$).

In summary, we observed a different result than we expected. The phagocytosis mutant *ced-2* embryos differed significantly from the control with reduced ventral movement of the P0 midbody at the late two-cell stage. In contrast, the polarity mutant *par-1*, in which we had expected decreased ventral movement of the midbody, moved to the ventral side similar to control midbodies. Given the difficulty determining the appropriate time points for the assay and unexpected results with the mutants, we decided not to analyze dorsoventral movement of the P0 midbody in septin mutants. Instead, we wanted to elucidate the fate of the midbody after internalization.

3.4. Midbodys are phagocytosed and undergo LC3-dependent degradation

3.4.1. Autophagy versus LC3-associated phagocytosis

In light of the distinct models of midbody fate that have been proposed (see 1.2), we wanted to elucidate the role of autophagy proteins and test whether proteins specific for macroautophagy are involved in midbody degradation.

LGG-1 and LGG-2 are homologs of mammalian GABARAP and LC3 and are required for elongation of the autophagosome membrane [74]. Previously, my workgroup had investigated whether these autophagy proteins are required for the degradation of phagocytosed midbodies in *C. elegans* embryos. Midbodies were labeled using an mCherry-tagged NMY-2/non-muscle myosin reporter to label the midbody ring and midbody remnants. In *lgg-1; lgg-2* double mutants, mCherry fluorescence on the P0 midbody remained constant, demonstrating that autophagy proteins like LGG-1 and LGG-2 are required for degradation of the midbody [29].

The molecular mechanisms of macroautophagy and LC3-associated phagocytosis (LAP) are very similar, with a few exceptions. For example, ULK1 and ATG14 are mammalian proteins that are specifically required for macroautophagy but not for LAP [56, 57, 83]. No one had tested a role for ULK1 or ATG14 in midbody degradation in any species, which would allow a distinction between macroautophagy and LAP. We first concentrated on

UNC-51, the *C. elegans* homolog of ULK1, which is responsible for the initiation of macroautophagy by phosphorylating Beclin1, but is not required for LAP [56].

The WEH176 strain has a nonsense allele of *unc-51(e369)* and fluorescently-labeled midbodies with an mCherry-tagged NMY-2/non-muscle myosin reporter. I quantified and analyzed NMY-2::mCh fluorescence of the P0 midbody in *unc-51(e369)* mutants (Fig. 26).
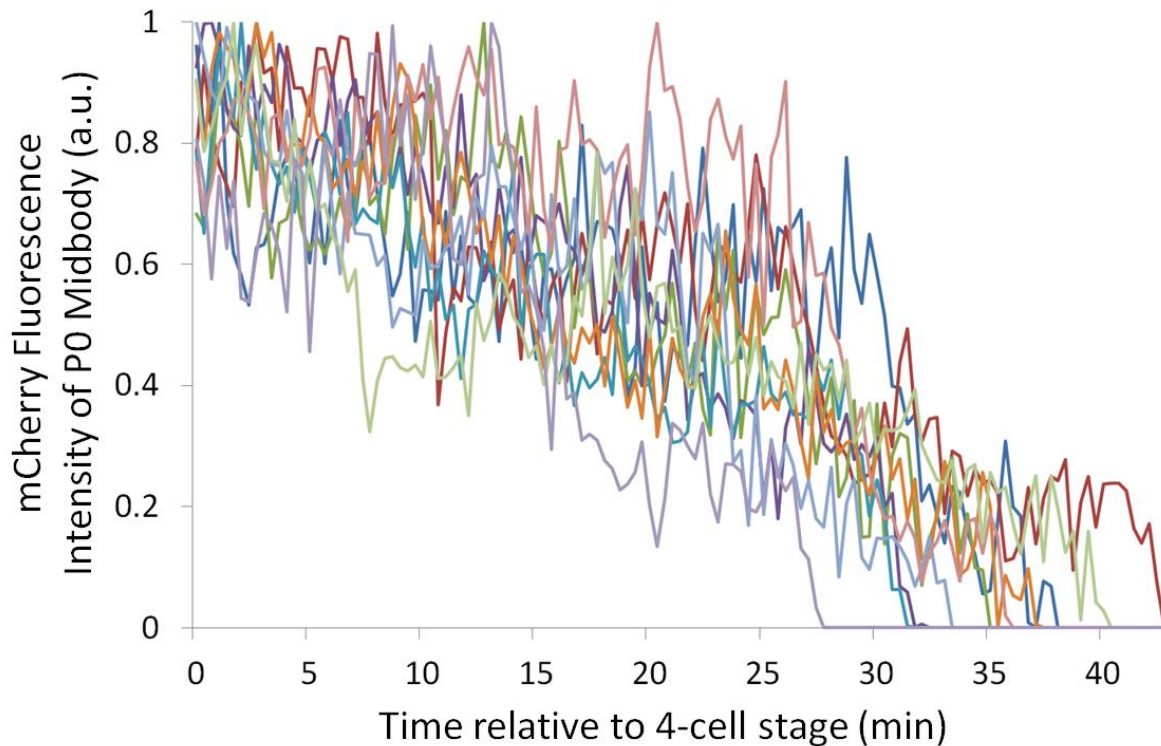
Fig. 26: NMY-2::mCh fluorescence intensity of the P0 midbody in *unc-51* mutants (n=10). Each embryo was plotted in a different color.

If autophagy initiated by UNC-51/ULK1 was required for midbody degradation, we expected fluorescence on the midbody to be stable in *unc-51* mutants, similar to *lgg-1; lgg-2* double mutants. However, analysis of fluorescence intensity of the P0 midbody in *unc-51* mutants showed a decrease in NMY-2::mCherry fluorescence, similar to the control (Fig.

27). In *unc-51* mutants, the P0 midbody disappeared 35 ± 4 minutes after the four-cell stage (n=10), while NMY-2::mCh disappeared from the P0 midbody 43 ± 3 minutes after the four-cell stage in control embryos (n=6). In contrast, fluorescence on the P0 midbody in *lgg-1; lgg-2* double mutants (n=6) remained constant, with no midbodies disappearing before the end of time-lapse recording (59 ± 11 minutes after four-cell stage, n=6).
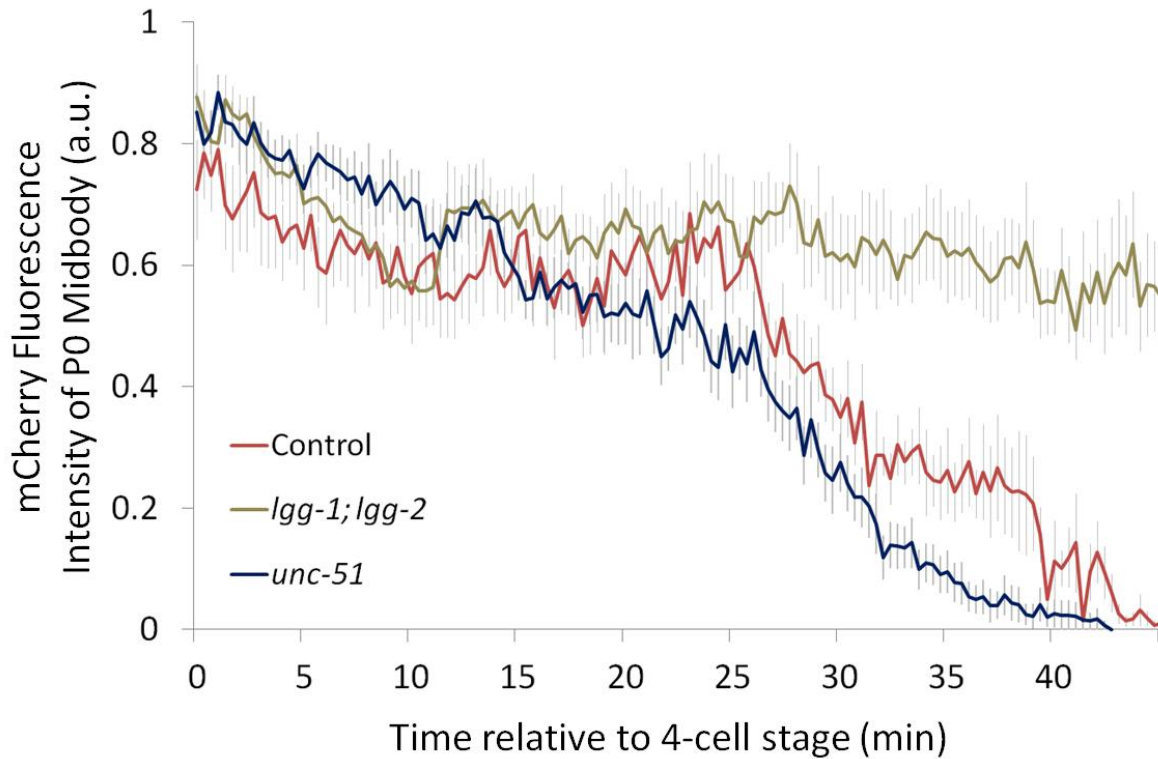
Fig. 27: NMY-2::mCh fluorescence intensity on the P0 midbody in control (n=6), *lgg-1; lgg-2* (n=6) and *unc-51* (n=10) mutant embryos. Fluorescence intensity is significantly different between *lgg-1; lgg-2* mutants and *unc-51* mutants, which drop similar to the control, starting at 24 minutes after the four-cell stage (p<0.01). Error bars indicate SEM.

Thus, no defect in midbody degradation was found in *unc-51* mutants. This finding shows that macroautophagy does not play a role in degradation of the midbody.

3.4.2. The role of ATG-7 in degradation of the midbody

To further demonstrate that midbody phagocytosis and degradation were independent of autophagy, we next analyzed the role of ATG-7 using the ZF1 degradation assay. ATG-7 is required for lipidation of the Atg8/LC3 family proteins LGG-1 and LGG-2 and thereby the recruitment of LGG-1 and LGG-2 to membranes such as phagophores or LC3-associated phagosomes [74]. G. Fazeli found that midbodies in *lgg-1; lgg-2* double mutants as well as in *atg-7* knockdowns internalize normally, suggesting that phagophore elongation does not play a role in phagocytosis [29]. However, ATG-7, LGG-1 and LGG-2 could still have played a role in sealing the phagosome in the cytoplasm.

To test whether autophagy proteins like LGG-1, LGG-2 and ATG-7 are needed to seal the midbody phagosome and further expand our understanding of the specific role of Atg8/LC3 in midbody internalization and degradation via LAP, we analyzed NMY-2::GFP::ZF1 fluorescence on the AB midbody in *atg-7* RNAi-treated WEH51 embryos.

In WEH51 control embryos, ZF1 fluorescence on the AB midbody began to diminish ~10 minutes after internalization (internalization taking place 5 ± 6 minutes after the six-cell stage; n=17) (Fig. 28). Midbody fluorescence disappeared 31 ± 10 minutes after the six-cell stage (n=18). This suggests that the midbody remains isolated from the cytoplasm for a period after internalization, likely because it remains protected by the phagosome.

In *atg-7* knockdowns, fluorescence began to diminish ~5 min after internalization (internalization taking place 11 ± 7 min after the six-cell stage; n=10) and disappeared 32 ± 8 minutes after the six-cell stage (n=10), similar to the control (p>0.05). No rapid fluorescence loss was seen prior to internalization like in septin-depleted embryos, as shown in Fig. 28. Indeed, the fluorescence in *atg-7* knockdowns differed significantly from *unc-59* mutants starting at 40 seconds before the six-cell stage (p<0.01), indicating that the AB midbody was released normally in *atg-7*-depleted embryos.
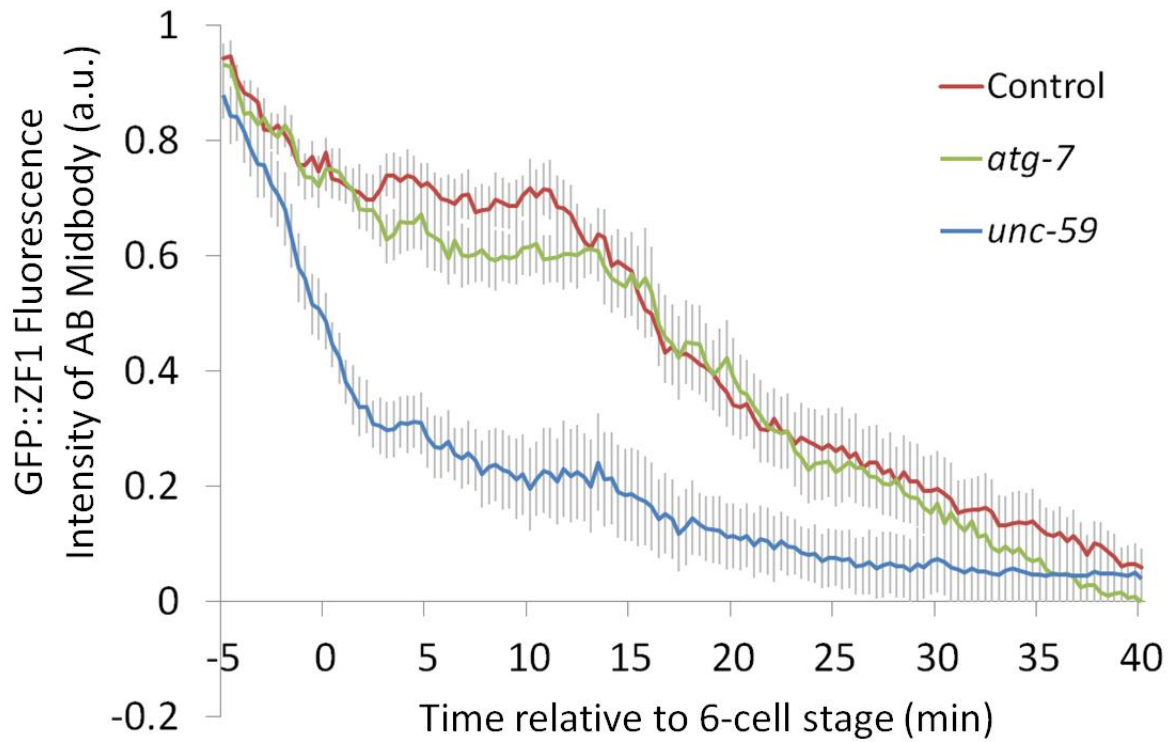
Fig. 28: NMY-2::GFP::ZF1 fluorescence intensity of the AB midbody in control (n=12), *atg-7* (n=10) and *unc-59* (n=6). Error bars indicate SEM.

Thus, consistent with their lack of a role in midbody internalization, autophagy proteins like LGG-1, LGG-2 and ATG-7 are not needed to seal the midbody phagosome, as the ZF1 reporter on the midbody is protected from degradation.

4. Discussion

In summary, we implemented the ZF1 degradation assay as a novel method to detect abscission defects (4.1). The abscission delay we found in septin mutants also resulted in a significant delay in internalization of the midbodies, associated with attached midbodies in the so-called bridge phenotype (4.3). Our analysis of the role of septins has deepened our understanding of abscission and midbody release into the extracellular space and is of high interest, as septins are involved in various human diseases (4.4) and the midbody remnant has been ascribed roles that may be linked to the pathogenesis of diseases (4.6). The ZF1-mediated technique was also applied to probe for a role of PI3K in abscission (4.5) and to elucidate the role of LC3 family proteins in resolving the midbody (4.2). These findings, in addition to the lack of a role for ULK1 in midbody degradation, lead to a new model of midbody fate in *C. elegans*, where the midbody is released and then internalized by LC3-associated phagocytosis (4.7).

4.1. The ZF1 degradation assay detects abscission defects in septin and *tsg-101* mutants

Unlike observations in septin knockdown in vertebrate cells [41], in our septin-depleted *C. elegans* embryos we did not observe contractile rings opening up again to result in multinucleated cells due to a defect in abscission. Our results are consistent with previous findings in *C. elegans*, that *unc-59* mutants have normal embryonic development [34] and Green et al. also observed no binucleation in septin-depleted *C. elegans* embryos, concluding that probably redundant mechanisms ensure formation of stable cell-cell boundaries [42]. However, as expected, we observed an abscission defect in our septin mutants, which we were able to analyze by applying the ZF1-mediated degradation technique.

The ZF1 degradation assay quickly and accurately eliminates both cytoplasmic and midbody-incorporated ZF1-tagged NMY-2 at the time of AB midbody formation. While midbodies are normally protected from ZF1 degradation due to bilateral abscission and

extracellular release in control embryos (Fig. 29), ZF1 marked NMY-2 can be degraded through the remaining connection to the cytoplasm in septin and ESCRT mutants (Fig. 30). Thus, defects in abscission can be sensitively detected by the ZF1-mediated degradation technique according to our experiments.
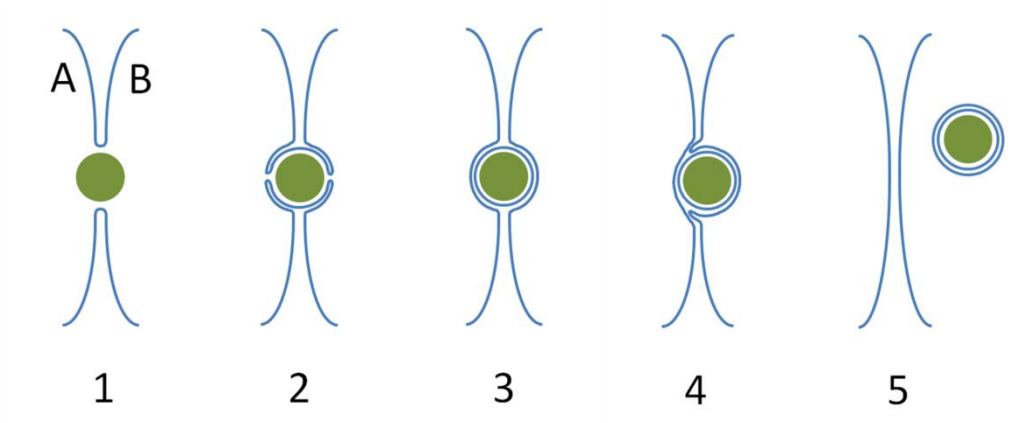
Fig. 29: Model of internalization of the midbody in control embryos. As the cleavage furrow draws towards the midbody, an intercellular connection between the two daughter cells remains, with the midbody (green) at its center (1-2). Abscission takes place on both sides of the midbody and the midbody is released into the extracellular space, protecting it from the process of NMY-2::GFP::ZF1 degradation (3). Cell B then internalizes the midbody via phagocytosis (4-5).
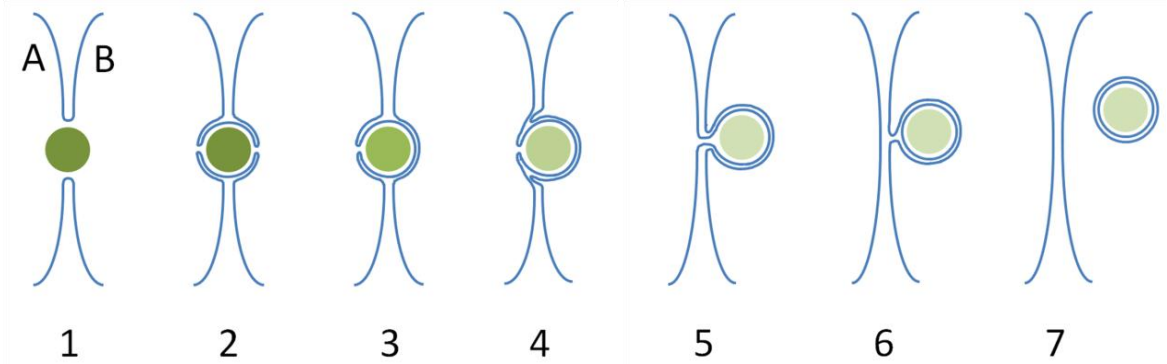
Fig. 30: Model of internalization of the midbody in septin mutants. Similar to wild type, as cleavage furrow draws in, an intercellular connection between the two daughter cells remains, with the midbody (green) at its center (1-2). In septin mutants, abscission is disturbed and a connection to cell A can persist (3), while cell B already begins engulfing the midbody (4). Through the connection to the cytoplasm of cell A, the midbody is not protected from ZF1 degradation (fluorescent intensity drops at (3)). Furthermore, a bridge phenotype can occur: the membrane around the midbody extends into cell B while still connected to cell A (5). Only upon completion of scission (6) can the midbody be internalized (7).

The abscission delay we observed in septin mutants is consistent with observations that the isolation of the cytoplasm of sister cells during the P0 cell division takes 2-3 minutes longer in *unc-59/septin* knockdowns than in control *C. elegans* embryos [42]. Green et al. observed that diffusion between sister cells ended 4 minutes after the beginning of P0 division in control cells versus 6-7 minutes after the beginning of P0 division in septin mutants. Applying the observations of Green et al. to the AB midbody, cytoplasmic isolation would be predicted to take place roughly 6-7 minutes after the onset of AB division in septin mutants. However, we observed a severe drop of ZF1 fluorescence on the AB midbody until ~14 minutes after AB division (Results section 3.1.3, also Fig. 31). This suggests that cytoplasmic isolation of the daughter cells is an earlier and distinct step than abscission of the membrane on both sides of the midbody. One possible explanation is that cytoplasmic isolation occurs after the first cut, while the ZF1 assay requires cuts on both sides of the AB midbody to hinder ZF1 degradation on the midbody, as both AB daughter cells have initiated ZF1 degradation at this time. In electron microscopy experiments, both single and double cuts have been observed around midbodies [16, 21, 84], indicating that abscission takes place asynchronously on both sides of the midbody, which would be consistent with the model, where abscission takes place consecutively on each side (see Fig. 30 part 3).

When analyzing the fluorescence of the AB midbody in control embryos, a slight decrease in ZF1 reporter fluorescence for the first three minutes after the onset of ZF1 degradation can be seen (see Fig. 17 in 3.1.3). This raises the question whether the AB midbody in controls is also initially accessible to ZF1 degradation. However, we see a similar early decrease for the P0 midbody, where ZF1 degradation has not yet begun. Thus, it is not likely due to ZF1 degradation. Though the reason remains unclear, fluorescence is stable and thus abscission has definitely occurred by the six-cell stage in control embryos, which is about five minutes before internalization happens. Thus, abscission normally takes place before internalization of the midbody.

Green et al. found that TSG-101-depleted embryos did not have a delay in cytoplasmic isolation [42], while in our experiments, testing for final separation of the two cells, they did show a significant drop in ZF1 fluorescence compared to the control (section 3.1.3). Thus, the ZF1 mediated degradation technique is more sensitive than the cytoplasmic diffusion assay. This also provides further evidence that the end of cytoplasmic diffusion is not equivalent to abscission. Thinning of the intercellular bridge could end diffusion between the daughter cells without the membrane being cut on either side of the midbody. Alternatively, endosomal and secretory vesicles accumulating at the midbody could serve as a diffusion barrier before abscission [23]. Although *tsg-101* are also abscission mutants, we did not see as severe a drop in fluorescence as in septin mutants, but instead a slow, continuous drop. This could be due to RNAi used for ESCRT being an incomplete knockdown. However, it is consistent with a previous report suggesting that septin and ESCRT are involved in distinct sequential contractile machineries that coordinate successful abscission [40].
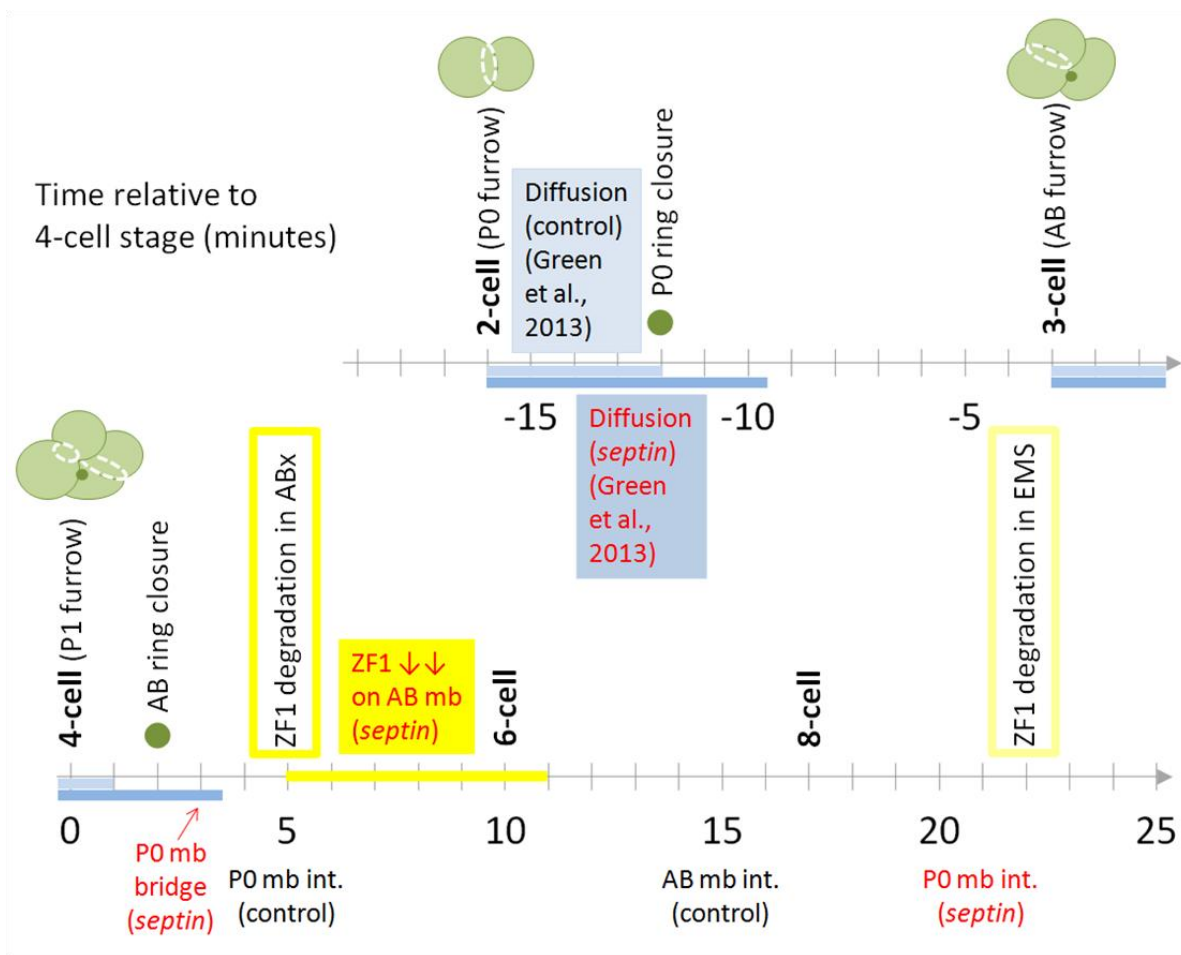
Fig. 31: The timeline depicts early embryonic cell stages relative to 4-cell stage in minutes. Contractile ring closure of the AB midbody takes place right before the onset of ZF1 degradation in ABx. In septin mutants, a drop of ZF1 fluorescence on the AB midbody (mb) can be observed for ~6 minutes. "mb int." stands for time of midbody internalisation.

Although the ZF1 technique works well for probing connections to the AB midbody, it could not be applied to the P0 or P1 midbody. In germ line progenitor cells, ZF1-tagged proteins are not degraded because the ZIF-1 (zinc finger interacting factor 1) protein that targets them for ubiquitination and degradation is not present in germ cells (P0, P1, P2, etc.). For example, the ZIF-1 target PIE-1 is an essential regulator of germ cell fate and is

enriched in the germ line precursor cell [67]. ZIF-1 expression starts in the somatic AB cell after it has separated from the germ line P1 cell.

At the time of ring closure of the P0 midbody, ZIF-1 expression has not yet begun and ZF1 degradation does not yet occur. For the P0 midbody to be accessible to ZF1 degradation in the AB cell, abscission would have to be blocked for more than 15 minutes after midbody remnant formation. Thus, isolation of the P0 midbody from the cytoplasm of the AB cell must happen within 15 minutes of ring closure in septin mutants, because we did not observe a drop in ZF1-tagged NMY-2 fluorescence for the P0 midbody at this stage (see Fig. 14 in 3.1.3 and Fig. 30). Similarly, for the P0 midbody to be accessible to ZF1 degradation in EMS, abscission would have to be blocked for more than 30 minutes after midbody remnant formation. Thus, isolation of the P0 midbody from the cytoplasm of EMS must happen within 30 minutes of ring closure in septin mutants. Otherwise, a fluorescence drop on the P0 midbody would have been seen at the onset of ZF1 degradation. The P0 midbody is internalized around the same time as the onset of ZF1 degradation in EMS, consistent with complete abscission being required for midbody internalization.

As mentioned above, the ZF1 degradation technique cannot be applied to the P1 midbody, which evolves from the division of the germ line progenitor cell P1 into EMS and P2. However, we speculate that if we induced NMY-2 degradation at the time of P0 or P1 midbody formation, we would observe a similar drop in fluorescence as seen in the AB midbody in septin mutants. A possible approach for defining the timing of abscission on P0 and P1 midbodies would be to use the auxin-inducible degradation (AID) system. The AID system is taken from plants, but is also able to induce degradation in *C. elegans.* It requires the expression of TIR1, a plant-specific F-box protein, the substrate recognition component of an ubiquitin ligase complex. Recognition only takes place in the presence of auxin, making temporal control possible through guided auxin exposure [85]. Thus, if we tagged NMY-2 with the AID degron, we could control the timing of degradation by adding the hormone auxin. This would allow us to determine the precise timing of midbody release from all cells.

In conclusion, we observed a delay in abscission by several minutes in septin and ESCRT mutants, but did not observe multinucleation due to abscission failure. We show that the ZF1 degradation technique can be used to sensitively detect a connection between the midbody and the cytoplasm, thus sensitively detecting abscission defects. Furthermore, tagging NMY-2 on the midbody with ZF1 is a helpful technique to elucidate the fate of the P0 and AB midbody. Using additional degron systems could also be helpful to gain further insights into abscission.

4.2. Further applications of the ZF1 degradation technique

In addition to testing the role of proteins in abscission, we also applied the ZF1 degradation assay to test whether autophagy proteins are required to seal the midbody phagosome. We found that ATG-7, LGG-1 and LGG-2 do not play a role in sealing the phagosome from the cytoplasm, as the AB midbody was released normally in *atg-7*-depleted embryos and the phagosome is sealed after internalization, protecting ZF1 on the midbody from degradation (see section 3.4.2). These results demonstrate that midbody phagocytosis and degradation are independent of macroautophagy. They are consistent with the finding by G. Fazeli that midbodies in *lgg-1; lgg-2* double mutants as well as in *atg-7* knockdowns internalize normally, suggesting that phagophore elongation does not play a role in phagocytosis [29].

The loss of ZF1 fluorescence in *atg-7* ~10 minutes after internalization is likely to be because acidification of the phagosome takes place, as G. Fazeli has observed in control embryos. The fluorescence of the GFP variant used in the NMY-2::GFP::ZF1 construct is known to be sensitive to pH [29]. Acidification of the midbody despite the lack of autophagy proteins further supports that the midbody is sealed in a phagosome, as an unsealed phagosome would not be able to acidify. This provides additional evidence that the midbody is not released into the cytoplasm. Thus, consistent with their lack of a role in midbody internalization, autophagy proteins like LGG-1, LGG-2 and ATG-7 are not needed to seal the midbody phagosome. Rather, they are recruited to the sealed phagosome for degradation of the midbody phagosome.

Thus, the ZF1-mediated degradation technique delivers valuable insights on the fate of the midbody by revealing connections to the cytoplasm. These findings strongly suggest that the midbody is not resolved by macroautophagy, which is consistent with our model of abscission on both sides of the midbody, followed by midbody internalization via phagocytosis (see 4.7).

4.3. Delay in midbody internalization in septin mutants

In addition to the abscission defect, we also observed a significant delay in midbody internalization times in our septin-depleted *C. elegans* embryos. In contrast to our data, Green et al. reported that UNC-59 is essential for internalization of the P0 midbody [42]. They predicted that abscission had not occurred in *unc-59* knockdown mutants because they did not observe midbody internalization. One possible explanation for the different observations made on midbody internalization in septin mutants is the different methods used to create *unc*-59 mutants. Green et al. injected dsRNA into wild type animals [42], while we fed a mutant strain with dsRNA. These techniques could give rise to different efficiencies in UNC-59 knockdown. However, Green et al. reported midbody internalization failure in septin mutants based on analysis of midbody internalization only through the four-cell stage. By analyzing midbodies through the 15-cell stage, we revealed that midbodies in septin mutants do internalize, albeit with a significant delay. To be sure that internalization of the midbodies would be completely blocked in the absence of septins, it would be necessary to create a complete deletion allele of *unc-59* or *unc-61* and analyze midbody internalization in this deletion strain. Although interesting, this experiment may be technically difficult as our RNAi results suggest that these mutant worms would likely be sterile.

The bridge phenotype seen in the P0 midbody offers a possible explanation for the observed delay in internalization in the first three midbodies in early *C. elegans* embryos. We propose that through disturbed abscission, the midbody remains attached to at least one daughter cell, while another cell begins to internalize it (Fig. 30 part 5). Internalization of

the midbody suggests that daughter cell separation always completed in our abscission mutant embryos. There are two possible explanations for this.

First, abscission could be slowed in septin mutants, but not completely blocked. We estimate this delay to be 3-15 minutes compared to the control. This is consistent with the delays in internalization times of the midbodies (see section 3.1.1). Internalization of the P0 midbody is delayed by 16 minutes (all P0 midbodies) to 25 minutes (P0 midbodies with bridge phenotype) in septin mutants. Similarly, internalization of the AB midbody is delayed by 13 minutes relative to control embryos. Therefore, abscission could complete with a delay and subsequently allow phagocytosis of the released midbody.

A second possibility is that phagocytosis could force the completion of abscission in septin mutants. Abdu et al. found that *C. elegans* primordial germ cells form lobes that are removed and digested by endodermal cells. Endoderm cells phagocytose lobes before they are released from germ cells with the help of molecular mechanisms that resemble vesicle endocytosis. F-actin and dynamin accumulate at lobe necks and subsequently lobe scission takes place. Thus, proteins like dynamin have to resolve four membranes instead of just two as in scission of endocytic vesicles [86]. Similarly, in the model as shown in Fig. 30, four membranes need to be resolved before the midbody can be released and phagocytosed. Thus, phagocytosis could also complete scission when abscission fails in septin mutant *C. elegans* embryos. An interesting future experiment could be to block phagocytosis in septin mutants, as then abscission can no longer be rescued, possibly resulting in ZF1 degradation on the P0 midbody or even multinucleated cells due to failure of abscission.

Overall, the bridge phenotype provides further evidence that abscission normally takes place on both sides of the midbody (Fig. 29). In septin mutants, abscission is disturbed and therefore phagocytosis of the released midbodies takes longer to complete (Fig. 30).

In contrast to the P0 midbody, a bridge phenotype was not seen for the AB and P1 midbodies. Since the AB midbodies rapidly lost their GFP fluorescence due to ZF1 degradation, tracking of this midbody was limited. Indeed, we regularly observed that fluorescence disappeared or almost disappeared before the normal time of AB midbody

internalization. A follow up experiment could be to analyze septin mutant embryos with midbodies marked with an NMY-2 reporter lacking the ZF1 tag. This would allow better tracking of the AB midbody and its internalization phenotype.

In addition to the AB midbody, we also did not observe a bridge phenotype for the P1 midbody. A possible explanation is that the bridge was too small to be seen with the limited resolution of our wide-field microscopy. Consistent with this idea, the daughter cells of the AB and P1 cell division are smaller than the P0 division. The P0 midbody bridge measured 1.5-2 μm, but the AB cells have higher surface tension and appear to push the P0 midbody into EMS. This difference in cortical tension also does not occur between EMS and P2, the daughter cells of P1. Imaging these mutants with super-resolution techniques could reveal bridges on the AB and P1 midbody. We think the bridge phenotype is likely to occur, as internalization is significantly delayed for the AB and P1 midbodies. Thus, further investigations are required to determine why the bridge phenotype was only observed with the P0 midbody.

Another possibility is that we do not see a bridge for other midbodies because our mutants are not null. Thus, it would be interesting to analyze the extent of the bridge phenotype in an *unc-59* null allele. The two *C. elegans* septins, UNC-59 and UNC-61, are thought to form heterodimers and then filaments together [37]. Previously it had been shown that *unc-61* mutants have a stronger phenotype than *unc-59(e261)* [87], which could either mean that UNC-61 protein has roles independent of UNC-59 or alternatively that the *e261* mutant is hypomorphic. The mutation *e261* is a missense allele of the septin *unc-59* and Nguyen et al. showed that UNC-59 protein is still expressed in *e261* mutants [34]. Therefore, we additionally treated the WEH132 strain bearing the *e261* allele with *unc-59* or *unc-61* RNAi in order to create a stronger loss-of-function phenotype. Our observation of increased sterility in RNAi treated worms, the bridge phenotype and later internalization times in *unc-59* treated with *unc-59* RNAi shows that the *e261* mutation is not a null allele. However, as we observed large variability in midbody internalization times after adding *unc-59* RNAi, our septin mutants treated with RNAi are probably still not a complete null. Therefore, the

e261 mutation is a hypomorphic or partial loss-of-function allele and it is plausible that a bridge phenotype could be seen for other midbodies in *unc-59* null allele.

In conclusion, we found that in septin mutants, abscission completes with a delay of 3-15 minutes, resulting in similar delays in phagocytosis. It would be interesting to look at true *unc-59* nulls to further understand the role of septins in *C. elegans* embryos.

4.4. Septins and human diseases

In humans, the septin family GTPases have a broad variety of functions, depending on the isoform of the septin and its interaction partners. Among others, functions in cell division, chromosome segregation, protein scaffolding, cell polarity and motility, membrane dynamics, vesicle trafficking, exocytosis, apoptosis, and the DNA damage response have been reported (reviewed in [88]). Thus, it is not surprising that various human diseases have been associated with septins.

Much has been discovered, especially in the field of neurological diseases, including observations of septins associating with Alzheimer-specific neurofibrillary tangles [89] or interacting with Parkin, the loss of which is thought to play a pathogenic role in Parkinson's disease [90]. Furthermore, mutations in SEPT9, which is thought to have a role in completing cytokinesis as well as structural functions [91, 92], have been found to cause hereditary neuralgic amyotrophy, a rare autosomal dominant disorder. This was the first monogenetic disease described to be caused by mutations in a gene of the septin family [93].

SEPT2 and SEPT11 are involved in the entry of intracellular organisms such as *Listeria* into non-phagocytic cells. Interestingly, while the first is essential for invasion, the latter restricts it [94, 95], demonstrating again the diversity of septin functions.

Several associations with oncogenesis have been discovered for septins thus far. Multiple septin genes have been identified as fusion partners of the mixed lineage leukemia protooncogene in acute myeloid leukemia [96], originally the first association of septins to

neoplasia. Also, SEPT4 acts as a tumor suppressor in leukemias and solid tumors: SEPT4 can promote apoptosis [97] and is associated with inhibition of colorectal carcinoma tumorigenesis [98]. SEPT2 has been associated with Von Hippel-Lindau, a cancer predisposition syndrome [99].

Thus, septins have many essential cellular and molecular functions in humans. Much remains to be elucidated. A deepened understanding of how septins work could help us comprehend the pathogenesis of diseases like Alzheimer's, listeriosis and neoplasia.

4.5. Delayed cell cycle in class III PI3K complex mutants

The class III PI3K complex has different known roles in membrane trafficking, including during abscission, phagocytosis and macroautophagy [27-29, 31]. Previously, a developmental delay in mutants for the PI3K subunit BEC-1 had been observed, but not quantified [100]. We quantified the delay in cell cycle progression in embryos of two PI3K mutants *bec-1* and *vps-34* and tested possible causes for the delay.

The analyses of this work showed that the significant developmental delay in PI3K mutants could not be attributed to slowed cytokinetic ring contraction (see section 3.2.3). Furthermore, we tested for a role of PI3K in abscission using the ZF1 degradation assay as a method to detect a possible defect in abscission, as discussed above. In *bec-1* mutants, fluorescence analyses showed no fluorescence drop of NMY-2::GFP::ZF1 on the AB midbody in contrast to *unc-59*/septin mutants (3.2.4.). Thus, in contrast to previously published evidence that PI3K is involved in abscission in mammalian cells [30], PI3K is not required for isolation of the midbody from the cytoplasm of daughter cells and is therefore not required for abscission in *C. elegans*. Since abscission is not delayed according to the ZF1 degradation assay, it is not a likely cause for the cell cycle delay. Moreover, we found that septin mutants have a normal cell cycle time, despite their abscission defects. Therefore, we show that the delay in cell cycle progression in PI3K mutants is not due to a delay in cytokinesis and propose that it is due to a delay during another phase of the cell cycle.

Additional analyses of G. Fazeli showed that midbodies of *bec-1* and *vps-34* mutants failed to internalize and ZF1 reporter fluorescence on the midbody remained steady, just as in *ced-1* phagocytosis mutants. We concluded that PI3K is involved in midbody phagocytosis [29]. However, my results showed that phagocytosis mutants also did not show a delay in cell cycle time. Thus, it is not likely that the cell cycle delay in PI3K mutants is due to its role in midbody phagocytosis. In the end, the delay could be caused by another membrane trafficking event. Considering the complex roles of the class III PI3K complex, the delay could also be due to a sum of delays at various times during the cell cycle.

Furthermore, we found that exposure to high-intensity excitation light during fluorescence microscopy did not bias our cell cycle results (see section 3.2.2). This is consistent with a report by Tinevez et al., who showed that lengthening of cell division times is not the main effect of light exposure. Rather, the embryo arrests upon reaching a threshold of exposure [101]. Thus, although intense light exposure is toxic for live cells [81], this was of no relevance for the observed slower developing embryos such as PI3K mutants in our experiments, where light exposure was not intense.

As *bec-1* and *vps-34* are components of the same complex, we expected both mutations to lead to a similar delay in cell cycle time. However, we found a delay of 28% in *bec-1* and 16% in *vps-34* (see section 3.2.1). The *vps-34* mutants are rescued with an extrachromosomal array carrying the wild type *vps-34* gene. Though repetitive DNA sequences are normally turned off in the germ line [102], it remains possible that these mutants inherited some maternal *vps-34* protein transcribed from the array. In contrast, the *bec-1* mutants do not have any copies of the wild type *bec-1* gene as they are simple deletion mutants. Furthermore, *bec-1* homozygous mutants arrest at late larval stage or at adult stage [103], while *vps-34* mutants arrest at early larval stage [104], showing that the proteins do not behave identically. This could mean that BEC-1 and VPS-34 have independent functions. However, this could also indicate that BEC-1 protein is more stable than VPS-34. Thus, there are multiple possible explanations why the extent of cell cycle delay was stronger in *bec-1* than in *vps-34*. Thus, the cause of the developmental delay in

75

C. elegans PI3K mutants remains to be determined, and it will be interesting to uncover how these two subunits of the class III PI3K complex contribute to cell cycle progression.

4.6. Roles of the midbody remnant

Motivated by recent reports suggesting that post-mitotic midbody positioning impacts cell polarity and cell fate [46, 60, 61], we analyzed the change of position of the P0 midbody in several control and mutant *C. elegans* embryos. Our results confirmed dorsoventral movement of the P0 midbody in control embryos, however, they were not as strong as found by Singh and Pohl [61]. Even after elongating the observation time by 40 seconds, dorsoventral movement was not as stereotypical as expected (see section 3.3).

Furthermore, it was unclear whether the midbody was moving or moved by the movement of the neighboring cells. Singh and Pohl ablated the cortex of the AB cell with a pulsed UV laser to prevent midbody movement, and also ablated the midbody to show its role in dorsoventral axis formation through mediating spindle rotation in P1 [61]. However, laser ablation of the midbody is likely to damage neighboring regions as well, leaving these results open to interpretation. Furthermore, how the P0 midbody remnant would regulate dorsoventral axis formation in *C. elegans* remains unclear.

Apart from dorsoventral movement, several other exciting signaling roles of the midbody have been proposed. Accumulation of midbodies in tumor cells has been found to be associated with higher tumorigenicity [46]. Pluripotent stem cells and cancer cells tend to accumulate midbodies in culture, thus midbody inheritance could play a role in stem cell status [45, 46]. Moreover, stem cells have also been found to release midbodies *in vivo* [48]. However, it remains to be determined how the midbody or related factors impact stem cell behaviour, as these correlations may or may not be causative. Salzmann et al. made interesting observations on midbody inheritance in *Drosophila* germline stem cells (GSC). While male GSCs release the midbody and leave inheritance up to the differentiating daughter cell, female GSCs inherit the midbody. Thus, it is unlikely that the midbody is a determinant of stem cell fate. These results show that midbody inheritance is highly

stereotyped, yet varies depending on the cell type [53]. Furthermore, these examples demonstrate that midbody fate needs to be tightly regulated, but that different cells can choose different fates [59, 105].

Recent studies by Bernabe-Rubio et al. found the midbody to play a role in primary ciliogenesis in polarized epithelial cells [106]. The midbody moves along the apical surface to meet the centrosome and thereby enables cilium formation. Defects in ciliary function cause diverse human developmental and degenerative disorders [107]. Therefore, it is important to understand where the midbody is positioned and how it is able to signal to a cell.

Thus, the midbody remnant is more than a leftover byproduct of cytokinesis. Determining whether abscission occurs on one or both sides of the midbody is relevant because signaling proteins of the midbody could be a potential source of misregulation of cellular functions. The midbody should at no point have unchecked access to the cytoplasm. By showing that the midbody is regularly released extracellularly through bilateral abscission in *C. elegans* embryos, we provide insights into the cell's strategy to safely resolve the midbody. That the released midbody is rapidly internalized by a daughter cell or neighboring cell and not left in the extracellular space, further underlines the importance of this strategy.

4.7. New model of midbody fate

Previously it had been suggested that macroautophagy plays a role in midbody degradation [45, 46]. We investigated the fate of the midbody after internalization and showed that autophagy proteins are not involved in macroautophagy during midbody degradation.

LGG-1 and LGG-2 are proteins classically associated with autophagy, as they are required for elongation of the phagophore membrane [74]. My workgroup showed that LGG-1 and LGG-2 are indeed required for degradation of the midbody [29]. However, I found that the *C. elegans* homolog of ULK1, UNC-51, does not play a role in degradation of the midbody (see section 3.4.1). ULK1 is responsible for the initiation of macroautophagy, but is not

77

required for LC3-associated phagocytosis (LAP) [56]. My results were further confirmed in my workgroup with another *unc-51* mutant allele, as well as a deletion in a second macroautophagy-specific regulator, the Atg14 homolog *epg-8* [29, 57]. G. Fazeli discovered that the disappearance time of the P0 midbody in *unc-51(e1189)* and *epg-8(e1189)* was also not significantly different from controls. My fluorescence measurements in *unc-51(e369)* mutants established a basis for validating these disappearance times and concluding that macroautophagy-specific genes are not involved in midbody degradation. Thus, we proposed that LGG-1 and LGG-2 mediate maturation of the midbody phagosome independent of macroautophagy, but instead via LAP, which was a novel discovery by our group.

Taken together, we propose the following new model for midbody fate: the ZF1-degradation technique *in vivo* showed that midbodies are released into the extracellular space, with abscission happening on both sides of the midbody. Released midbodies are internalized by receptor-mediated phagocytosis. The PI3K complex recruits LC3 to the midbody phagosome, leading to fusion of the phagosome with lysosomes for degradation of the midbody [29]. Thus, VPS-34, BEC-1, ATG-7, LGG-1 and LGG-2 mediate the maturation of the midbody-phagosome via LAP.

In both macroautophagy and LAP, a second membrane must be degraded with the help of LC3 proteins. In macroautophagy, the phagophore consists of a double membrane starting to form near the endoplasmic reticulum (reviewed in [108]). In LAP, one membrane is wrapped around the cell corpse [55, 56] or the midbody and the other is derived from engulfment. Therefore, the double membrane observed around cytoplasmic mammalian midbodies [48] is consistent with both macroautophagy and LAP models.

The LAP model is consistent with the observed roles of proteins involved in both phagocytosis and autophagy in midbody degradation in *C. elegans*, *Drosophila,* and mammals [45, 50, 52, 53]. Analyzing the role of ULK1 and ATG14 allowed us to distinguish between macroautophagy and LAP. No one had previously tested a role for ULK1 or ATG14 in midbody degradation in any species. Therefore, it remains unclear

whether internalized midbodies in other species are degraded via macroautophagy. Midbody release followed by LAP could be the primary *in vivo* fate of midbodies in animals.

Various human diseases are connected to a defect in autophagy (reviewed in [109]). Since autophagy and LAP share many proteins, it will be interesting to see to what extent a role for LAP in human diseases will be uncovered in the future. For example, LAP has been shown to be responsible for degradation of shed photoreceptor outer segments by the retinal pigment epithelium, which is important for ensuring the function and longevity of the photoreceptors [110]. Furthermore, LAP eliminates engulfed dying cells in mice and when LAP fails, inflammatory cytokine production is increased, resulting in a lupus-like syndrome. Thus, LAP is involved in inflammatory responses and protects mice from lupus [111]. This raises the question, whether LAP possibly protects embryonic cells from inflammatory signals by the midbody. Given the possible signaling roles of the midbody, exploring its fate and the role of LAP in midbody degradation in other organisms is a path worth further investigation.

5. Conclusion

Abscission marks the last step of cytokinesis and gives rise to two physically separated daughter cells and a midbody remnant. As midbodies have important signaling roles during and perhaps even after cytokinesis, they need to be carefully resolved. We further developed the ZF1-tag technique to elucidate the fate of the midbody and test whether midbodies are released into the extracellular space in *C. elegans* embryos. Similar degron strategies could be a sensitive technique to apply to studying abscission and the fate of the midbody in mammalian cells in the future.

We applied the ZF1 technique to detect abscission defects in septin and ESCRT mutants. Using a ZF1-tagged midbody reporter, I confirmed that septins are required for proper abscission in *C. elegans* embryos and revealed that midbodies are hindered from release in septin mutants, resulting in delayed internalization of the midbodies. The ZF1 reporter diminished rapidly on midbodies in septin mutants, demonstrating that a connection to the cytoplasm remained, while in control embryos it was protected from degradation. The ZF1 reporter on midbodies in ESCRT mutants diminished similarly. Thus, the ZF1 mediated degradation technique can sensitively detect connections between the midbody and the cytoplasm as in abscission defects. Moreover, these findings show that midbodies are regularly released into the extracellular space before internalization and do not remain attached to the cytoplasm of one daughter cell.

The internalization delay in septin mutants was associated with the so-called bridge phenotype, where the midbody is still attached to one cell, while another begins to internalize it. The bridge phenotype provides further evidence that abscission normally takes place on both sides of the midbody. In septin mutants, abscission is disturbed and therefore phagocytosis of the released midbodies takes longer to complete. Given that the midbody eventually internalizes, we propose that abscission could either be slowed in septin mutants, or alternatively another mechanism like phagocytosis could cause the completion of abscission. Further research is required to test whether phagocytosis can rescue abscission defects in *C. elegans* and possibly other organisms. In humans, abscission marks a crucial step of cytokinesis and has been linked to promoting tumorigenesis. Septins

have many essential functions beyond abscission. A deeper understanding of the mechanisms of abscission and of how septins work could therefore help us comprehend the pathogenesis of many human diseases.

Using the ZF1 degradation assay, we also found that the class III PI3K complex is not required for abscission in *C. elegans*. Rather, my workgroup showed that it is required for phagocytosis of the released midbody and after internalization for recruitment of LGG-1/2 to the phagosome. Further experiments on the fate of the midbody after internalization revealed that unlike previously proposed, midbody degradation is independent of macroautophagy. A key finding leading to this conclusion was that ULK1/UNC-51, a protein required specifically for macroautophagy, does not play a role in the degradation of the midbody in *C. elegans*. Furthermore, we found that the autophagy proteins ATG-7, LGG-1 and LGG-2 are not required to seal the midbody phagosome. These results served as a foundation for the novel discovery that LGG-1 and LGG-2 mediate the maturation of the midbody phagosome via LC3-associated phagocytosis (LAP). LAP is a non-canonical autophagy pathway where autophagy proteins help mature phagosomes. It is consistent with the observed roles of phagocytic and autophagic proteins during midbody degradation in worms, flies, and mammals. Thus, although more research is required to confirm this hypothesis in other species, midbody release followed by LAP is likely to be the primary *in vivo* fate of midbodies in animals.

Taking all findings together, we propose that midbodies are released into the extracellular space, with abscission happening on both sides of the midbody. Released midbodies are then internalized by phagocytosis. The PI3K complex recruits LC3 to the midbody phagosome, facilitating the fusion of the phagosome with lysosomes for degradation of the midbody via LAP.

This work contributes to resolving the previously debated fate of the midbody during and after abscission. Considering the importance of abscission and the potential signaling roles of the midbody, the fate of the midbody will continue to be a promising area to explore in future work.

6. Zusammenfassung

Durch Abszission, den letzten Schritt der Zytokinese, entstehen zwei physisch voneinander getrennte Tochterzellen und ein Mittelkörper, auch Flemming-Körper oder Midbody genannt. Der Midbody muss sorgfältig beseitigt werden, insbesondere in Hinblick auf verschiedene Signalrollen, die dem Midbody während und möglicherweise auch nach der Zytokinese zugeschrieben werden. Um das Schicksal des Midbodys zu klären und zu testen, ob Midbodies in den extrazellulären Raum freigesetzt werden, wurde hier die sogenannte ZF1-vermittelte Abbautechnik in *C. elegans* Embryonen weiter entwickelt und angewendet. Ähnliche Degradationsstrategien könnten als sensitive Techniken dienen, um zukünftig Abszission und das Schicksal des Midbodys in Säugetierzellen zu studieren.

Die ZF1-Technik wurde eingesetzt, um Abszissionsdefekte in Septin- und ESCRT-Mutanten zu detektieren. Mithilfe eines ZF1-markierten Midbody-Reporters konnte ich bestätigen, dass Septine für eine ungestörte Abszission in *C. elegans* Embryonen erforderlich sind. Die Untersuchungen zeigten auch, dass die Freilassung der Midbodies in Septin Mutanten gehindert ist, was zu einer verzögerten Internalisierung der Midbodies führte. Während der ZF1 Reporter der Midbodies in Kontrollembryonen vor dem Abbau geschützt war, nahm er in Septin-Mutanten rasch ab, was auf eine verbleibende Verbindung zum Zytoplasma hinweist. In ESCRT-Mutanten nahm der ZF1 Reporter der Midbodies ebenso ab. Daher kann die ZF1-vermittelte Abbautechnik zum sensitiven Detektieren von Verbindungen zwischen dem Midbody und dem Zytoplasma, so wie bei Abszissionsdefekten, eingesetzt werden. Zusätzlich konnte damit gezeigt werden, dass Midbodies regulär in den Extrazellularraum freigesetzt und im Anschluss internalisiert werden und dabei keine Verbindung zum Zytoplasma einer der Tochterzellen bestehen bleibt.

Die signifikant verzögerte Internalisierungszeit der Midbodies in Septin-Mutanten war außerdem mit dem sogenannten Brücken-Phänotyp assoziiert, bei dem der Midbody noch mit einer Tochterzelle verbunden ist, während eine andere Zelle beginnt, diesen zu internalisieren. Dieser Phänotyp liefert weitere Evidenz, dass Abszission normalerweise auf beiden Seiten des Midbodys stattfindet. In Septin-Mutanten führt die gestörte Abszission

dazu, dass die Phagozytose des freigelassenen Midbodys nur verzögert abgeschlossen werden kann. Da der Midbody letztendlich internalisiert wird, könnte Abszission in Septin-Mutanten lediglich verlangsamt sein, oder aber ein anderer Mechanismus wie z.B. Phagozytose könnte die Vollendung der Abszission herbeiführen. Weitere Untersuchungen sind erforderlich um zu testen, ob Phagozytose in *C. elegans* Embryonen und möglicherweise anderen Organismen Abszissionsdefekte retten kann. Beim Menschen ist Abszission ein entscheidender Schritt der Zytokinese und eine Verbindung zur Tumorgenese konnte bereits gezeigt werden. Septinen werden viele wesentliche Funktionen, auch über Zytokinese hinaus, zugeschrieben. Ein tieferes Verständnis der Mechanismen, die zu Abszission führen, und der Aufgaben von Septinen könnten daher dazu beitragen, die Pathogenese vieler Krankheiten beim Menschen besser zu begreifen.

Mithilfe der ZF1-Technik konnte auch gezeigt werden, dass der Klasse III PI3K Komplex nicht notwendig ist für Abszission. Meine Arbeitsgruppe bestätigte jedoch seine Rolle in der Phagozytose des freigesetzten Midbodys und in der Rekrutierung von LGG-1/2 zum Phagosom nach der Internalisierung. Weitere Experimente zum Erforschen des Schicksals des Midbodys nach der Internalisierung ergaben, dass im Gegensatz zu vorherigen Annahmen der Abbau von Midbodies unabhängig von Makroautophagie geschieht. Eine Schlüsselentdeckung war, dass ULK1/UNC-51, ein Protein, das spezifisch für Makroautophagie benötigt wird, keine Rolle im Abbau des Midbodys in *C. elegans* spielt. Des Weiteren sind die Autophagieproteine ATG-7, LGG-1 und LGG-2 nicht für das Abdichten des Midbodyphagosoms erforderlich. Diese Ergebnisse dienten als Basis für die neue Entdeckung, dass LGG-1 und LGG-2 die Reifung des Midbodyphagosoms mittels LC3-assoziierter Phagozytose (LAP) vermitteln. LAP ist ein nicht-kanonischer Autophagie-Pathway, bei dem Autophagieproteine am Heranreifen von Phagosomen beteiligt sind. Er ist stimmig mit der beobachteten Beteiligung von Phagozytose- und Autophagieproteinen am Midbodyabbau in Würmern, Fliegen und Säugetieren. Auch wenn noch weitere Forschung erforderlich ist, um diese Hypothese in anderen Spezies zu bestätigen, ist die Freilassung der Midbodies, gefolgt von LAP, möglicherweise das primäre Schicksal von Midbodies *in vivo* in Tieren.

Zusammengefasst schlagen wir vor, dass Midbodys durch Abszission auf beiden Seiten des Midbodys in den Extrazellularraum freigelassen werden. Die freigelassenen Midbodies werden dann mittels Phagozytose internalisiert. Mittels LAP rekrutiert der PI3K Komplex LC3 zum Midbodyphagosom, was folglich zur Fusion des Phagosoms mit Lysosomen für die Vollendung des Abbaus führt.

Diese Arbeit liefert einen wichtigen Beitrag zum Aufdecken des zuvor umstrittenen Schicksals des Midbodys während und nach Abszission. In Anbetracht der Bedeutung von Abszission und möglicher Signalrollen des Midbodys, ist das Schicksal des Midbodys weiterhin ein vielversprechendes Forschungsgebiet.

7. References

1. Green, R.A., E. Paluch, and K. Oegema, *Cytokinesis in animal cells.* Annu Rev Cell Dev Biol, 2012. **28**: p. 29-58.
2. Normand, G. and R.W. King, *Understanding cytokinesis failure.* Adv Exp Med Biol, 2010. **676**: p. 27-55.
3. Brown, H.M., A.E. Knowlton, and S.S. Grieshaber, *Chlamydial infection induces host cytokinesis failure at abscission.* Cell Microbiol, 2012. **14**(10): p. 1554-67.
4. Xavier de Carvalho, A., et al., *Reed-Sternberg cells form by abscission failure in the presence of functional Aurora B kinase.* PLoS One, 2015. **10**(5): p. e0124629.
5. Gordon, D.J., B. Resio, and D. Pellman, *Causes and consequences of aneuploidy in cancer.* Nat Rev Genet, 2012. **13**(3): p. 189-203.
6. Bement, W.M., H.A. Benink, and G. von Dassow, *A microtubule-dependent zone of active RhoA during cleavage plane specification.* J Cell Biol, 2005. **170**(1): p. 91-101.
7. Watanabe, S., et al., *mDia2 induces the actin scaffold for the contractile ring and stabilizes its position during cytokinesis in NIH 3T3 cells.* Mol Biol Cell, 2008. **19**(5): p. 2328-38.
8. Matsumura, F., *Regulation of myosin II during cytokinesis in higher eukaryotes.* Trends Cell Biol, 2005. **15**(7): p. 371-7.
9. Reichl, E.M., et al., *Interactions between myosin and actin crosslinkers control cytokinesis contractility dynamics and mechanics.* Curr Biol, 2008. **18**(7): p. 471-80.
10. Field, C.M. and B.M. Alberts, *Anillin, a contractile ring protein that cycles from the nucleus to the cell cortex.* J Cell Biol, 1995. **131**(1): p. 165-78.
11. Piekny, A.J. and A.S. Maddox, *The myriad roles of Anillin during cytokinesis.* Semin Cell Dev Biol, 2010. **21**(9): p. 881-91.
12. Joo, E., M.C. Surka, and W.S. Trimble, *Mammalian SEPT2 is required for scaffolding nonmuscle myosin II and its kinases.* Dev Cell, 2007. **13**(5): p. 677-90.
13. Mavrakis, M., et al., *Septins promote F-actin ring formation by crosslinking actin filaments into curved bundles.* Nat Cell Biol, 2014. **16**(4): p. 322-34.
14. Carvalho, A., A. Desai, and K. Oegema, *Structural memory in the contractile ring makes the duration of cytokinesis independent of cell size.* Cell, 2009. **137**(5): p. 926-37.
15. Mierzwa, B. and D.W. Gerlich, *Cytokinetic abscission: molecular mechanisms and temporal control.* Dev Cell, 2014. **31**(5): p. 525-38.
16. Guizetti, J., et al., *Cortical constriction during abscission involves helices of ESCRT-III-dependent filaments.* Science, 2011. **331**(6024): p. 1616-20.
17. Schiel, J.A., et al., *FIP3-endosome-dependent formation of the secondary ingression mediates ESCRT-III recruitment during cytokinesis.* Nat Cell Biol, 2012. **14**(10): p. 1068-78.
18. Carlton, J.G. and J. Martin-Serrano, *Parallels between cytokinesis and retroviral budding: a role for the ESCRT machinery.* Science, 2007. **316**(5833): p. 1908-12.

19. Carlton, J.G., M. Agromayor, and J. Martin-Serrano, *Differential requirements for Alix and ESCRT-III in cytokinesis and HIV-1 release.* Proc Natl Acad Sci U S A, 2008. **105**(30): p. 10541-6.

20. Elia, N., et al., *Computational model of cytokinetic abscission driven by ESCRT-III polymerization and remodeling.* Biophys J, 2012. **102**(10): p. 2309-20.

21. Elia, N., et al., *Dynamics of endosomal sorting complex required for transport (ESCRT) machinery during cytokinesis and its role in abscission.* Proc Natl Acad Sci U S A, 2011. **108**(12): p. 4846-51.

22. Schiel, J.A., et al., *Endocytic membrane fusion and buckling-induced microtubule severing mediate cell abscission.* J Cell Sci, 2011. **124**(Pt 9): p. 1411-24.

23. Gould, G.W. and J. Lippincott-Schwartz, *New roles for endosomes: from vesicular carriers to multi-purpose platforms.* Nat Rev Mol Cell Biol, 2009. **10**(4): p. 287-92.

24. Schiel, J.A. and R. Prekeris, *Membrane dynamics during cytokinesis.* Curr Opin Cell Biol, 2013. **25**(1): p. 92-8.

25. Kinchen, J.M., et al., *A pathway for phagosome maturation during engulfment of apoptotic cells.* Nat Cell Biol, 2008. **10**(5): p. 556-66.

26. Campa, C.C., et al., *How PI3K-derived lipids control cell division.* Front Cell Dev Biol, 2015. **3**: p. 61.

27. Funderburk, S.F., Q.J. Wang, and Z. Yue, *The Beclin 1-VPS34 complex--at the crossroads of autophagy and beyond.* Trends Cell Biol, 2010. **20**(6): p. 355-62.

28. Levine, B., et al., *Beclin orthologs: integrative hubs of cell signaling, membrane trafficking, and physiology.* Trends Cell Biol, 2015. **25**(9): p. 533-44.

29. Fazeli, G., et al., *C. elegans midbodies are released, phagocytosed and undergo LC3-dependent degradation independent of macroautophagy.* J Cell Sci, 2016. **129**(20): p. 3721-3731.

30. Sagona, A.P., et al., *PtdIns(3)P controls cytokinesis through KIF13A-mediated recruitment of FYVE-CENT to the midbody.* Nat Cell Biol, 2010. **12**(4): p. 362-71.

31. Schink, K.O., K.W. Tan, and H. Stenmark, *Phosphoinositides in Control of Membrane Dynamics.* Annu Rev Cell Dev Biol, 2016. **32**: p. 143-171.

32. Hartwell, L.H., *Genetic control of the cell division cycle in yeast. IV. Genes controlling bud emergence and cytokinesis.* Exp Cell Res, 1971. **69**(2): p. 265-76.

33. Mostowy, S. and P. Cossart, *Septins: the fourth component of the cytoskeleton.* Nat Rev Mol Cell Biol, 2012. **13**(3): p. 183-94.

34. Nguyen, T.Q., et al., *The C. elegans septin genes, unc-59 and unc-61, are required for normal postembryonic cytokineses and morphogenesis but have no essential function in embryogenesis.* J Cell Sci, 2000. **113 Pt 21**: p. 3825-37.

35. Kinoshita, M., *Assembly of mammalian septins.* J Biochem, 2003. **134**(4): p. 491-6.

36. Hall, P.A., et al., *Expression profiling the human septin gene family.* J Pathol, 2005. **206**(3): p. 269-78.

37. John, C.M., et al., *The Caenorhabditis elegans septin complex is nonpolar.* EMBO J, 2007. **26**(14): p. 3296-307.

38. Weirich, C.S., J.P. Erzberger, and Y. Barral, *The septin family of GTPases: architecture and dynamics.* Nat Rev Mol Cell Biol, 2008. **9**(6): p. 478-89.

39. Spiliotis, E.T. and A.S. Gladfelter, *Spatial guidance of cell asymmetry: septin GTPases show the way.* Traffic, 2012. **13**(2): p. 195-203.

40. Renshaw, M.J., et al., *Anillin-dependent organization of septin filaments promotes intercellular bridge elongation and Chmp4B targeting to the abscission site.* Open Biol, 2014. **4**: p. 130190.

41. Estey, M.P., et al., *Distinct roles of septins in cytokinesis: SEPT9 mediates midbody abscission.* J Cell Biol, 2010. **191**(4): p. 741-9.

42. Green, R.A., et al., *The midbody ring scaffolds the abscission machinery in the absence of midbody microtubules.* J Cell Biol, 2013. **203**(3): p. 505-20.

43. Schiel, J.A., C. Childs, and R. Prekeris, *Endocytic transport and cytokinesis: from regulation of the cytoskeleton to midbody inheritance.* Trends Cell Biol, 2013. **23**(7): p. 319-27.

44. Djeddi, A., et al., *Sperm-inherited organelle clearance in C. elegans relies on LC3-dependent autophagosome targeting to the pericentrosomal area.* Development, 2015. **142**(9): p. 1705-16.

45. Pohl, C. and S. Jentsch, *Midbody ring disposal by autophagy is a post-abscission event of cytokinesis.* Nat Cell Biol, 2009. **11**(1): p. 65-70.

46. Kuo, T.C., et al., *Midbody accumulation through evasion of autophagy contributes to cellular reprogramming and tumorigenicity.* Nat Cell Biol, 2011. **13**(10): p. 1214-23.

47. Dubreuil, V., et al., *Midbody and primary cilium of neural progenitors release extracellular membrane particles enriched in the stem cell marker prominin-1.* J Cell Biol, 2007. **176**(4): p. 483-95.

48. Ettinger, A.W., et al., *Proliferating versus differentiating stem and cancer cells exhibit distinct midbody-release behaviour.* Nat Commun, 2011. **2**: p. 503.

49. Arai, Y., et al., *Lipidome of midbody released from neural stem and progenitor cells during mammalian cortical neurogenesis.* Front Cell Neurosci, 2015. **9**: p. 325.

50. Crowell, E.F., et al., *Engulfment of the midbody remnant after cytokinesis in mammalian cells.* J Cell Sci, 2014. **127**(Pt 17): p. 3840-51.

51. Chai, Y., et al., *Apoptotic regulators promote cytokinetic midbody degradation in C. elegans.* J Cell Biol, 2012. **199**(7): p. 1047-55.

52. Ou, G., C. Gentili, and P. Gonczy, *Stereotyped distribution of midbody remnants in early C. elegans embryos requires cell death genes and is dispensable for development.* Cell Res, 2014. **24**(2): p. 251-3.

53. Salzmann, V., et al., *Centrosome-dependent asymmetric inheritance of the midbody ring in Drosophila germline stem cell division.* Mol Biol Cell, 2014. **25**(2): p. 267-75.

54. Sanjuan, M.A., et al., *Toll-like receptor signalling in macrophages links the autophagy pathway to phagocytosis.* Nature, 2007. **450**(7173): p. 1253-7.

55. Florey, O., et al., *Autophagy machinery mediates macroendocytic processing and entotic cell death by targeting single membranes.* Nat Cell Biol, 2011. **13**(11): p. 1335-43.

56. Martinez, J., et al., *Microtubule-associated protein 1 light chain 3 alpha (LC3)-associated phagocytosis is required for the efficient clearance of dead cells.* Proc Natl Acad Sci U S A, 2011. **108**(42): p. 17396-401.

57.   Martinez, J., et al., *Molecular characterization of LC3-associated phagocytosis reveals distinct roles for Rubicon, NOX2 and autophagy proteins.* Nat Cell Biol, 2015. **17**(7): p. 893-906.

58.   Fazeli, G. and A.M. Wehman, *Rab GTPases mature the LC3-associated midbody phagosome.* Communicative & Integrative Biology, 2017. **10**(2): p. e1297349.

59.   Chen, C.T., et al., *Resurrecting remnants: the lives of post-mitotic midbodies.* Trends Cell Biol, 2013. **23**(3): p. 118-28.

60.   Morais-de-Sa, E. and C.E. Sunkel, *Connecting polarized cytokinesis to epithelial architecture.* Cell Cycle, 2013. **12**(23): p. 3583-4.

61.   Singh, D. and C. Pohl, *Coupling of rotational cortical flow, asymmetric midbody positioning, and spindle rotation mediates dorsoventral axis formation in C. elegans.* Dev Cell, 2014. **28**(3): p. 253-67.

62.   Corsi, A.K., B. Wightman, and M. Chalfie, *A Transparent Window into Biology: A Primer on Caenorhabditis elegans.* Genetics, 2015. **200**(2): p. 387-407.

63.   Hochbaum, D., A.A. Ferguson, and A.L. Fisher, *Generation of transgenic C. elegans by biolistic transformation.* J Vis Exp, 2010(42).

64.   Fire, A., et al., *Potent and specific genetic interference by double-stranded RNA in Caenorhabditis elegans.* Nature, 1998. **391**(6669): p. 806-11.

65.   Schneider, S.Q. and B. Bowerman, *Cell polarity and the cytoskeleton in the Caenorhabditis elegans zygote.* Annu Rev Genet, 2003. **37**: p. 221-49.

66.   Gonczy, P., et al., *Dissection of cell division processes in the one cell stage Caenorhabditis elegans embryo by mutational analysis.* J Cell Biol, 1999. **144**(5): p. 927-46.

67.   Reese, K.J., et al., *Asymmetric segregation of PIE-1 in C. elegans is mediated by two complementary mechanisms that act through separate PIE-1 protein domains.* Mol Cell, 2000. **6**(2): p. 445-55.

68.   DeRenzo, C., K.J. Reese, and G. Seydoux, *Exclusion of germ plasm proteins from somatic lineages by cullin-dependent degradation.* Nature, 2003. **424**(6949): p. 685-9.

69.   Nance, J., E.M. Munro, and J.R. Priess, *C. elegans PAR-3 and PAR-6 are required for apicobasal asymmetries associated with cell adhesion and gastrulation.* Development, 2003. **130**(22): p. 5339-50.

70.   Armenti, S.T., et al., *Repurposing an endogenous degradation system for rapid and targeted depletion of C. elegans proteins.* Development, 2014. **141**(23): p. 4640-7.

71.   Wehman, A.M., et al., *The P4-ATPase TAT-5 inhibits the budding of extracellular vesicles in C. elegans embryos.* Curr Biol, 2011. **21**(23): p. 1951-9.

72.   Brenner, S., *The genetics of Caenorhabditis elegans.* Genetics, 1974. **77**(1): p. 71-94.

73.   Lu, N., et al., *Two PI 3-kinases and one PI 3-phosphatase together establish the cyclic waves of phagosomal PtdIns(3)P critical for the degradation of apoptotic cells.* PLoS Biol, 2012. **10**(1): p. e1001245.

74.   Manil-Segalen, M., et al., *The C. elegans LC3 acts downstream of GABARAP to degrade autophagosomes by interacting with the HOPS subunit VPS39.* Dev Cell, 2014. **28**(1): p. 43-55.

75.   Fraser, A.G., et al., *Functional genomic analysis of C. elegans chromosome I by systematic RNA interference.* Nature, 2000. **408**(6810): p. 325-30.

76.   Kamath, R.S. and J. Ahringer, *Genome-wide RNAi screening in Caenorhabditis elegans.* Methods, 2003. **30**(4): p. 313-21.

77.   Sonnichsen, B., et al., *Full-genome RNAi profiling of early embryogenesis in Caenorhabditis elegans.* Nature, 2005. **434**(7032): p. 462-9.

78.   Sulston, J.E., et al., *The embryonic cell lineage of the nematode Caenorhabditis elegans.* Dev Biol, 1983. **100**(1): p. 64-119.

79.   Bourdages, K.G., et al., *Quantitative analysis of cytokinesis in situ during C. elegans postembryonic development.* PLoS One, 2014. **9**(10): p. e110689.

80.   Johnston, W.L., A. Krizus, and J.W. Dennis, *The eggshell is required for meiotic fidelity, polar-body extrusion and polarization of the C. elegans embryo.* BMC Biol, 2006. **4**: p. 35.

81.   Magidson, V. and A. Khodjakov, *Circumventing photodamage in live-cell microscopy.* Methods Cell Biol, 2013. **114**: p. 545-60.

82.   Cheng, N.N., C.M. Kirby, and K.J. Kemphues, *Control of cleavage spindle orientation in Caenorhabditis elegans: the role of the genes par-2 and par-3.* Genetics, 1995. **139**(2): p. 549-59.

83.   Russell, R.C., et al., *ULK1 induces autophagy by phosphorylating Beclin-1 and activating VPS34 lipid kinase.* Nat Cell Biol, 2013. **15**(7): p. 741-50.

84.   Konig, J., et al., *Analysis of cytokinesis by electron microscopy.* Methods Cell Biol, 2017. **137**: p. 225-238.

85.   Zhang, L., et al., *The auxin-inducible degradation (AID) system enables versatile conditional protein depletion in C. elegans.* Development, 2015. **142**(24): p. 4374-84.

86.   Abdu, Y., et al., *Developmentally programmed germ cell remodelling by endodermal cell cannibalism.* Nat Cell Biol, 2016. **18**(12): p. 1302-1310.

87.   Finger, F.P., K.R. Kopish, and J.G. White, *A role for septins in cellular and axonal migration in C. elegans.* Dev Biol, 2003. **261**(1): p. 220-34.

88.   Peterson, E.A. and E.M. Petty, *Conquering the complex world of human septins: implications for health and disease.* Clin Genet, 2010. **77**(6): p. 511-24.

89.   Kinoshita, A., et al., *Identification of septins in neurofibrillary tangles in Alzheimer's disease.* Am J Pathol, 1998. **153**(5): p. 1551-60.

90.   Choi, P., et al., *SEPT5_v2 is a parkin-binding protein.* Brain Res Mol Brain Res, 2003. **117**(2): p. 179-89.

91.   Nagata, K., et al., *Filament formation of MSF-A, a mammalian septin, in human mammary epithelial cells depends on interactions with microtubules.* J Biol Chem, 2003. **278**(20): p. 18538-43.

92.   Surka, M.C., C.W. Tsang, and W.S. Trimble, *The mammalian septin MSF localizes with microtubules and is required for completion of cytokinesis.* Mol Biol Cell, 2002. **13**(10): p. 3532-45.

93.   Kuhlenbaumer, G., et al., *Mutations in SEPT9 cause hereditary neuralgic amyotrophy.* Nat Genet, 2005. **37**(10): p. 1044-6.

94.   Mostowy, S., et al., *Septins regulate bacterial entry into host cells.* PLoS One, 2009. **4**(1): p. e4196.

95.   Mostowy, S., et al., *Septin 11 restricts InlB-mediated invasion by Listeria.* J Biol Chem, 2009. **284**(17): p. 11613-21.

96.   Cerveira, N., S. Bizarro, and M.R. Teixeira, *MLL-SEPTIN gene fusions in hematological malignancies.* Biol Chem, 2011. **392**(8-9): p. 713-24.

97.   Larisch, S., *The ARTS connection: role of ARTS in apoptosis and cancer.* Cell Cycle, 2004. **3**(8): p. 1021-3.

98.   Tanaka, M., et al., *Impaired expression of a human septin family gene Bradeion inhibits the growth and tumorigenesis of colorectal cancer in vitro and in vivo.* Cancer Gene Ther, 2002. **9**(6): p. 483-8.

99.   Yu, W., et al., *The phosphorylation of SEPT2 on Ser218 by casein kinase 2 is important to hepatoma carcinoma cell proliferation.* Mol Cell Biochem, 2009. **325**(1-2): p. 61-7.

100.   Aladzsity, I., et al., *Autophagy genes unc-51 and bec-1 are required for normal cell size in Caenorhabditis elegans.* Genetics, 2007. **177**(1): p. 655-60.

101.   Tinevez, J.Y., et al., *TrackMate: An open and extensible platform for single-particle tracking.* Methods, 2016.

102.   Kelly, W.G., et al., *Distinct requirements for somatic and germline expression of a generally expressed Caernorhabditis elegans gene.* Genetics, 1997. **146**(1): p. 227-38.

103.   Johnsen, R.C., S.J. Jones, and A.M. Rose, *Mutational accessibility of essential genes on chromosome I(left) in Caenorhabditis elegans.* Mol Gen Genet, 2000. **263**(2): p. 239-52.

104.   McDowall, J.S. and A.M. Rose, *Genetic analysis of sterile mutants in the dpy-5 unc-13 (I) genomic region of Caenorhabditis elegans.* Mol Gen Genet, 1997. **255**(1): p. 60-77.

105.   Dionne, L.K., X.J. Wang, and R. Prekeris, *Midbody: from cellular junk to regulator of cell polarity and cell fate.* Curr Opin Cell Biol, 2015. **35**: p. 51-8.

106.   Bernabe-Rubio, M., et al., *Novel role for the midbody in primary ciliogenesis by polarized epithelial cells.* J Cell Biol, 2016. **214**(3): p. 259-73.

107.   Hildebrandt, F., T. Benzing, and N. Katsanis, *Ciliopathies.* N Engl J Med, 2011. **364**(16): p. 1533-43.

108.   Carlsson, S.R. and A. Simonsen, *Membrane dynamics in autophagosome biogenesis.* J Cell Sci, 2015. **128**(2): p. 193-205.

109.   Levine, B., M. Packer, and P. Codogno, *Development of autophagy inducers in clinical medicine.* J Clin Invest, 2015. **125**(1): p. 14-24.

110.   Kim, J.Y., et al., *Noncanonical autophagy promotes the visual cycle.* Cell, 2013. **154**(2): p. 365-76.

111.   Martinez, J., et al., *Noncanonical autophagy inhibits the autoinflammatory, lupus-like response to dying cells.* Nature, 2016. **533**(7601): p. 115-9.

Danksagungen

Mein Dank gilt zunächst Dr. Ann Wehman und Dr. Gholamreza Fazeli für ihre professionelle und warmherzige Betreuung, mit der sie mich in das wissenschaftliche Arbeiten eingeführt und darin auch herausgefordert haben – ich habe wirklich sehr viel lernen dürfen.

Außerdem danke ich meinem Promotionskomitee, insbesondere meiner Referentin Prof. Gohla, für die Unterstützung und Auseinandersetzung mit meiner Dissertation.

Mein besonderer Dank gilt Fr. Mewis für die exzellente Beratung im Promotionsbüro.

Ich danke meinen Labmates der AG Wehman – für viele gemeinsame Stunden sowie alle Ermutigung und Unterstützung im Labor.

Mein Dank gilt auch meinen lieben Freunden in Würzburg, allen voran Conny und Iris, meine größten Cheerleader, wenn es ums Durchhalten ging.

Tief dankbar bin ich meinen Eltern für ihre bedingungslose Unterstützung auf meinem Weg in und durch mein gesamtes Medizinstudium – solche Ermutigung und solcher Zuspruch sind ein wahrer Segen!

Und ich danke dem Gott der Bibel, der als Schöpfer dieser Welt nicht zu begreifen ist und dem jeder einzelne Mensch doch so wichtig ist, der mich trägt und über dessen Schöpfung ich nach dieser Arbeit nur noch mehr staunen kann.

Lebenslauf

Linda Irmisch

geboren 1993 in Karlsruhe

Schulausbildung

6/2010   Allgemeine Hochschulreife

Studium

10/2011 – 5/2018   Studium der Humanmedizin an der Julius-Maximilians-Universität
                     Würzburg

10/2014   Beginn der Dissertation am Rudolf-Virchow-Zentrum in Würzburg
                   unter der Betreuung von Dr. Ann Wehman

5/2018   Approbation